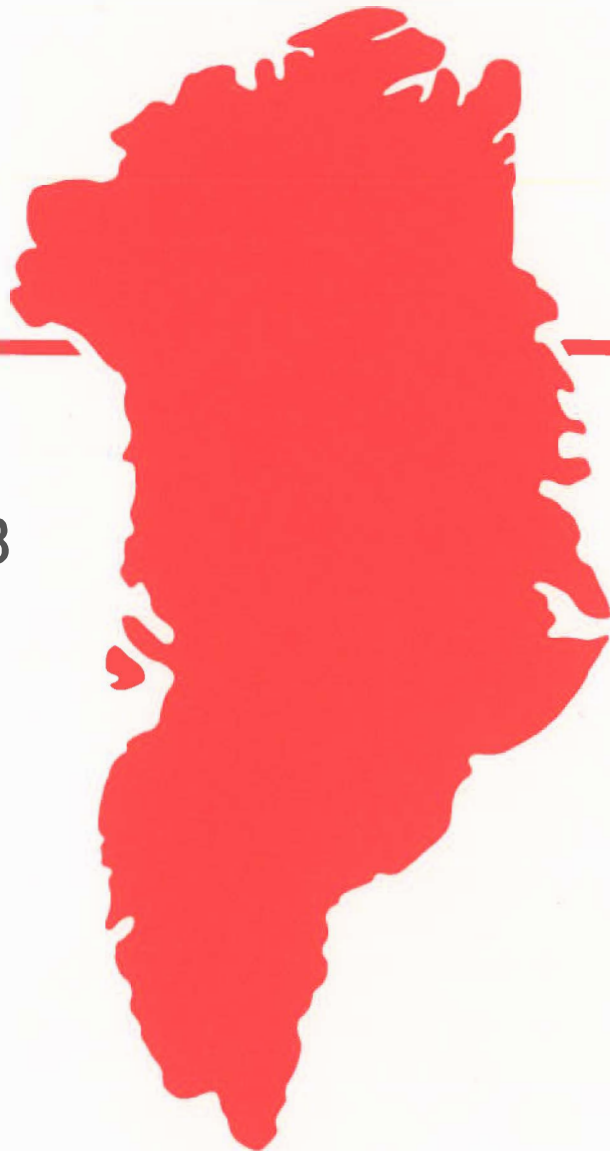


Mass balance and related topics of the Greenland ice sheet

Report of the 4th workshop

Jaap J. M. van der Meer and
Roger J. Braithwaite (editors)



Open File Series 94/13

June 1994



GRØNLANDS GEOLOGISKE UNDERSØGELSE
Ujarassioortut Kalaallit Nunaanni Misissuisoqarfiat
GEOLOGICAL SURVEY OF GREENLAND

GRØNLANDS GEOLOGISKE UNDERSØGELSE
Open File Series 94/13

Report of the
4th Workshop on

Mass balance
and related topics
of the Greenland ice sheet

Jaap J. M. van der Meer and Roger J. Braithwaite
(editors)

held at
Fysisch Geografisch en Bodemkundig Laboratorium
University of Amsterdam, The Netherlands
22nd – 24th November 1993

June 1994

Page intentionally left empty in printed version

INTRODUCTION

The Fourth Workshop on 'Mass Balance and Related Topics of the Greenland Ice Sheet' was held at the Fysisch Geografisch en Bodemkundig Laboratorium of the University of Amsterdam, The Netherlands from 22 to 24 November 1993 . The workshop attracted 35 registered participants from Europe and North America, and was also followed by a number of Dutch students.

In the Introduction to Open File Series 93/5, which contains the extended abstracts to the Third Workshop, it is stated that the workshops were started as a forum to exchange and discuss mass and energy balance studies carried out in Greenland by Austrian, Danish, Dutch, German and Swiss groups. Furthermore it was stated hopefully that the workshops should develop into real symposia dealing with all aspects of Greenland glaciology.

Although the size of the Fourth Workshop was similar to that of the Third, the number of countries represented increased from five to eight as researchers from Belgium, France and the USA participated in the Fourth Workshop. In this sense the Fourth Workshop was another step towards reaching 'real' symposium status.

An essential purpose of the workshops is to discuss and exchange results of the preceding summer's campaign. As such many of the presentations, and consequently the abstracts, should not be considered as 'matured' products of research. Instead some contributions express ideas, or present the results of trials, which later appear in the form of papers in Journals. It is hoped that a change towards real symposia on Greenland glaciology will not conflict with this essential trait of the workshops.

Most, if not all, of the European groups active in glaciological research in Greenland seem to be represented at the workshops. However, there is ongoing research on the Holocene development of the Greenland Ice Sheet that is hardly represented up to now. It is hoped that future Workshops will attract representatives of this paleo-glaciological component. The next opportunity will be the Fifth Workshop, which will be held in Innsbrück, Austria, in November 1994.

June 1994

Jaap van der Meer/Roger J. Braithwaite

Page intentionally left empty in printed version

CONTENTS	Page
Introduction	3
Participants and addresses	7
Presentations at the workshop:	
C.S. Benson - Glacier facies: with special reference to Greenland	11
C.S. Benson, G. Bender & S.A. Bowling - Distribution of accumulation on the Greenland ice sheet	15
C.E. Bøggild, N. Reeh & H. Oerter - Past and present energy-balance studies of Northeast Greenland	18
R.J. Braithwaite - Degree-day factor, energy balance and ablation in Greenland	23
M. van den Broeke, P.G. Duynkerke & E.A.C. Henneken - A heat budget study of the boundary layer overlying the melting zone of the West-Greenland ice sheet in summer	25
P. Calanca & A. Ohmura - Atmospheric moisture flux and flux convergence in the Greenland area	28
P.G. Duijnkerke - Linear stability of katabatic flows: effect of Froude number, slope angle and surface friction	32
J. Forrer & M. Rotach - Exchange of heat and momentum in a very stable boundary layer	35
H. Gallée, O.Fontaine de Ghélin & G. Schayes - Simulation of atmospheric circulation during the GIMEX 91 experiment using a Meso- γ primitive equations model	39
Ch. Genthon - Resolution sensitivity of Greenland surface mass balance in a GCM	43
R. Greve - EGIG line simulations with a 2-D polythermal ice sheet model	46
M. Haefliger - Net radiation derived from AVHRR for the Greenland ice sheet - preliminary results	49
L. Hempel - Deep radio echo soundings in the vicinity of GRIP and GISP2 drill sites, Greenland	53
E.A.C. Henneken - On the use of the profile method on the Greenland ice sheet	56
H. Jiskoot & J. Oerlemans - Model simulation of the Greenland ice sheet in an East-West transect	59
F. Jung-Rothenhäusler, S. Kipfstuhl & T. Thorsteinsson - First field report from the AWI North Greenland traverse	62
K. Keller, N. Gundestrup, C.C. Tscherning, R. Forsberg & S. Ekholm - Mass balance studies at Dome GRIP using GPS & gravity	65
T. Konzelman - Energy balance of dry and wet snow covers at ETH camp	69
I. Marsiat - Modelling the mass balance of ice sheets. Long-term simulation with a simple climate model	72
J.J.M. van der Meer, K. van der Borg, C. Laban & F.G.M. van Tatenhove - Dating deglaciation and its aftermath in Søndre Strømfjord/Sandflugtdalen	76

	Page
A. Meesters - Energy balance of the ablation zone: influence of tundra and katabatic wind	80
G. Niederbäumer - Synoptic observations during two years from automatic weatherstation at the ETH camp	83
H. Oerter, N. Reeh & C.E. Bøggild - Glaciological fieldwork at the ice margin in Kronprins Christian Land, NE Greenland, 1993	86
A. Ohmura - ETH Greenland climate programme - balance of four years' field experiment	90
A.J. Russell - The role of infrequent hydrological events in glacialfluvial sediment transport from the western margin of the Greenland ice sheet, near Kangerlussuaq (Søndre Strømfjord)	94
C. Schøtt Hvidberg, K. Keller & N. Gundestrup - Mass balance calculations around GRIP, Central Greenland	98
M. Stober - Investigations about refraction influences in trigonometric leveling on the Greenland ice surface	101
F.G.M. van Tatenhove & C.M. Roelfsema - Changes in position and altitude of a small outlet glacier and adjacent moraines during the period 1943-1992, Leverett glacier, West Greenland	108
R.H. Thomas, W. Krabill, S. Manizade & K. Jezek - Greenland ice sheet thickness changes measured by laser altimetry	110
A. Weidick - Neoglacial changes of the inland ice margin	114
Z. Zuo & J. Oerlemans - Albedo variations in the melting zone of the Greenland ice sheet: observations and modelling	119

PARTICIPANTS TO THE FOURTH WORKSHOP ON THE MASS BALANCE OF THE GREENLAND ICE SHEET AND RELATED TOPICS

Carl S. Benson tel. ++1.907.4747450
 Geophysical Institute fax. ++1.907.4747290
 University of Alaska
 Fairbanks, Alaska 99775, United States

Norbert Blindow tel. ++49.251.833593
 Institut für Geophysik fax. ++49.251.838397
 Corrensstrasse 24
 4400 Münster, FRG

Carl Egede Bøggild tel. ++45.33.118866
 Grønlands Geologiske Undersøgelse fax. ++45.33.935352
 Øster Voldgade 10
 1350 København K, Denmark

Roger J. Braithwaite tel. ++45.33.118866
 Grønlands Geologiske Undersøgelse fax. ++45.33.935352
 Øster Voldgade 10
 1350 København K, Denmark

Michiel R. van den Broeke tel. ++31.30.934780
 Instituut voor Marien en Atmosferisch Onderzoek
 Princetonplein 5 fax. ++31.30.543163
 3584 CC Utrecht, The Netherlands

Peter G. Duijnkerke tel. ++31.30.532909
 Instituut voor Marien en Atmosferisch Onderzoek
 Princetonplein 5 fax. ++31.30.543163
 3584 CC Utrecht, The Netherlands

Jann Forrer tel. ++41.1.2575221
 Geographisches Institut ETH fax. ++41.1.3625197
 Winterthurerstrasse 190
 8057 Zürich, Switzerland

Hubert Gallée tel. ++32.10.473302
 Institut d'Astronomie et de Géophysique fax. ++32.10.474722
 Université catholique de Louvain
 2, Chemin du Cyclotron
 1325 Louvain-le-Neuve, Belgium

Christophe Genthon tel. ++33.76.824264
 Laboratoire de Glaciologie et Géophysique de l'Environnement/CNRS
 54 Rue Molière fax. ++33.76.824201
 38402 Saint Martin d'Hères Cedex, France

- Ralf Greve**
 Technische Hochschule
 Institut für Mechanik III
 Hochschulstraße 1
 64289 Darmstadt, FRG
 tel. ++49.6151.163093
 fax. ++49.6151.166869
- Marcel Haefliger**
 Geographisches Institut ETH
 Winterthurerstrasse 190
 8057 Zürich, Switzerland
 tel. ++41.1.
 fax. ++41.1.3625197
- Ludwig Hempel**
 Institut für Geophysik
 Corrensstrasse 24
 4400 Münster, FRG
 tel. ++49.251.834704
 fax. ++49.251.838397
- Edwin A.C. Henneken**
 Instituut voor Aardwetenschappen
 Free University Amsterdam
 De Boelelaan 1085
 1081 HN Amsterdam, The Netherlands
 tel. ++31.20.5485772
 fax. ++31.20.6462457
- Hester Jiskoot**
 Fysisch Geografisch en Bodemkundig Laboratorium
 University of Amsterdam
 Nieuwe Prinsengracht 130
 1018 VZ Amsterdam, The Netherlands
 tel. ++31.20.5257451
 fax. ++31.20.5267431
- Friedrich Jung-Rothenhäusler**
 Alfred-Wegener-Institut
 Postfach 120161
 27515 Bremerhaven, FRG
 tel. ++49.471.4831347
 fax. ++49.471.4831149
- Kristian Keller**
 Niels Bohr Institutet for Astronomi, Fysik og Geofysik
 University of Copenhagen
 Haraldsgade 6
 2200 København N, Denmark
 tel. ++45.35.320586
 fax. ++45.35.822565
- Wouter H. Knap**
 Instituut voor Marien en Atmosferisch Onderzoek
 Princetonplein 5
 3584 CC Utrecht, The Netherlands
 tel. ++31.30.934780
 fax. ++31.30.543163
- Thomas Konzelman**
 Geographisches Institut ETH
 Winterthurerstrasse 190
 8057 Zürich, Switzerland
 tel. ++41.1.2575208
 fax. ++41.1.3625197

- Isabelle Marsiat**
Institut d'Astronomie et de Géophysique
2, Chemin du Cyclotron
1325 Louvain-le-Neuve, Belgium
tel. ++32.10.473397
fax. ++32.10.474722
- Jaap J.M. van der Meer**
Fysisch Geografisch en Bodemkundig Laboratorium
University of Amsterdam
Nieuwe Prinsengracht 130
1018 VZ Amsterdam, The Netherlands
tel. ++31.20.5257420
fax. ++31.20.5267431
- Antoon Meesters**
Instituut voor Aardwetenschappen
Free University Amsterdam
De Boelelaan 1085
1081 HN Amsterdam, The Netherlands
tel. ++31.20.5485772
fax. ++31.20.6462457
- Gunthard Niederbäumer**
Geographisches Institut ETH
Winterthurerstrasse 190
8057 Zürich, Switzerland
tel. ++41.1.2575208
fax. ++41.1.3625197
- Hans Oerlemans**
Instituut voor Marien en Atmosferisch Onderzoek
Princetonplein 5
3584 CC Utrecht, The Netherlands
tel. ++31.30.934780
fax. ++31.30.543163
- Hans Oerter**
Alfred-Wegener-Institut
Postfach 120161
27515 Bremerhaven, FRG
tel. ++49.471.4831347
fax. ++49.471.4831149
- Atsumu Ohmura**
Geographisches Institut ETH
Winterthurerstrasse 190
8057 Zürich, Switzerland
tel. ++41.1.2575220
fax. ++41.1.3625197
- Hisashi Ozawa**
Geographisches Institut ETH
Winterthurerstrasse 190
8057 Zürich, Switzerland
tel. ++41.1.2575217
fax. ++41.1.3625197
- Chris Roelfsema**
Faculty of Geodesy, TU Delft
Thijsseweg 11
2600 GA Delft, The Netherlands

Andy Russell
School of Geography
Kingston University
Penrhyn Ross
Kingston upon Thames, Surrey KT1 2EE, U.K.

tel. ++44.81.5472000
fax. ++44.81.5477419

Christine Schøtt Hvidberg
Geofysisk Afdeling
University of Copenhagen
Haraldsgade 6
2200 København N, Denmark

tel. ++45.35.320560
fax. ++45.35.822565

Manfred Stober
Fachhochschule für Technik Stuttgart
Postfach 101452
70013 Stuttgart, FRG

tel. ++49.711.1212563
fax. ++49.711.1212666

Frank van Tatenhove
Fysisch Geografisch en Bodemkundig Laboratorium
University of Amsterdam
Nieuwe Prinsengracht 130
1018 VZ Amsterdam, The Netherlands

tel. ++31.20.5257420
fax. ++31.20.5267431

Robert H. Thomas
Code YS
NASA Headquarters
Washington DC 20546, United States

tel. ++1.202.3580766
fax. ++1.202.3583098

Hans F. Vugts
Instituut voor Aardwetenschappen
Free University Amsterdam
De Boelelaan 1085
1081 HV Amsterdam, The Netherlands

tel. ++31.20.5484151
fax. ++31.20.6462457

Anker Weidick
Grønlands Geologiske Undersøgelse
Øster Voldgade 10
1350 København K, Denmark

tel. ++45.33.118866
fax. ++45.33.935352

Zhizheng Zuo
Instituut voor Marien en Atmosferisch Onderzoek
Princetonplein 5
3584 CC Utrecht, The Netherlands

tel. ++31.30.533155
fax. ++31.30.543163

GLACIER FACIES: WITH SPECIAL REFERENCE TO GREENLAND

Carl S. Benson
Geophysical Institute
University of Alaska
Fairbanks, Alaska 99775 U.S.A.

The concept of glacier facies, introduced in 1960, permits a classification of glaciers that has proven useful in subdividing the Greenland ice sheet, and permits evaluation and comparison of other glacier masses as well.

The facies are generalized in the figure which is modified from Benson (1961, 1962). Annual layers are schematically drawn with constant thickness for simplicity; they slope upward to indicate increasing altitude. Below the *snow line* the annual accumulation of snow is completely stripped away in the *ice facies*. Immediately above the snow line and extending up to the *wet-snow line* the entire year's accumulation is raised to the melting point and wetted in the *wet-snow facies*. Above the wet-snow line the annual increment of snow is not completely wetted, nor does its temperature reach the melting point. Percolation of melt water occurs along selected channels and, as this percolating water freezes in the snow, ice lenses and vertical pipe-like ice glands form. The amount of percolation decreases with altitude and becomes negligible at the *dry-snow line* which forms the upper limit of the *percolation facies*. Above the dry-snow line negligible melt occurs in the *dry-snow facies*.

The *superimposed ice zone* overlaps the wet-snow facies and the ice facies. Superimposed ice forms where melt water in the snow freezes on cold, impermeable glacier ice. Part of the superimposed ice is lost to ablation, but part of it becomes an increment added to the glacier. The lower limit of the superimposed ice zone, in the ice facies, is the *equilibrium line* which separates the *ablation area* from the *accumulation area*. The *slush zone* occurs within the lower end of the wet-snow facies where the snow is not only wetted, but soaked or saturated with melt water to the extent that free water is present and slush flows occur; it extends up to the *slush limit*. The concept of a slush zone and slush limit was introduced by Müller (1962).

The facies boundaries were located by physical measurements of temperature, density and ram-hardness together with stratigraphic determinations of annual units in Greenland. The overburden pressure (load) at a depth of 5m below the snow surface provided one of the best indicators of the facies boundaries measured along traverses extending nearly 2000 km on the Ice Sheet. Where complete wetting of the annual unit occurs there is a sharp drop in the load values from >250 to 220 g cm^{-3} at the wet-snow line. The load values gradually decrease as one proceeds up the percolation facies from 220 to 200 g cm^{-3} at the dry snow line. Within the dry-snow facies the load values are below 200 and mostly lie in the range of 180 g cm^{-3} . The wet-snow line and the dry-snow line have no surface expression so they cannot be determined from aircraft or space vehicles which rely on sensors which see only the surface (Williams, Hall and Benson, 1991). However, the potential of SAR imagery to see below the surface opens a new chapter of polar glaciology. The zonation of the Greenland ice sheet observed on SAR imagery by Fahnestock et al. (1993), Fahnestock (1993), and Rignot et al. (1993) was very close to the glacier facies boundaries mapped from field measurements in the mid 1950's. The possibility of mapping large areas by satellite is exciting and may

eliminate the need for digging holes all over the place.

Comparison of Antarctic and Greenland Stations, at places which have essentially the same mean annual temperatures and rates of accumulation, demonstrates that the definition of facies boundaries, needs to consider additional variables. This is because the overall wind environment did not vary significantly across the region studied in Greenland, nor did the range of annual temperature vary to the extent that it does when the two hemispheres are compared. However, this does not affect the conceptual framework of the glacier facies. The stations considered were Byrd Station, Antarctic ice sheet, (80°S.; 120°W., 1500 m) and Benson's station 4-0, North Greenland Ice Sheet (77°N.; 47°W., 2616m); the mean annual temperatures are -28°C and -31°C respectively, the accumulation rates at both stations are between 16 and 17 cm water equivalent (Benson, 1971).

Research on Alaskan glaciers has helped define the limits of glacier facies in this complex mountain area and has helped to refine the concepts of percolation warming. The dry-snow facies occurs on high parts (>4000m) of the Wrangell-St. Elias Mountains and in the Alaska Range (Benson and Follett, 1986). The McCall Glacier in the Brooks Range is of special interest because its 10m deep temperatures are in the range of -7 to -10°C in the ablation area, but 0 to -3°C in its accumulation area. This is because percolating meltwater releases latent heat as it freezes in the firn; this process does not occur in the impermeable ice of the ablation area. The upper reaches of McCall glacier lie below the wet-snow line (Trabant, Harrison and Benson, 1975). The process of percolation and freezing in the percolation and wet-snow facies is responsible for a "warm band" around Greenland. The existence of a warm band around the Greenland ice sheet, and its characteristics, such as its location, width, and the amount of warming in it (on the order of 10°C) require further investigation.

When the temperature gradient measured in the dry-snow facies of the Greenland Ice Sheet is projected to the latitude of 90°N, and an altitude of 3000m is assumed (as at the South Pole) we obtain a hypothetical mean annual temperature of -47°C. This is close enough to the measured mean annual temperature at the South Pole (-50°C) to suggest that the Greenland Ice Sheet behaves as if it were part of a larger and polar-symmetric Ice Sheet.

References:

- Benson, C.S. 1961. Stratigraphic Studies in the Snow and Firn of the Greenland Ice Sheet. *Folia Geographica Danica* IX, 13-37, and SIPRE, (CRREL) Research Report 70, 93 pp., 3 Appendices, 11 fold-out, graphical data sheets, 1962.
- Benson, C.S. 1971. Stratigraphic Studies of the Snow at Byrd Station, Antarctica, Compared with similar Studies in Greenland. *Antarctic Research Series, A.G.U., Antarctic Snow and Ice Studies* II 16, 333-353.
- Benson, C.S., and A. B. Follett. 1986. Application of Photogrammetry to the Study of Volcano-Glacier Interactions on Mount Wrangell, Alaska. *Photogrammetric Engineering and Remote Sensing* 52, 813-827.
- Fahnestock, M. A., R.A. Bindshadler, R. Kwok and K. Jezek. 1993. Greenland Ice Sheet Surface Properties and Ice Dynamics from ERS-1 SAR Imagery. *Science* 262, 1530-1534. (see also: Melt-Related Hydrologic Zones on the Greenland Ice Sheet Imaged with ERS-1 Synthetic Aperture Radar, *EOS supplement* 73, 175; 1992)

Fahnestock, M. A. 1993. Ice Sheet Research Using SAR. SAR Users Meeting Abstracts, Alaska SAR Facility, Battelle Conference Center 27-29 July 1993, Seattle, Washington USA. G4-G6.

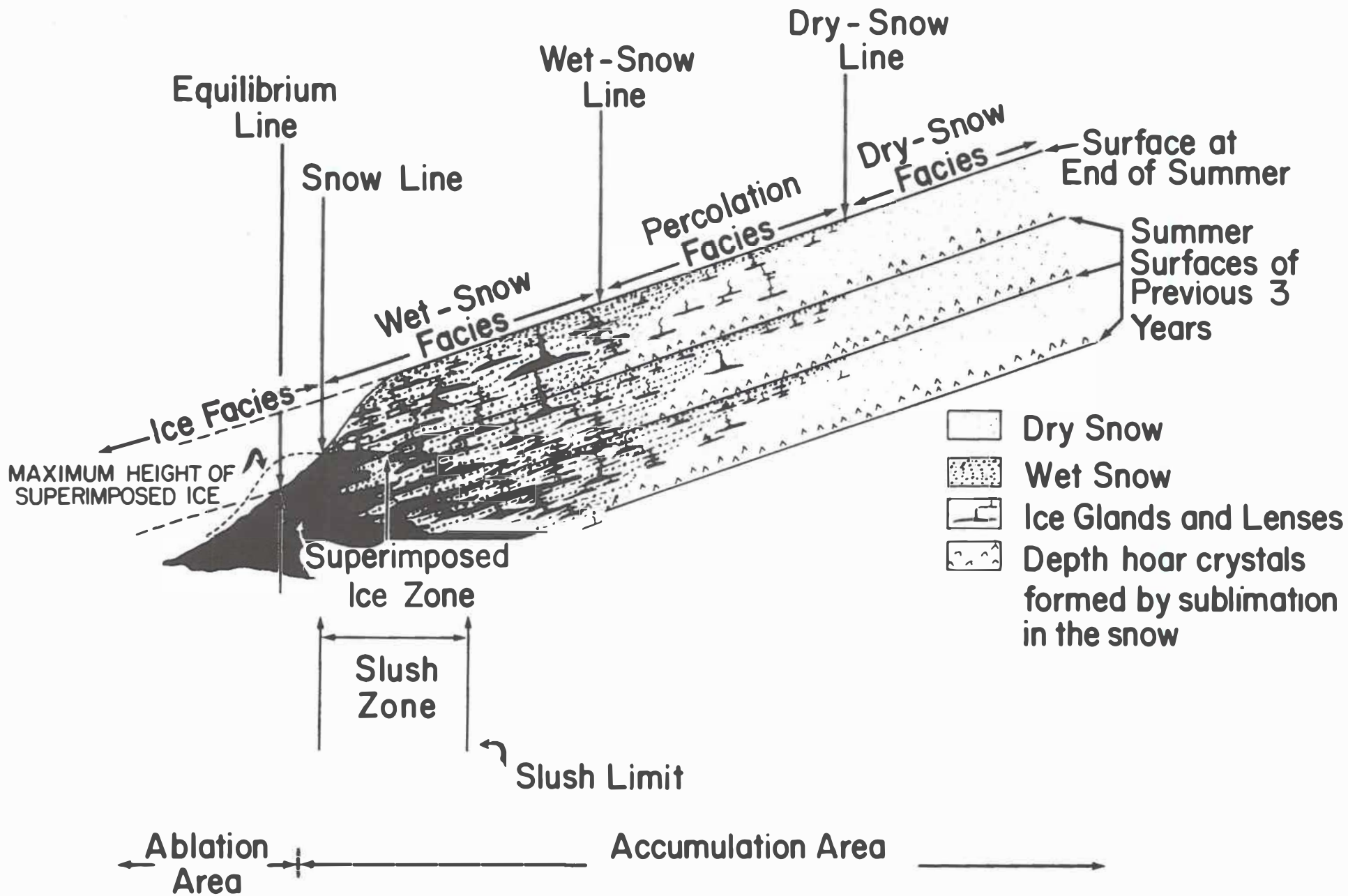
Müller, F. 1962. Zonation in the Accumulation Area of the Glaciers of Axel Heiberg Island, NWT, Canada. *Journal of Glaciology* 4, 302-313.

Rignot, E.J., S.J. Ostro, J.J. van Zyl and K. C. Jezek. 1993. Unusual Radar Echoes from the Greenland Ice Sheet. *Science* 261, 1710-1713.

Trabant, D. C., W. D. Harrison and C. S. Benson. 1975. Thermal Regime of McCall glacier, Brooks Range, Northern Alaska. *Climate of the Arctic: Proceedings of the AAAS-AMS Conference, Fairbanks, Alaska, August 1973, Geophysical Institute, University of Alaska*, 347-349.

Williams, R. S., Jr., D. K. Hall and C. S. Benson. 1991. Analysis of Glacier Facies using Satellite Techniques. *Journal of Glaciology* 37, 120-128.

Acknowledgements: This research has been supported by the U.S. National Science Foundation: Grant No. DPP 90-02345. My transportation to the 4th workshop on mass balance of the Greenland Ice Sheet and related topics was provided by Alaska Airlines (ASA) and Scandinavian Airlines (SAS).



ACCUMULATION ON THE GREENLAND ICE SHEET

Carl S. Benson, Gary Bender & Sue Ann Bowling
Geophysical Institute
University of Alaska, Fairbanks, U.S.A.

More is known about accumulation than the other mass balance parameters for the Greenland Ice Sheet, even though information is steadily increasing on ablation and ice-berg flux. Accumulation data on the ice sheet itself come from snow pit studies and deeper cores, spaced along traverses extending back to expeditions in 1912-1913 (De Quervain and Mercanton, 1925; Koch and Wegener, 1930). The measurements include simply measuring the snow height on stakes, as well as detailed profiles of temperature, density, hardness, grain size, electrical conductivity, and chemical and isotopic composition. In addition to data from the ice sheet itself, there is a set of meteorological stations along the coast of Greenland, (and on Canadian Islands to the West and Iceland to the East) some of which have operated for over 100 years. This paper represents another attempt to pull all this material together to give an overall distribution of accumulation on the ice sheet.

There are about 250 places on the ice sheet where measurements of accumulation have been made. Pit studies done repeatedly for several years along the same traverses demonstrate that stratigraphy in the snow is preserved for years and can be interpreted to yield annual accumulation values; close spacing of stations shows a smooth areal variation in the values. Where data points lie close to coastal meteorological stations the accumulation and precipitation values don't match very well. For example, the total annual precipitation recorded at Thule Air Base is 13% of the accumulation measured on the ice sheet about 20 km away. Similarly, the total annual precipitation measured at Upernavik and Jakobshavn is about 46% of the accumulation values measured at points on the ice sheet along the French traverse, or the EGIG Line (Benson, 1961). One of the key problems is to relate meteorological station data with the data set from pit studies on the ice sheet. A critical step in doing this is to examine the performance of precipitation gages and how their efficiency varies with wind and the rate of snowfall.

Concerns about the accuracy of gages in measuring precipitation in the form of snow have been with us for many years (Brooks, 1938; Warnick, 1953; Jackson, 1960; Benson, 1982; Legates, 1993). On the Arctic Slope of Alaska comparison of the Weather Service's unshielded gages with gages shielded by the Wyoming Shield (basically two concentric snow fences around the gage) show that the unshielded gages caught about 30% of the catch of the shielded gages (Benson, 1982). This study has now been extended for over 12 years with the same results (Clagett, U.S. Soil Conservation Service, personal communication). Unshielded gages, including the Hellmann Gage used in Greenland, catch about 30% or less of the precipitation which comes as snow when wind speed exceeds 5 m s^{-1} (Legates, 1993; Günther, 1993; Goodison, 1993). The wind-speed on the Arctic Slope exceeds 5 m s^{-1} for about half of the year (Wendler, 1978). Our measured undercatch of 30% by the unshielded gages is consistent with experiments on gage catch as a function of wind speed and the wind regime of the Arctic Slope.

In reassessing winter precipitation on the Arctic Slope it was found that snow-fall exceeded the Weather Service's record of total annual precipitation (Benson, 1982). As a first approximation, it was decided to use the total precipitation at Greenland Weather Stations as

a measure of accumulation. Thus each Weather Station is treated as an accumulation data point. This makes our values come out higher than those of Ohmura and Reeh (1991).

One could contour accumulation over the entire ice sheet from the existing data points in a variety of ways, and get a variety of results. It is necessary to seek some guiding principles. We have focused on storm tracks which affect Greenland and then assumed orographic control of precipitation. Georgi (1933) referred to Greenland as a “switch for cyclones”. Cyclonic depressions from the south move up either the east or west coast of Greenland. These primary storm tracks are combined with a secondary one in the northeast (Radok et al. 1982). The storm tracks move in such a way as to provide storm winds which ascend the slopes of the ice sheet nearly normal to the coast. If we assume an adequate supply of storms we may concentrate on the orographic precipitation produced by them as they interact with the topography of the ice sheet. Places where vigorous storms are forced to ascend the slopes will have maximum zones of precipitation close to the coast. Places where the air flows over an obstacle and descends on the lee side will have relatively low precipitation; in some cases, such as Inglefield Land and Peary Land, deserts will occur.

A simple orographic model was developed by one of us (S.A.B.) based on the model for precipitation from an ascending air mass (Fulks, 1935) to determine the location of maximum precipitation along a given path normal to the altitude contours. The model was not used for information on the magnitude of precipitation. The model assumptions are simple, in keeping with the available data set. The location of the maximum is most affected by wind speed. An average speed of slightly over 7 m s⁻¹ locates the maxima close to where they were determined by field traverses at 70°N and 77°N (Benson, 1962). A first attempt at our contour map of accumulation was presented by Bender (1984), and a version of it was published by Bromwich et al, 1993. It gives an average annual accumulation for the Ice Sheet of 41 cm H₂O

The map of Greenland has useful information on precipitation sources. Where ice comes directly to the sea one can assume there is a persistent source of precipitation which impinges on the coast. Where there is a broad desert region one can assume there is no such persistent source of precipitation impinging on the coast. Indeed desert regions indicate the existence of a precipitation shadow. A precipitation shadow occurs in the lee of the Sukkertoppen Ice Cap in west Greenland and extends out onto the Ice Sheet. This is also well documented in the case of Thule Peninsula, where the effect extends out onto the ice sheet itself, for at least 250 km (Benson, 1962).

References:

- Bender, G. 1984. The Distribution of Snow Accumulation on the Greenland Ice Sheet. M. S. Thesis, Geophysical Institute, University of Alaska, Fairbanks, Alaska, 110 pp.
- Benson, C.S. 1961. Stratigraphic Studies in the Snow and Firn of the Greenland Ice Sheet. *Folia Geographica Danica*, IX, 13-37, and SIPRE, (CRREL) Research Report 70, 93 pp., 3 Appendices, 11 fold-out, graphical data sheets, 1962.
- Benson, C.S. 1982. Reassessment of Winter Precipitation on Alaska's Arctic Slope and Measurements of the Flux of Wind Blown Snow. Geophysical Institute UAG R-288 University of Alaska, Fairbanks, Alaska, 26 pp.

- Bromwich, D. A., F. M. Robasky, R. A. Keen and J. F. Bolzan 1993. Modeled Variations of Precipitation over the Greenland Ice Sheet, *Journal of Climate*, 6, 1253-1268.
- Brooks, C. R. 1938. Need for Universal Standards for Measuring Precipitation, Snowfall, and Snowcover. Bull 23 IAHS, IUGG Riga.
- DeQuervain, A. and P. L. Mercanton 1925. Resultats Scientifiques de l'Expedition Suisse au Groenland 1912-1913. *Meddelelser Om Grønland*, 59 (5), 55-271.
- Fulks, J. R. 1935. Rate of Precipitation for Adiabatically Ascending Air. *Monthly Weather Review*, 63, 291-294.
- Georgi, J. 1933. Greenland as a switch for Cyclones. *Geographical Journal*, 81, 344-345.
- Goodison, B. 1993. Personal Communication on a Report to WMO.
- Günther, Th. 1993. German Participation in the WMO Solid Precipitation Intercomparison: Final Results, *Precipitation Measurement & Quality Control*. B. Sevruck & M. Lupin (eds.) Proc. of Symp. on Precipitation and Evaporation. Vol. 1 Bratislava, Slovakia, 20-24 Sept. 1993.
- Jackson, C. I. 1960 Snowfall Measurements in Northern Canada. *Quarterly Journal of the Royal Meteorological Society*, 86, 273-275.
- Koch, J. P. and A. Wegener. 1930. *Wissenschaftliche Ergebnisse der Danischen Expedition nach Dronning Louises-Land und quer über das Inlandeis von Nordgrønland (1912-13 unter Leitung von Hauptmann J.P. Koch)*. *Meddelelser Om Grønland*, Bd. 75.
- Legates, D. 1993. The Need for Removing Biases from Rain and Snowgauge Measurements. Snow Watch '92, *Detection Strategies for Snow and Ice: An International Workshop on Snow and Lake Ice Cover and the Climate System*. Eds. R. Barry, B. Goodison, E. Le Drew, *Glaciological Data, Report GD-25*, World Data Center A for Glaciology, Boulder, CO, USA.
- Ohmura, A., and N Reeh, 1991. New Temperature Distribution Maps for Greenland. *Journal of Glaciology*, 37, 140-148.
- Radok, U., R.G. Barry, D. Jensen, R.A. Keen, G.N. Kiladis and B. McInnes. 1982. Climatic and Physical Characteristics of the Greenland Ice Sheet, Parts 1 and 2. CIRES, University of Colorado, Boulder, CO, USA.
- Warnick, C.C. 1953. Experiments with Windshields for Precipitation Gages. *Transactions AGU*, 34, 379-388.
- Wendler, G. 1978. Snow Blowing and Snow Fall on the North Slope, Alaska. Geophysical Institute UAG R-288 University of Alaska, Fairbanks, Alaska.

Acknowledgements: This research has been supported by the U.S. National Science Foundation: Grant No. DPP 90-02345. My transportation to the 4th workshop on mass balance of the Greenland Ice Sheet and related topics was provided by Alaska Airlines (ASA) and Scandinavian Airlines (SAS).

PAST AND PRESENT ENERGY-BALANCE STUDIES OF NORTHEAST GREENLAND

Carl Egede Bøggild

*The Geological Survey of Greenland, Øster Voldgade 10, DK-1350 København K,
Denmark*

Niels Reeh

*Danish Polar Center/ The Geological Survey of Greenland, Øster Voldgade 10, DK-1350 København
K, Denmark*

Hans Oerter

*Alfred Wegener Institut für Polar- und Meeresforschung, Postfach 12016, D-27515 Bremerhaven,
Germany*

Introduction

The main aim of an EC project in 1991 and 1992 was to reconstruct the mass-balance of the Storstrømmen glacier by means of a time series of meteorological data from Danmarkshavn on the outer coast (Bøggild et Al., in press). It became apparent that the degree-day method was most suitable for this mass-balance reconstruction. However, it was also apparent that the data from a lightly equipped glacier climate station, located 900 m from the ice-margin in 1990, could be applied to an existing energy-balance model (Bøggild, 1991) to gain some insight into the physics of melting in Northeast-Greenland.

In this presentation the energy-balance model, as well as some results are shown briefly. Due to the remoteness of Northeast Greenland, only two similar studies have been carried out previously (see Fig. 1). The first study was on Frøya Glacier, a Swedish expedition to Clavering Island from 1939 to 1940 (e.g. Ahlmann, 1942). From 1952 to 1954 the British North Greenland Expedition were operating out of two locations, namely at the ice margin of Northeast Greenland (Britannia SØ) and near the ice-divide of the North-Greenland ice-sheet (Northice). At Britannia Gletscher near Britannia SØ, the energy-balance studies were conducted on two separate locations at 620 m a.s.l. and 460 m a.s.l., respectively (Lister and Taylor, 1961). In this presentation only the lowest energy-balance station will be considered here since this locality shows most resemblance with our Storstrømmen studies.

The Storstrømmen studies

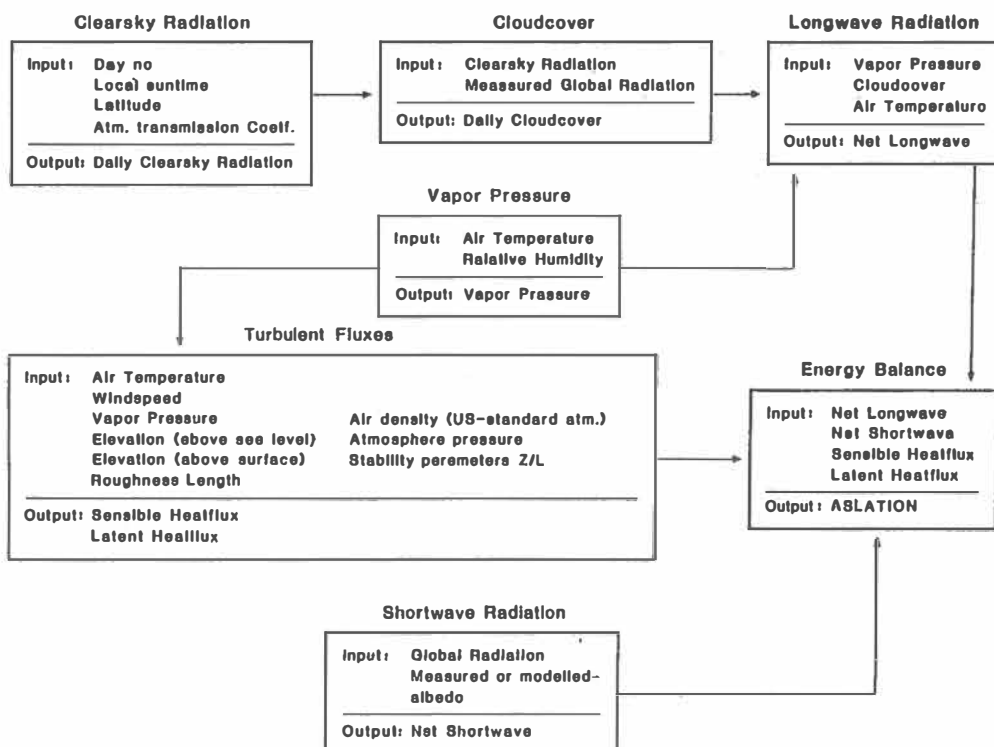
As temperature, wind speed and humidity was measured in just one level, the turbulent fluxes could only be determined from the fact that values of the wind speed, temperature and vapour pressure are known for a melting ice-surface. Also, the radiation fluxes were measured only in the short-wave range. In order to determine the radiation balance in the long wave spectral range, some information about the cloudiness was necessary. This could be circumvented by applying a model to calculate global radiation from information about the cloudiness. The clearsky radiation has been calculated theoretically and, in conjunction with the observed global radiation, this provided us with a value of the daily mean cloud cover of 51% in average over the observation period from July 6 to August 21 in 1990. 51% cloudiness is some 21% less



Fig 1. Map of locations where energy-balance studies have been carried out (marked *)

Fig. 2

Energy Balance Procedure



than observed at Danmarkshavn, and is in agreement with the observed decrease in cloudiness from Danmarkshavn toward Britannia Sø (Hamilton and Rollitt, 1957). An overview of the energy-balance model applied to Storstrømmen is given in fig 2. The cumulated modelled ablation matches very well the observed ablation (fig. 3). However, this match is only to the nearest ablation-stake but is some 20% less than the mean of all stakes in the vicinity of the climate station.

Energy-balance studies at the lower Britannia Gletscher

The studies of energy-balance on Britannia Gletscher are so far the most comprehensive in Northeast Greenland in terms of instrumentation. During three intensive campaigns in 1953 the temperature and humidity were measured in as much as eight different levels ranging from 2 to 400 cm above the ice-surface, and wind was measured in four levels from 30 cm to 400 cm. The standard measurements were carried out from June 14 until August 18. Wind, as well as temperature and humidity was measured manually four times per day. Unfortunately the radiation were only measured in the short-wave range, and the authors does offer little detail on retrieval of the long wave radiation balance (Lister and Taylor, 1961). In addition to this instrumentation a self-recording ablatograph registered ablation continuously as well.

The Fröya glacier on Clavering island

50 years ago any expedition to Northeast Greenland was associated with great difficulties to access the coast due to severe pack-ice in the Greenland sea. This expedition lead by Ahlman took part in a Norwegian journey to the coast, to exchange provision with furs collected by Norwegian trappers in Northeast Greenland. At arrival the scientific programme had to be reduced dramatically. So, only at sea-level recordings could be performed continuously. At the energy-balance site (453 m a.s.l.) all observations had to be collected manually on daytrips out of the camp at sea-level. Wind, temperature and humidity were measured close to the surface and at another level 145 cm above surface. Any radiation measurements had to be given up, so the radiation balance was estimated from observations of the cloudiness. However, details on this matter are lacking (Erikson, 1942).

The Fröya glacier is different from the Storstrømmen and Britannia glaciers since it is a 6.3 km² valley glacier located on the outer coast at Clavering Island. Also, the glacier is only 1 km at the widest, which must affect the glacier climate from the ice-free area surrounding the glacier. During the period of measurements from July 30 until August 18, 1939 the surface was snow-covered and the prescribed albedo was set to 61%. Given an approximate angle of the horizon of 25° toward north-east and south-west, respectively, this has caused a negative radiation balance during most of the period (Erikson, 1942). By means of which the turbulent fluxes were more important for the ablation.

During conditions with mist on the Fröya glacier the airmasses some 2-4 m elevation above the snow surface were found to blow up along the glacier. The wind nearest to the snow surface, however, had a downward direction, and the two layers were highly separated. Today it is apparent that at this early time of energy-balance studies, scientists were not aware of the difficulties related to measuring sensible and latent

heatfluxes within a thin catabatic layer. E.g. the highest sensors on Frøya glacier were placed 174 cm above the snow surface. This elevation could well have been near the point of maximum wind speed within the catabatic layer, where the wind flow is nearly laminar. Application of a bulk transfer coefficient for neutral conditions most probably have resulted in an overestimation of the sensible and latent heat fluxes on Frøya glacier.

Summary and conclusions

For comparison of the importance of components in the ablation processes table 1 lists the results of Storstrømmen as similarly compiled by Lister and Taylor (1961) for Britannia and Frøya glacier. This provides the only means of comparison of results since the former studies are presented mainly graphically. It can be seen that results from Britannia Gletscher and Storstrømmen are almost contrary in terms of radiation and convective fluxes. This is somehow surprising since the two locations are only 40 km apart and are climatically dominated by the high pressure in the interior of the ice-sheet. Moreover, albedo and the general surface characteristics as reported by Lister and Taylor (1961) were very similar to our observations on Storstrømmen.

The following points suggests possible reasons for the different results from the two studies:

- 1) Year to year differences in climate are known to be higher in the high Arctic (Mitchell et al., 1990). The summer of 1953 was reported to be an "average" summer (Hamilton and Rollitt, 1957) whereas the summer of 1990 was a wet and cloudy summer as compared to our experience from other years.
- 2) Due to the lack of stability corrections all observations above 30 cm in the Britannia Gletscher studies were rejected because profile analysis showed data from above this height to deviate from the log-linear profile. However, measurements of fluxes within the narrow range from 9 to 30 cm can be a source of severe errors since measured gradients are extremely small.
- 3) Our estimation of the incoming long wave radiation was calculated to be as little as 210 W/m. This is some 30% less than observed in direct measurements in the ETH-camp with the same cloudiness (Greuell, 1992). We had to estimate the long wave radiation from a calculated cloud cover as well as the empirical "Brunt" and "Bolz" approaches. Incoming long wave radiation is probably the greatest source of uncertainty in our study, which we hope to improve in the future by direct measurements.

Acknowledgements

Besides the Alfred Wegener Institutes involvement in the Northeast Greenland research, additional funding was provided by the Danish National Science Foundation, The Commission for Scientific Research in Greenland, The Nordic Council of Minister's Environmental Research Programme, and the EC EPOC and ENVIRONMENT programme.

Literature

Ahlmann, H.W:son, 1942. Studies in north-east Greenland 1939-1940. Part III: Accumulation and ablation on the Frøya glacier; its regime in 1938-39 and in 1939-40. Geogr. Annalr 24, 1-22.

Bøggild, C.E., N. Reeh, H. Oerter 1994: Modelling ablation and mass-balance sensitivity to climate change of Storstrømmen, North-east Greenland. Global and Planetary Change 9, 79 - 90.

Bøggild, C. E. 1991s En smeltende snepakkes masse og energifluxe - belyst ved beregningsmetoder. (Numerical methods for determining mass- and energyfluxes in a melting snowpack) Thesis. University of Copenhagen. 94 pp.

Erikson, B. E. 1942. Meteorological records and the ablation on the Frøya glacier in relation to radiation and meteorological conditions. Geogr. Ann. XXIV, 23-50.

Greuell, W., 1992. Numerical modelling of the energy balance and englacial temperature at the ETH Camp, West Greenland. Zürcher Geografische Schriften (51) 81 pp.

Hamilton, R.A., and G. Rollitt, 1957. Climatological tables for the site of the expedition's base at Britannia Sø and the station on the Inland ice "Northice". Medd. om Grønland 158 (2), 83 pp.

Lister, H. and P.F. Taylor, 1961, Heat balance and ablation on an arctic glacier. Medd. om Grønland 1958 (7), 54 pp.

Mitchell, J.F.B., Manabe, S., Meleshko, V., Tokioka, T., 1990. Equilibrium Climate Change - and its Implications for the Future. In: Houghton, J.T., Jenkins, G.J., and Ephraums, J.E (eds), Climate Change, the IPCC Scientific Assessment, Cambridge University Press, 131-172.

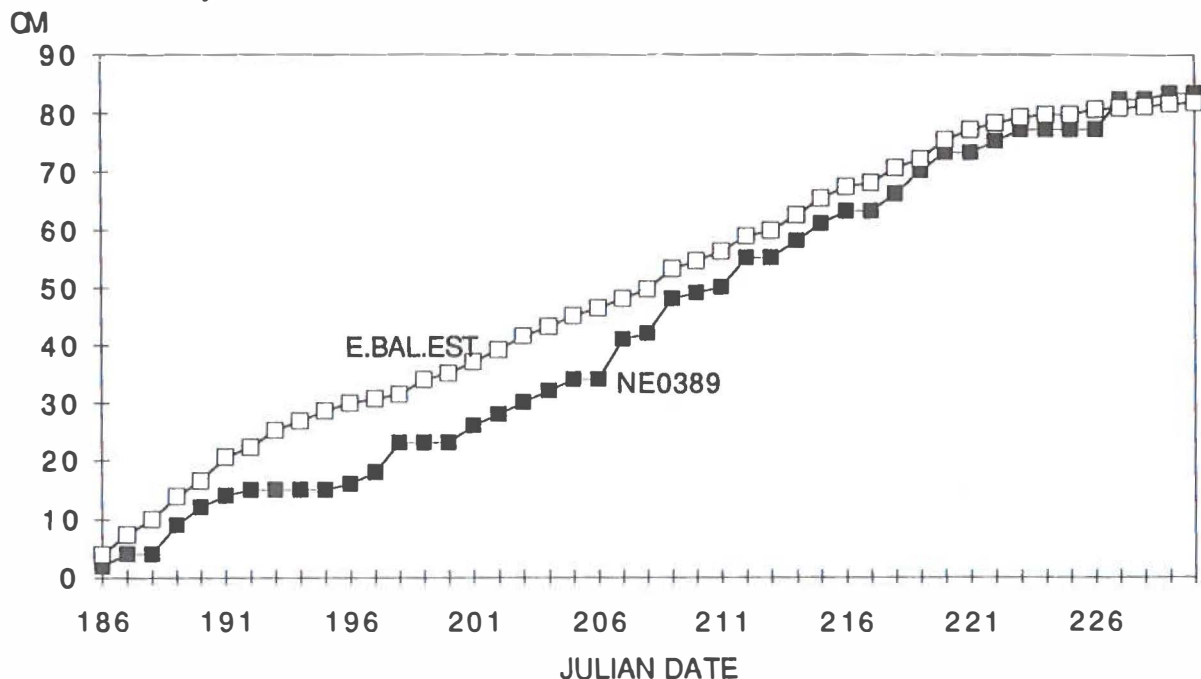


Fig 3. observed and modelled cumulative ablation (in cm ice) at Storstrømmen.

Glacier	Year	Lat	Long	Elevation	Convection (%)	Condensation (%)	Radiation (%)
Froya Glacier	1939	74°24'N	20°50'W	453	83	9	8
Britannia Glacier	1953	77°12'N	23°48'W	470	20	5	75
Storstrømmen	1990	77°11'N	22°04'W	230	88	2	10

Table 1 Energy-balance terms from the studies described in the text.

DEGREE-DAY FACTOR, ENERGY BALANCE AND ABLATION IN GREENLAND

Roger J. Braithwaite
The Geological Survey of Greenland
Copenhagen, Denmark

Ablation is often linked to positive temperature sums by the degree-day factor. On the other hand, ablation energy can also be estimated from climatological data by energy balance modelling. The degree-day and energy balance approaches are both simplifications of a complex system where ablation is estimated from some input variables and some parameters. In the degree-day approach, the only input variable is temperature and there are only two parameters, representing degree-day factors for ice and snow. By contrast, the energy balance model needs more input data but its parameters are also more closely identifiable with physical processes. For example, a typical energy balance model (Fig. 1) uses data for temperature, humidity, wind speed, insolation and cloud amount to estimate ablation according to whether the glacier surface is snow or ice.

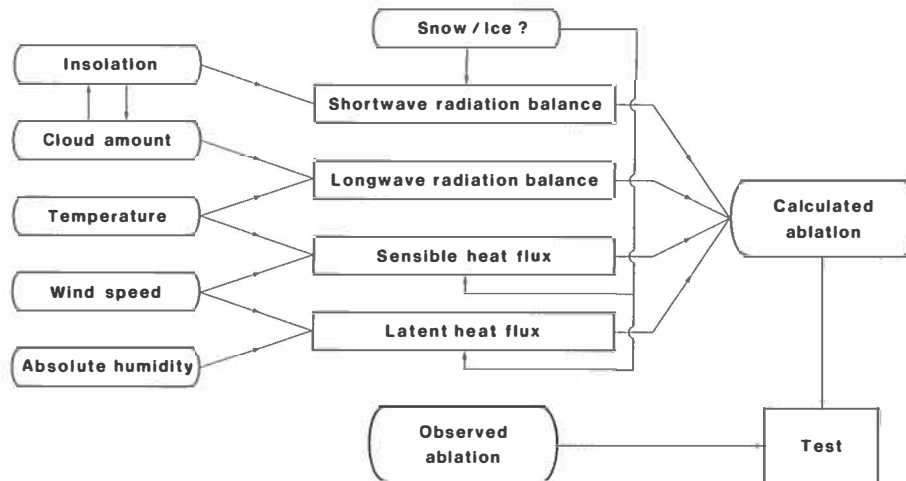


Fig. 1. Calculation of ablation by a simple energy balance model (Braithwaite & Olesen, 1990).

The energy balance approach seems more 'physical' than the degree-day approach but the distinction is not so clear because it is difficult to define all inputs to the energy balance model on the scale of the whole Greenland ice sheet. For example, the scheme in Fig. 1 works well for a site where climate data are available but even such simple data are rare in most parts of the ice sheet. This problem can be partly overcome by further parameterization, e.g. the need for wind data in the energy balance model is commonly avoided by using constant exchange coefficients, but this further blurs the distinction between degree-day and energy balance models. The real distinction is rather uncertainty in the parameters (degree-day model) versus uncertainty in almost all the input data (energy balance model).

The relation between ice ablation and degree-days is illustrated in Fig. 2 where the straight line is the model assumed by Huybrechts *et al* (1991). Although lying outside the general pattern, the two points with relatively high ablation and low degree-days, from Ambach (1988) and van der Wal (1992) respectively, cannot be simply ignored as exceptions to a constant degree-day factor. Indeed, these measurements (made at relatively high elevation in the ablation area at exposed locations) may be more 'representative' of the whole ice sheet than the other data (made closer to the ice sheet margin).

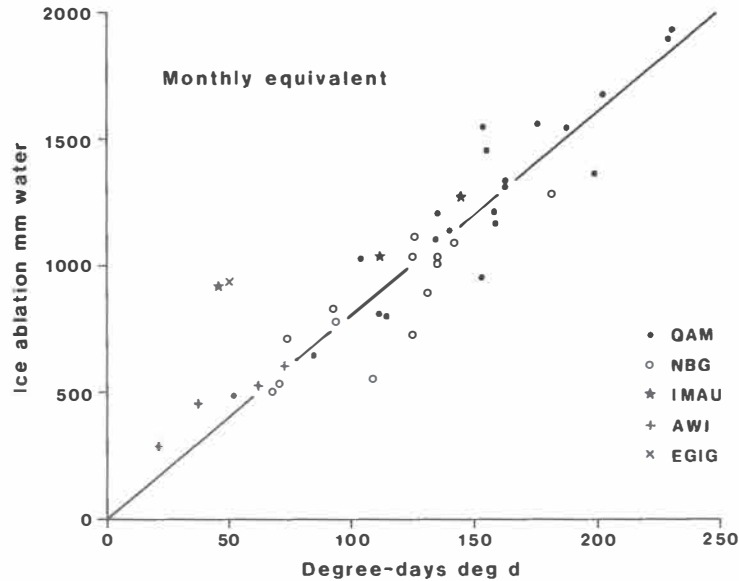


Fig. 2. Monthly equivalent ice ablation on the Greenland ice sheet versus positive degree-days for various studies: QAM & NBG = Qamanârssûp sermia and Nordbogletscher, W. Greenland (Braithwaite and Olesen, 1989); IMAU = E. of Søndre Strømfjord (van der Wal, 1992); AWI = Storstrømmen, NE Greenland (Reeh and others, 1993); EGIG = NE of Jakobshavn, W. Greenland (Ambach, 1988). Straight line is assumed by Huybrechts and others (1991).

Systematic variations in degree-day factor are now being studied by energy balance modelling using data from Nordbogletscher (415 days) and Qamanârssûp sermia (512 days). The key here is that degree-day factors can be estimated from modelled ablation in just the same way as from measured ablation. Inputs to the energy balance model can then be varied to study the effect of different assumptions on the degree-day factor.

For actual climate data, the energy balance model gives degree-day factors that agree reasonably well with those for measured data. Sensitivity experiments to simulate climate change confirm that the degree-day factor is not strictly constant with temperature in agreement with Ambach (1988). Low ice albedo favours a high degree-day factor at lower temperatures while high wind speeds generally favour a high-degree factor. If these model-based conclusions are correct, the degree-day approach will benefit from a better understanding of albedo and wind speed variations over the ice sheet.

Acknowledgements

This research is supported by the European Community through contracts EPOC-CT90-0015 and EV5V-CT91-0051a

References

- Ambach, W. 1988. Heat balance characteristics and ice ablation, western EGIG-profile, Greenland. In Thomsen, T., Søgaard, H. & Braithwaite, R. J. (editors) *Applied hydrology in the development of northern basins*, 59-70. Copenhagen: Danish Society for Arctic Technology
- Braithwaite, R. J. & Olesen, O. B. 1989. Calculation of glacier ablation from air temperature, West Greenland. in Oerlemans, J. (ed.) *Glacier Fluctuations and Climatic Change*. Dordrecht. Kluwer Academic Publishers, 219-233.
- Braithwaite, R. J. & Olesen, O. B. 1990. A simple energy balance model to calculate ice ablation at the margin of the Greenland ice sheet. *J. Glaciol* 36(123), 222-228.
- Huybrechts, P., Letréguilly, A. & Reeh, N. 1991a The Greenland ice sheet and greenhouse warming. *Palaeogeogr. Palaeoclim. Palaeoecol. (Global planet. Change Sect.)* 89, 399-412.
- Reeh, N., H. Oerter & C. E. Bøggild. 1993. *Mass balance and ice dynamics of the North-East Greenland ice-sheet margin*. Final report to the European Community under Contract no. EPOC-CT90-0015. Alfred Wegener Institut für Polar- und Meeresforschung, Bremerhaven.
- Wal, R. van de. 1992. *Ice and climate*. Ph. D. Thesis, Utrecht: Rijksuniversiteit Utrecht.

A HEAT BUDGET STUDY OF THE BOUNDARY LAYER OVERLYING THE MELTING ZONE OF THE WEST-GREENLAND ICE SHEET IN SUMMER

Michiel R. van den Broeke, Peter G. Duynkerke
 Institute for Marine and Atmospheric Research Utrecht
 Utrecht University, The Netherlands
Edwin A.C. Henneken
 Faculty of Earth Sciences
 Free University, Amsterdam, The Netherlands

Preliminary results concerning the heat budget of the atmospheric boundary layer overlying the melting zone of the Greenland ice sheet are presented. The structure of this boundary layer differs significantly from the stable nocturnal boundary layer that is normally found over land. First, the surface temperature is fixed at 0°C due to the continuous melting of ice. Secondly, partly as a result of that, wind speeds are relatively large due to katabatic forcing. The governing stationary heat budget equation in flux form reads:

$$\int_{\text{ice edge}}^{\text{equilibrium line}} \left(\overline{\frac{\partial(u\theta h)}{\partial x}} + \gamma \left[\frac{\partial(\overline{u}h_s h)}{\partial x} - (h_s + \frac{h}{2}) \frac{\partial(\overline{u}h)}{\partial x} \right] \right) = \frac{-1}{\rho_0 c_p} (F_{h_s+h} - F_{h_s}) - \left[\overline{(w'\theta')}_{h_s+h} - \overline{(w'\theta')}_{h_s} \right] dx$$

where u is downslope wind speed, v is cross slope wind speed, γ is the background temperature gradient $\partial\theta/\partial z$, F denotes long wave radiation flux and $(w'\theta')$ is the turbulent heat flux. The double bar denotes the vertically integrated value from the surface h_s to a level h_s+h (h is chosen to be 500 m, and it is assumed that the flux equals zero there). All terms are integrated over the horizontal domain from ice edge towards the equilibrium line, to indicate that we are mainly interested in the time averaged bulk heat budget of a slab of air with depth h and horizontal extent dx . According to Mahrt (1982) we adopted the values of u and θ to be generated entirely by the katabatic flow, meaning that θ equals the temperature difference compared to the reference background state $\theta_0(z)$, while u is the actual wind speed, since the large scale flow is neglected in the present study.

The budget equation states that in stationary conditions the horizontal advection of temperature deviation (HAD), down slope vertical advection (VA) and subsidence (SUB) in a stable atmosphere are balanced by vertical divergence of radiation (RAD) and turbulent cooling through the surface heat flux (TC). The turbulent flux at h_s+h is zero by definition. The effect of a stable background atmosphere on the development of katabatic flow can be understood as follows: when the air descends it encounters colder surroundings that act to decrease the potential temperature deficit of the layer, decreasing katabatic forcing.

We applied the budget equation to the average vertical profiles of wind and temperature for the period 8-15 July 1991, and presented in Fig. 1. The background potential temperature profile θ_0 was obtained by averaging balloon soundings at Egedesminde, yielding a stable lapse rate $\gamma = 5.1 \text{ K km}^{-1}$. Surface turbulent fluxes (TC) were taken from Duynkerke and Van den Broeke (1994); a longwave radiation model was used to calculate the radiation divergence (RAD).

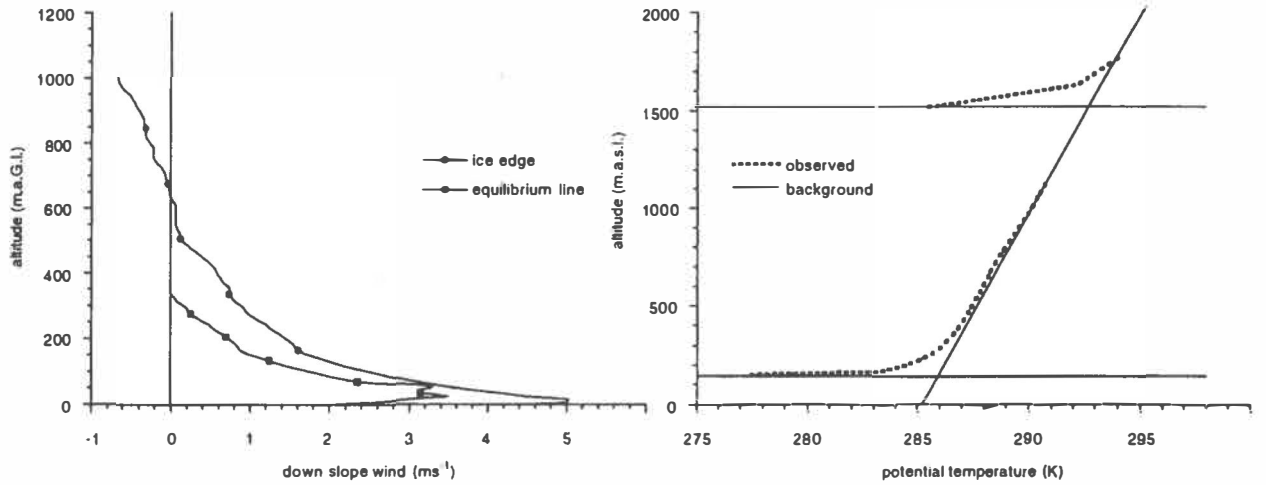


Fig. 1: Average vertical profiles of down slope wind speed u (left) and potential temperature (right) during the period 8-15 July 1991. Note vertical scale for u in meter above ground level and for θ in meter above sea level. The background potential temperature profile is based on daily balloon soundings at Egedesminde.

The balance of the different terms is presented in Fig. 2. It appears that all terms, except horizontal advection HAD, are important for determining the potential temperature deficit of the boundary layer. The contribution of subsidence (SUB) to the heating budget is surprisingly large. The heating caused by vertical advection and subsidence in the stable atmosphere is partly balanced by turbulent cooling and for the rest by long wave radiative divergence.

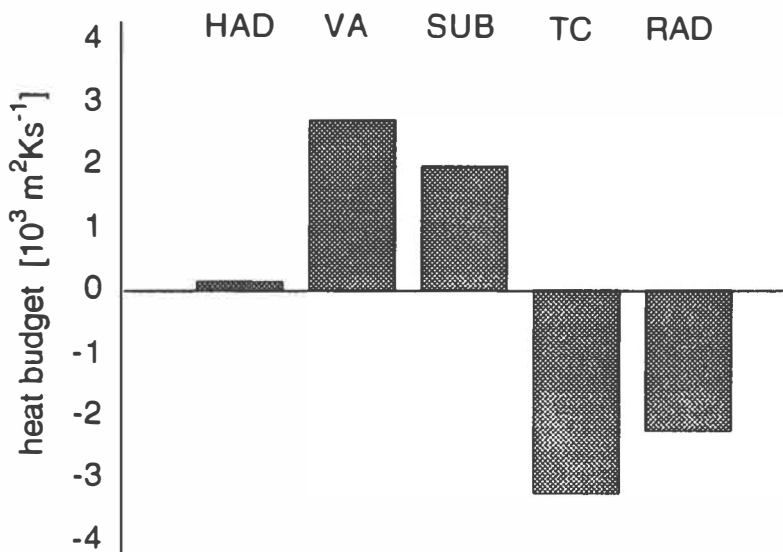


Fig. 2: Heat budget for the period 8-15 July. See text for explanation.

In this analysis the daily cycle is not included. A previous study showed that on a daily time scale the horizontal gradients might become important due to increasing wind speed near the ice edge in the afternoon, whereas the wind speed closer to the equilibrium line is just out of phase with this pattern (Van den Broeke et al. 1994). This matter will be discussed more thoroughly in a forthcoming paper.

references

- Duynkerke, P. G. and M. R. van den Broeke, 1994: Surface energy balance and katabatic flow over glacier and tundra during GIMEX-91, *Global and Planetary Change*.
- Mahrt, L., 1982: Momentum balance of gravity flow, *J. Atmos. Sci.* **39**, 2701-2711.
- Oerlemans, J. and Vugts, H. F., 1993: A meteorological experiment in the melting zone of the Greenland ice sheet, *Bull. Am. Meteorol. Soc.* **74** (3), 355-365.
- Van den Broeke, M. R., P. G. Duynkerke and J. Oerlemans, 1994: The observed katabatic flow at the edge of the Greenland ice sheet during GIMEX-91, *Global and Planetary Change*.

ATMOSPHERIC MOISTURE FLUX AND FLUX CONVERGENCE IN THE GREENLAND AREA

Pierluigi Calanca and Atsumu Ohmura
Department of Geography
Swiss Federal Institute of Technology
Zürich, Switzerland

In order to better understand the precipitation regime of Greenland, climatological fields of the atmospheric water vapour flux and flux convergence have been derived from the instantaneous spatial distribution of wind- and moisture fields provided by the European Center for Medium-Range Weather Forecasts (ECMWF). The ECMWF analyses are believed to represent one of the best description of the actual state of the atmosphere. In the form normally employed in climatological studies, but rearranged so as to yield an expression for the precipitation, the atmospheric moisture budget reads:

$$\bar{P} = \bar{E} + \left\{ -\nabla_h \cdot g^{-1} \int_{p_t}^{\bar{p}_s} \overline{v_h q} dp \right\}, \quad (1)$$

where P and E are the precipitation and evaporation at the Earth's surface, ∇_h the two-dimensional Nabla operator, g is the acceleration due to gravity, v_h is the horizontal wind vector, q the specific humidity, p_s the surface pressure and p_t the pressure at the top of the atmosphere. An overbar indicates a time average. In this form, the equation emphasizes the relation between the precipitation and the water vapour flux convergence (the term in the braces).

The annual mean, vertically-integrated moisture flux, averaged over the three years 1989 to 1991, is depicted in Fig. 1a. One of the most striking aspects is the orographic influence exerted by Greenland. The orographic forcing on the water vapour flux is stronger than that on the mass flux, since the moisture transport occurs prevalently in the lowest troposphere. The orographic forcing is evident along the western coast, where the westerly flow from the Canadian Arctic backs to become a southerly flow. But the orographic influence is also apparent at the southeastern coast, where the southeasterly moisture flux in the northern branch of the Icelandic Low is stopped abruptly as it hits on the coastal mountains.

The annual total convergence of the moisture flux field is shown in Fig. 2a. To eliminate the computational noise, the field was smoothed using an isotropic spatial filter (Calanca, 1993). For comparison, the annual total precipitation presented by Ohmura and Reeh (1991), for Greenland, and by Legates and Willmott (1990), for the surrounding areas,

is depicted in Fig. 3. Focussing the attention on Greenland, one can observe how the essential features of the precipitation distribution are also found in the distribution of the moisture flux convergence. In particular, one notes: the zone of low convergence in northeastern Greenland; the tendency for increased convergence along the central-western and northwestern coast; the strong zonal gradient in southern Greenland. Areally averaged, the moisture flux convergence amounts to 380 mm year^{-1} , which compares fairly well with the estimated annual precipitation of 340 mm year^{-1} (Ohmura and Reeh, 1991).

The breaking down of the total moisture flux $\overline{v_h q}$ into a component achieved by the mean circulation $\overline{v_h} \overline{q}$ and an eddy component $\overline{v_h' q'}$, that is:

$$\overline{v_h q} = \overline{v_h} \overline{q} + \overline{v_h' q'} , \quad (2)$$

where a prime denotes the deviation from the time average, reveals that the total flux is dominated by the contribution from the mean circulation (Figs. 1b and 1c). However, this latter is highly rotational (Salstein et al., 1980), and the moisture flux convergence contributions by the mean circulation and by the transient eddies are both of the same order of magnitude, although not similarly distributed (Figs. 2b and 2c). In particular, the Reynold's decomposition (2) stresses the different nature of the moisture flux convergence, and therefore of the precipitation, in western and eastern Greenland. Along the western coast of Greenland, precipitation is significantly enhanced owing to the interplay between the mean circulation and the orography (Fig. 2b). Along the eastern coast, the dominant term is the eddy contribution (Fig. 2c). This is not surprising, since cyclogenesis often occurs in this area (Whittacker and Horn, 1984). Along the eastern coast, in addition, orographic lifting of air masses associated with the transient disturbances and a simultaneous breaking effect for the onshore component of the eddy moisture flux (see Fig. 1c) must be taken into account. In northeastern Greenland the convergence of the eddy moisture flux more than compensate for the losses caused by the mean circulation. This compensation is determinant for the precipitation regime in this area.

References

- Calanca, P., 1993: *The atmospheric water vapour budget over Greenland*. Dissertation at the Swiss Federal Institute of Technology, Zürich, 119 pp.
- Legates, D.R. and C.J. Willmott, 1990: Mean seasonal and spatial variability in gauge-corrected, global precipitation. *Int. J. Climatology*, **10**, 111-127.
- Ohmura, A. and N. Reeh, 1991: New precipitation and accumulation maps for Greenland. *J. Glac.*, **37**, 140-148.

Salstein, D.A., R.D. Rosen and J.P. Peixoto, 1980: Hemispheric water vapor flux variability- Streamfunction and potential fields. In: Deepak, A., T.D. Wilkerson and L.H. Ruhnke (Eds.): *Atmospheric Water Vapor*. Academic Press, New York, 557-573.

Whittaker, L.M. and L.H. Horn, 1984: Northern Hemisphere extratropical cyclone activity for four mid-season months. *J. Climatology*, 4, 297-310.

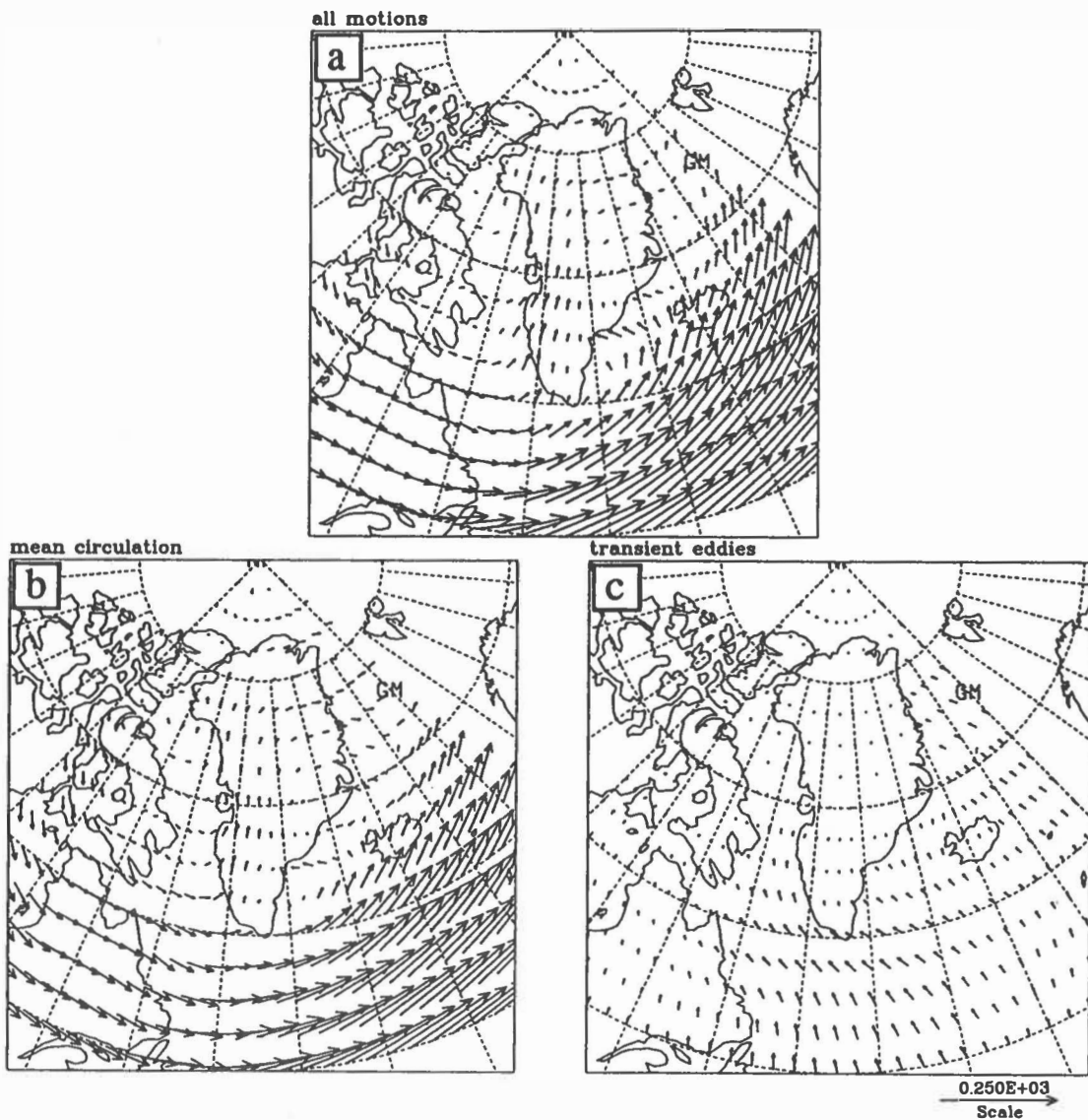


Fig. 1: Vertically-integrated, annual mean water vapour flux [$\text{kg m}^{-1} \text{s}^{-1}$]. The scale is shown in the lower right corner. The total flux is shown in the upper panel (a), the contribution achieved by the mean circulation in the lower left panel (b), and the transient eddy contribution in the lower right panel (c).

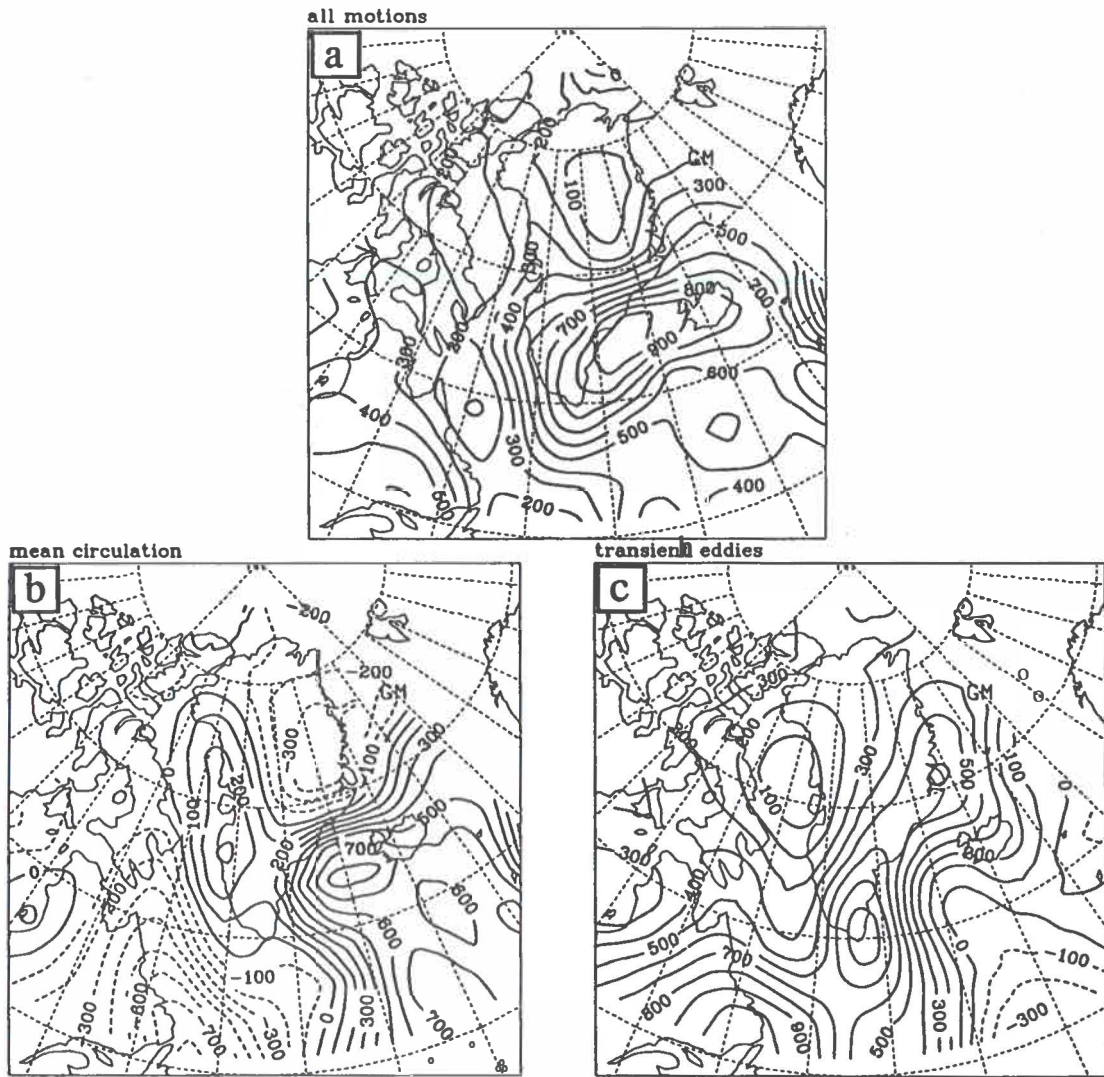


Fig. 2: Annual total water vapour flux convergence [mm year^{-1}]. The total field is shown in the upper panel (a), the contribution achieved by the mean circulation in the lower left panel (b), and the transient eddy contribution in the lower right panel (c).

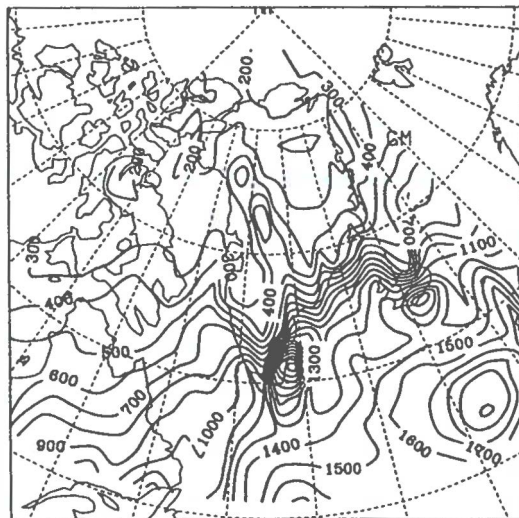


Fig. 3: Distribution of the annual total precipitation. Units are [mm year^{-1}]. Sources: Legates and Willmott (1990) and Ohmura and Reeh (1991).

LINEAR STABILITY OF KATABATIC FLOWS: EFFECT OF FROUDE NUMBER, SLOPE ANGLE AND SURFACE FRICTION

Peter G. Duynkerke

Institute for Marine and Atmospheric Research Utrecht
Utrecht University, The Netherlands

Several integral models have been proposed during the last decades (Mahrt, 1982; Lalaurette and André, 1985). The most general models are the ones proposed by Manins and Sawford (1979) and Lalaurette and André (1985) which include many important physical effects like surface radiative cooling, entrainment with overlying air, surface drag and stable stratification of the ambient flow. In these papers mostly stationary solutions of the equations are discussed. Implicitly it is assumed that these solutions are stable for small perturbations, i.e. no runaway occurs. In this study it will be analysed under which conditions the stationary solution becomes unstable.

For simplicity it will be supposed that the cold air has a definite depth (h) and that the potential temperature (θ) and velocity (u) of the cold air are independent of height. If there is no mixing across the inversion and cross-slope flow variations are neglected then the continuity equation takes the form:

$$\frac{\partial h}{\partial t} + \frac{\partial uh}{\partial x} = 0, \quad (1)$$

in which t is time and x is the horizontal distance measured downstream. If we neglect the Coriolis force and the horizontal background pressure gradient the equation of motion can be written as:

$$\frac{\partial uh}{\partial t} + \frac{\partial uuh}{\partial x} = g' h \alpha - g' h \frac{\partial h}{\partial x} - c_d |u| u, \quad \text{where } g' = g \frac{\theta'}{\theta_o} \quad (2)$$

α is the slope angle of the surface, c_d is the dimensionless drag coefficient, g is the acceleration due to gravity, θ_o is a reference potential temperature and θ' the potential temperature deficit of the cold air. The last term on the right-hand side of (2) represents the friction force, supposed proportional to the square of the velocity. The first two terms are the katabatic force dependent on the slope and the gradient force dependent on the gradient of h . The sum of these two terms vanishes when $\partial h/\partial x = \alpha$, that is when the inversion is horizontal.

In steady state conditions (1) reduces to $h u = Q$, where Q is a constant depending on the rate of supply of cold air down the slope. Under stationary conditions (2) can be written as:

$$\frac{\partial h}{\partial x} \left(h^3 - \frac{Q^2}{g'} \right) = \alpha \left(h^3 - \frac{c_d}{\alpha} \frac{Q^2}{g'} \right) \quad (3)$$

When the air has ceased to accelerate $\partial h/\partial x$ is zero and the depth of the flow, called the normal depth h_n is obtained by setting the right-hand side of (3) equal to zero:

$$h_n^3 = \frac{c_d}{\alpha} \frac{Q^2}{g'}. \quad (4)$$

The results from equation (3) can be expressed conveniently in terms of the Froude number, a dimensionless number defined as:

$$F_n = \frac{Q^2}{g' h^3}. \quad (5)$$

The Froude number for normal flow is α/c_d and thus depends only on the steepness and roughness of the slope and not on the temperature or rate supply of cold air.

If $\alpha \neq 0$ the general solution of (3) with α and c_d constant is:

$$x' = h' + (1 - F_n) \left[\frac{1}{6} \ln \left(\frac{(h' - 1)^2}{h'^2 + h' + 1} \right) - \frac{1}{\sqrt{3}} \arctan \left(\frac{2h' + 1}{\sqrt{3}} \right) \right] + c \quad (6)$$

in which $x' = x \alpha/h_n$, $h' = h/h_n$ and $F_n = Q^2/(g' h_n^3) = \alpha/c_d$. Equation (6) is slightly different from the one proposed by Ball (1956) and has been given correctly by Lalaurette and André (1985). From (6) it is clear that x' is only a function of h' and the Froude number for normal flow (F_n).

The question is now under which conditions the stationary solution (6) is stable for small perturbations. This will be investigated by performing a linear stability analysis of the complete equations (1) and (2) for the stationary solution (6). First we will substitute $u = u_0 + u''$ and $h = h_0 + h''$ into the equations (1) and (2), in which the stationary solution is denoted by u_0 and h_0 , respectively. After linearization we obtain the equations for u'' and h'' in which we substitute wave like solutions of the form $(u'', h'') = (U, H) \exp[i(\omega t - kx)]$, where ω is the frequency and k is the wave number. From this we obtain for the dispersion relationship for the dimensionless frequency: $\omega h_0/(c_d u_0) \equiv \Omega = \Omega(K, \alpha/c_d, F_0)$, in which $K = k h_0/c_d$ is the dimensionless wavenumber and $F_0 = u_0^2/(g' h_0)$ is the Froude number based on the stationary solution. From the dispersion relationship the following neutral stability curve can be obtained

$$\frac{\alpha}{c_d} = \frac{F_0 [2 + F_0 \pm \{2/\sqrt{F_0}\} (1 - F_0)^2]}{4 F_0 - 1}. \quad (7)$$

In Figure 1 we have drawn the solution for normal flow ($\alpha/c_d = F_0$) as a heavy line together with the neutral stability curves (7) as a function of F_{00} . From the dispersion relationship it

can now be determined that the flow is stable for the hatched area shown in Figure 1. For normal flow it is found that the flow is stable for $F_o < 4$, in agreement with the result mentioned by Ball (1956). From Figure 1 it is clear that the stability of the flow is very much dependent upon α/c_d . For $\alpha/c_d < 1$ only stable solutions exist for $F_o < 1$ whereas, for $\alpha/c_d > 1$ only stable solutions exist for $F_o > 1$. For $F_o > 1$ it can be shown that the stationary solution for large horizontal distances will asymptotically approach either the normal flow solution or create a horizontal inversion ($\partial h_o/\partial x = 0$). The solution in which the inversion becomes horizontal is for $\alpha/c_d > 1$ always unstable. For $\alpha/c_d > 4$ the normal flow becomes unstable too, so that no stable stationary solution exists over large horizontal distances.

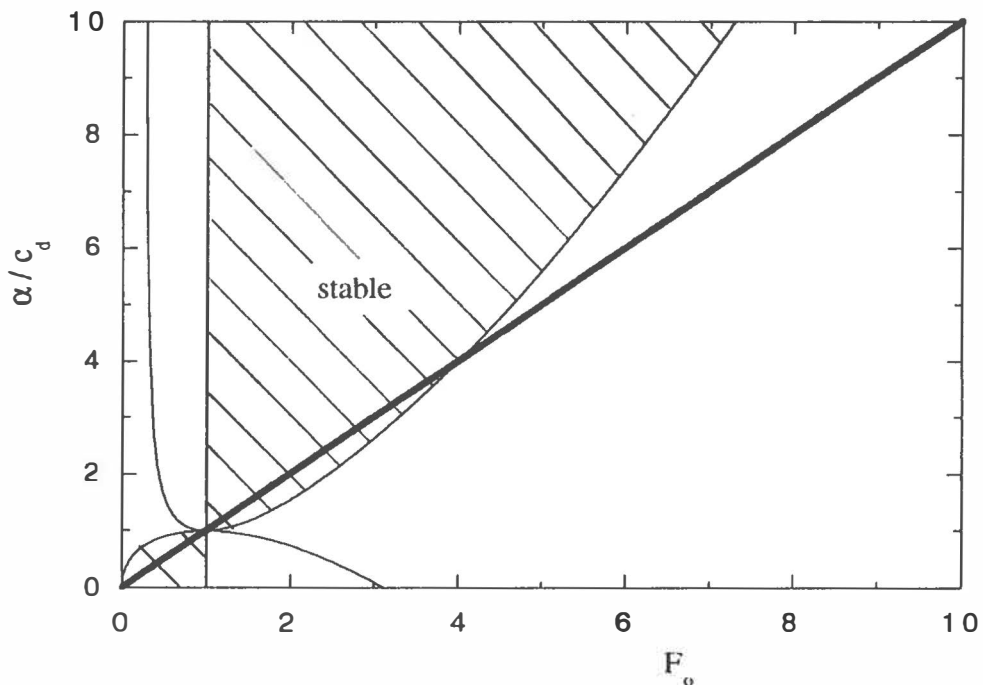


Figure 1 Stability diagram for downslope winds as a function of the Froude number (F_o) and the ratio of the slope angle and the drag coefficient (α/c_d). The hatched area corresponds to stable flows and the heavy line corresponds to normal flow.

REFERENCES

- Ball F. K., 1956: The theory of strong katabatic winds. *Australian J. Phys.*, **9**, 373-386.
 Lalaurette F. and J.-C. André, 1985: On the integral modelling of katabatic flows. *Boundary layer Meteorology*, **33**, 135-149.
 Mahrt, L., 1982: Momentum balance of gravity flows. *J. Atmos. Sci.*, **39**, 2701-2711.
 Manins, P.C., and B.L. Sawford, 1979: A model of katabatic winds. *J. Atmos. Sci.*, **36**, 619- 630.

COMPARISON BETWEEN MEASURED AND CALCULATED TURBULENT FLUXES

Jann Forrer and Mathias Rotach
 Department of Geography
 Swiss Federal Institute of Technology
 Zürich, Switzerland

EDDY CORRELATION METHOD

The measurements of the fluxes were performed with three eddy correlation systems. They include a sonic anemometer (Gill 3-dimensional research probe) for the measurement of u , v , w and temperature (sound velocity) with a sampling rate of 21 s^{-1} and a Ly- α hygrometer for the measurement of specific humidity fluctuations (q') with a sampling rate of 10 s^{-1} . The distance between these two sensors was 0.5 m. An advantage of the eddy correlation method is, that it directly yields the fluxes at the height or location the original time series was measured. But the fast-response sensors are very expensive and data intensive. On the other hand slow-response sensors are less expensive and often used to measure the mean profiles. The fluxes in the surface layer are then inferred from the profile method.

PROFILE METHOD

The friction velocity u_* is calculated from:

$$\phi_m(z/L) = \frac{\partial \bar{u}}{\partial z} \frac{kz}{u_*}$$

where $\partial \bar{u} / \partial z$ is the gradient of mean wind speed, $k=0.4$ the von Karman constant and z/L the non-dimensional stability. For the function ϕ_m the expression of Businger et al. (1971) modified by Högström (1988), $\phi_h = 1 + 6z/L$ ($z/L \geq 0$), was used.

Similarly θ_* and q_* are calculated from:

$$\phi_h(z/L) = \frac{\partial \bar{\theta}}{\partial z} \frac{kz}{\theta_*} \quad \text{and} \quad \phi_h(z/L) = \frac{\partial \bar{q}}{\partial z} \frac{kz}{q_*} ,$$

where the same function $\phi_h = 0.95 + 7.8z/L$ (Högström, 1988) was used due to lack of better knowledge. The stability measure z/L is obtained iteratively from the relation:

$$Ri = \frac{z/L \phi_h(z/L)}{\phi_m^2(z/L)}$$

where Ri is the gradient Richardson Number. We use 8 levels (0.5, 1, 2, 5, 10, 15, 22, 30 m a. g.) to calculate the gradients of wind speed, u , and potential temperature, θ , and the lower 5 levels to calculate the gradients of specific humidity, q with the help of the following interpolations:

$$\begin{aligned} x(z) &= a_1 + a_2 z + a_3 z^2 + a_4 \ln(z) & x &= u, T \\ y(z) &= b_1 + b_2 z & y &= q \end{aligned}$$

Finally the fluxes are determined from:

$$H = -\rho c_p u_* \theta_* \quad \text{sensible heat flux}$$

$$LE = -\rho L_v u_* q_* \quad \text{latent heat flux}$$

Where ρ is the density of air, L_v is the latent heat of vaporisation of water and c_p the specific heat at constant pressure for moist air.

RESULTS

A first comparison of calculated to measured fluxes exhibited an underestimation of the uncorrected eddy correlation method especially for the latent heat flux. Moore (1986) proposed a correction procedure for an eddy correlation system that mainly corrects for:

- sensor response (21 s⁻¹ for the Sonic, 10 s⁻¹ for the Ly- α)
- sensor line averaging
- sensor separation (0.5 m between sonic and Ly- α)

Under “normal” circumstances the correction (or flux loss) is between 5 and 10%. But the conditions on the Greenland ice sheet, with a high wind speed regime and the requirement to measure at relatively low levels above ground in order to apply surface layer scaling, can lead to substantially larger flux losses. Fig.1 shows a result of the correction procedure. The correction for the sensible heat flux, which was measured with one single instrument is typically less than 10% for $z/L = 0.1$. On the other hand, the correction for the latent heat flux is much larger. At the 2m level it accounts for about 40% if $z/L=0.1$ and for as much as 65% if $z/L=1$ (not shown). The main reason for that is the sensor separation between sonic and Ly- α . For a detailed description of the correction procedure see Moore (1986). A preliminary conclusion at this point is, that under conditions prevailing over the Greenland ice sheet it is often crucial to correct the fluxes measured with an eddy correlation system.

In the following the comparisons between measured and calculated u_* , sensible and latent heat flux at 2 m a. g. l. are presented. The eddy correlation measurements were checked for stationarity and statistical uncertainty, and if necessary excluded from the analysis. Fig. 2 shows that the calculated u_* (u_{*prof}) slightly overestimates the measured friction velocity (u_{*eddy}). This can also be seen from comparing of the present data of the non-dimensional wind profile, (ϕ_m) to the formulation given by Högström(1988). A linear regression (requiring that $\phi_m(0)=1$) yields $\phi_m=1+7.6z/L$ rather than the expression given by Högström (Fig. 3). However, Fig. 3 shows that this kind of result is very sensitive to some few runs of high stability. Spectral analysis of the few very stable runs indicates that gravity wave activity might have to be taken into account for the interpretation of the ϕ -functions.

Figs. 4 and 5 show the same as Fig. 2 for the sensible and latent heat flux. The data scatter around the 1:1 line for the sensible heat flux with an rms difference of 13 Wm⁻². There is an overestimation of the calculated latent heat fluxes, similar to that found for u_* . Apart from the relatively large correction necessary for LE_{eddy} , the comparison of latent heat fluxes appeared to be strongly influenced by the type of interpolation scheme used for q . In the relatively dry environment on the ice sheet, the accuracy of the humidity sensors (see Ohmura et al., 1992) is not good enough to allow for a higher order interpolation. However, using a linear interpolation in z (see above) makes it necessary to restrict

the number of included levels to the lowest five (in the present case), i.e., a height range of the lowest 10m, since often a kink in the profile of specific humidity between 10 and 15 m is observed.

Further analysis will have to focus on the following issues:

- How sensitive are the calculated turbulent fluxes on the interpolation scheme for the mean profiles.
- To what extent and under which conditions can the ϕ -functions be used in the case of continuously stable conditions, such as those over the Greenland ice sheet.

REFERENCES

- Businger, J.A., Wyngaard, J. C., Izumi, J., and Bradley, E. F., 1971: Flux-Profile relationships in the atmospheric surface layer. *J. Atm. Sci.*, 28, 181-189.
- Högstöm U., 1988: Non-dimensional wind and temperature profiles in the atmospheric surface layer: A re-evaluation. *Boundary-Layer-Meteor.* 42, 55-78.
- Moore C. J., 1986: Frequency response corrections for eddy correlation systems. *Boundary-Layer-Meteor.* 37, 17-35.
- Ohmura, A. et al., 1992: *Energy and mass balance during the melt season at the equilibrium line Altitude, Paakitsoq, Greenland Ice Sheet*. ETH Greenland Expedition Progress Report No.2, Department of Geography ETH-Zürich, 94 pp.

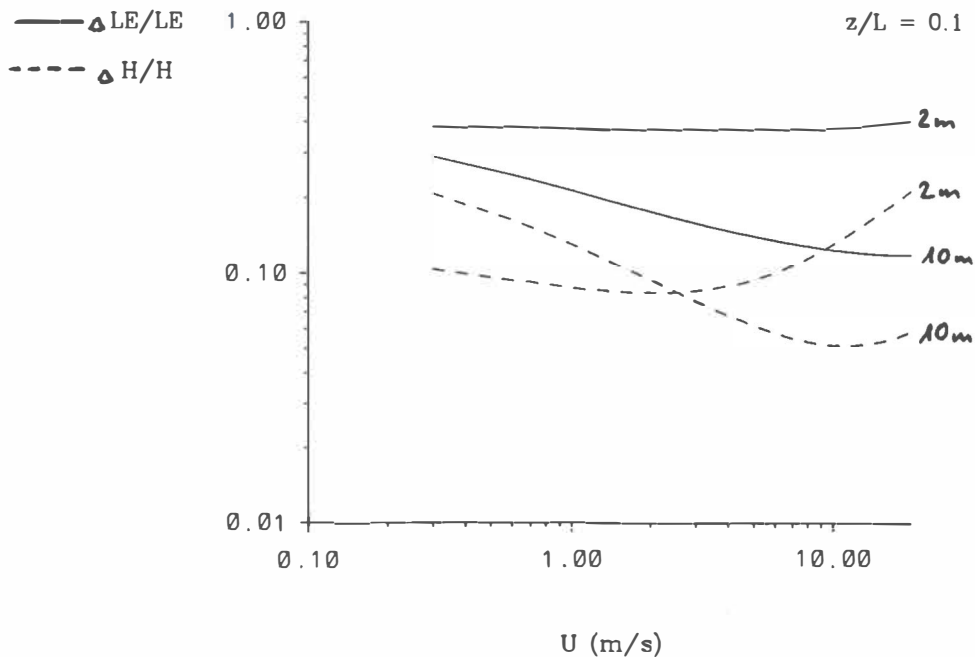


Fig. 1: Estimated percentage flux loss expected when measuring sensible heat flux (H), and latent heat flux (LE) for $z/L = 0.1$ at different heights.

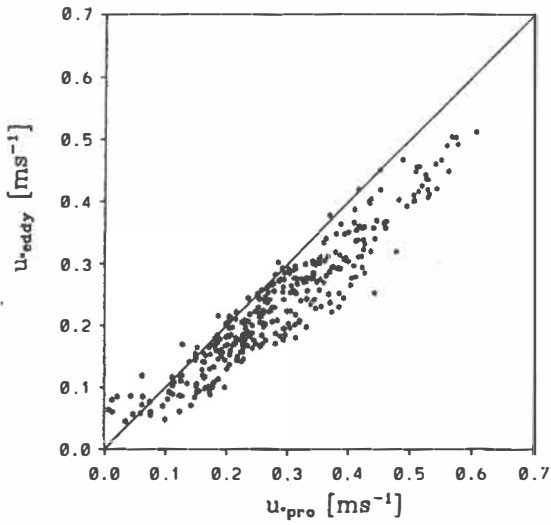


Fig.2: Comparison between calculated (u_{pro}) and measured (u_{eddy}) friction velocity.

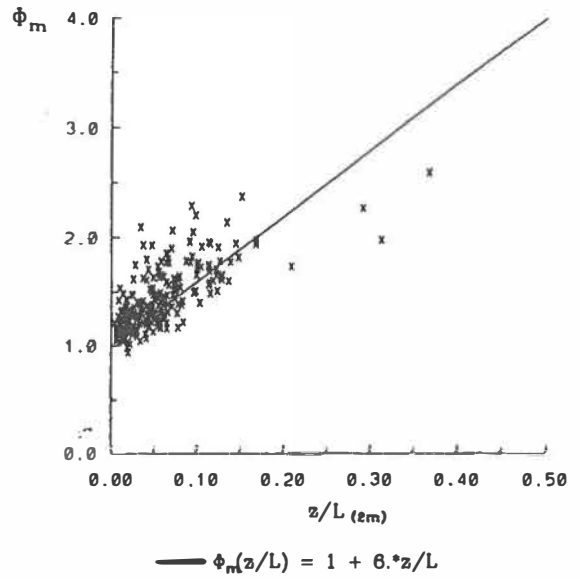


Fig. 3: ϕ_m against z/L for stable stratification. The solid line is ϕ_m given by Högström (1988).

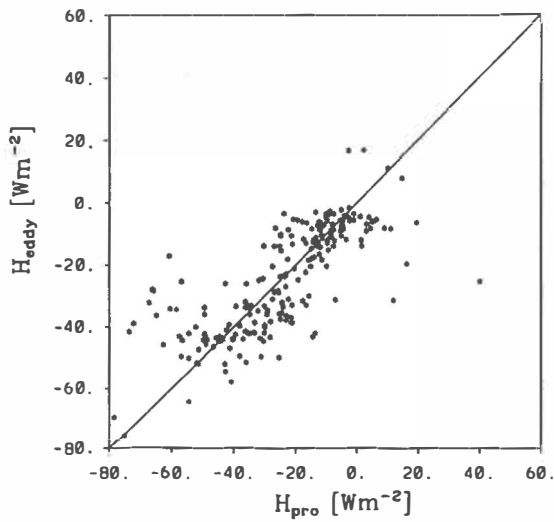


Fig. 4: As Fig.2, but for the sensible heat flux H .

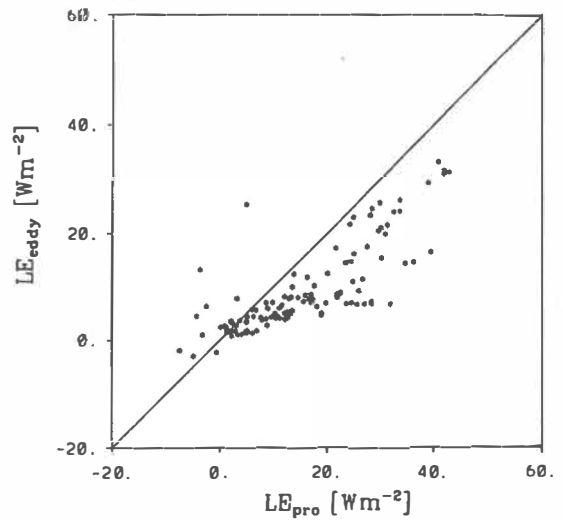


Fig. 5: As Fig. 2, but for the latent heat flux LE .

SIMULATION OF ATMOSPHERIC CIRCULATION DURING THE GIMEX 91 EXPERIMENT USING A MESO- γ PRIMITIVE EQUATIONS MODEL

Hubert Gallée, Olivier Fontaine de Ghélin and Guy Schayes
Institut d'Astronomie et de Géophysique G. Lemaître
Louvain-la-neuve, Belgium

Introduction

In this paper, one presents the first results obtained from a meso- γ scale atmospheric model used to simulate atmospheric circulations during the Greenland Ice Margin EXperiment [GIMEX, *Oerlemans and Vugts* 1993] which was carried out to improve our knowledge of the Greenland ice-sheet margin mass balance, in relation to meteorological conditions. The simulation shown here is 2-dimensional, and cover the period from 12 to 13 July 1991. Simulated wind, temperature, humidity and turbulent fluxes are compared with available observations.

The Model

The atmospheric model (referred hereafter as MAR¹) is that of *Gallée and Schayes* [1993]. It is a meso- γ scale primitive-equations model in which the vertical coordinate is the normalized pressure $\sigma = \frac{p}{p_s}$ (p and p_s being the pressure and the surface pressure respectively). The full continuity equation is taken into account. The model is extensively described in *Gallée and Schayes* [1993] and is used here with the following modifications: (i) except in the surface layer, the vertical subgrid scale fluxes are treated using the E- ϵ model of turbulence [*Duynkerke*, 1988], allowing to represent the turbulent mixing length as a function of the local flow characteristics. This is important because of the complex structure of the katabatic layer [*Pettré and André*, 1991; *Gallée and Schayes*, 1992]; (ii) to represent the vertical subgrid scale fluxes in the surface layer, the formulation of *Duynkerke and van den Broeke* [1994] is used; (iii) the lateral boundary conditions are modified to take into account large scale motions, and involve "relaxing" the model-predicted variables toward the large-scale analysis [*Anthes et al.*, 1989]; (iv) the *Deardorff* [1978] soil model has been adapted to the GIMEX situation. Soil parameters are taken from *Meesters et al.* [1994].

Initial Data

The GIMEX data were obtained along the western coast of Greenland at a latitude of 67°N along a line approximatively perpendicular to the general coastline. The most useful data come from a series of masts and a captive balloon site as given by *Oerlemans and Vugts* [1993].

¹MAR: Modèle Atmosphérique Régional

The data from the two days of July 12 and 13 are particularly interesting because of the calm and stationary large-scale weather, with few clouds. The present simulation is done with the model domain perpendicular to the coast. The grid size is 20 km and there are 17 non uniformly distributed vertical levels (i.e. 15365, 12224, 9386, 6862, 4717, 3028, 1819, 1032, 561, 295, 153, 78, 39, 20, 10, 5 and 2.50 m).

The model is initialized with the sounding (air temperature and humidity) of Egedesminde on 13 July 1991 at 00UT. The geostrophic forcing is not taken into account, as in *Meesters et al.* [1994]. Sea surface temperature is fixed at the freezing point (271.2 K). Over the tundra and the ice sheet, the mean soil temperature used in the *Deardorff* [1978] soil model are 289.2 K and 273.2 K respectively. The initial soil surface temperature is that of the sounding, except over the ice sheet when it exceeds 273.2 K. In this case it is reset to 273.2 K and the resulting meltwater flux is computed. The surface albedo is prescribed. It amounts to 0.2 over the tundra and is taken from the GIMEX data over the ice-sheet. The roughness length is chosen to be 0.0001 m, 0.01 m and 0.003 m over the sea, the tundra and the ice sheet respectively.

Simulation

The simulation shown here is done with the 2-dimensional model version. The simulation is started at 00UT on 12 July and is conducted over 48 hours. It is found that in the ice-sheet interior, katabatic flow is well simulated, with maximum wind speeds during night. The height of the wind maximum is between the fifth and sixth σ levels (i.e. between 40 m and 80 m above the surface). This is in agreement with the observations. During daytime, the wind speed maximum is localized near the ice-sheet margin. This could be explained by the fact that during daytime, an important temperature gradient is generated between the warm tundra and the cold ice sheet. The temperature gradient is then responsible for an ice-breeze effect [e.g. *van den Broeke et al.*, 1994].

On the Figure, the circulation characteristics observed at mast 9 (located on the ice-sheet, 88 km from the ice-sheet margin) are compared with the simulation for the 13 July 1991. The agreement is good for temperature, specific humidity and wind. Over the ice sheet, the observed wind direction is SE. This behaviour is also found in the simulation. Nevertheless, the simulated turbulent heat fluxes are underestimated when compared to those reconstructed from the observations using the profile method. As already mentioned by *Meesters* [1994], strong horizontal advection of heat, as it occurs at mast 9, can make the assumed flux-profile relations invalid. A consequence could be an overestimation of the observed turbulent heat fluxes. On the other hand, the simulation could be in error. For example, the geostrophic forcing, which is not included in the simulation input, could play a significant role in the katabatic flow behaviour, by increasing both entrainment at the top of the boundary layer and turbulent exchange with the surface. In conclusion, a direct consequence of the geostrophic forcing could be a larger heat amount supplied to the surface, but this hypothesis has yet to be verified.

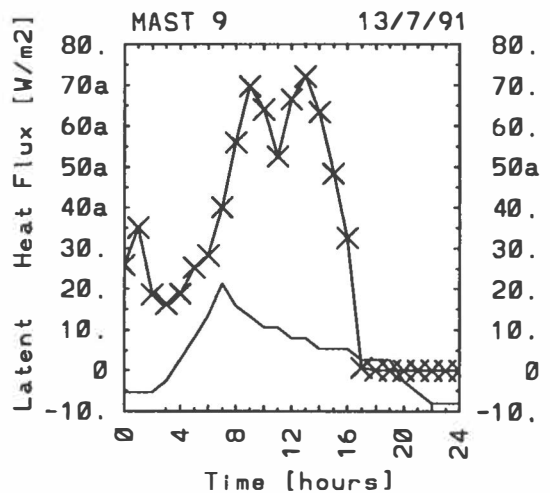
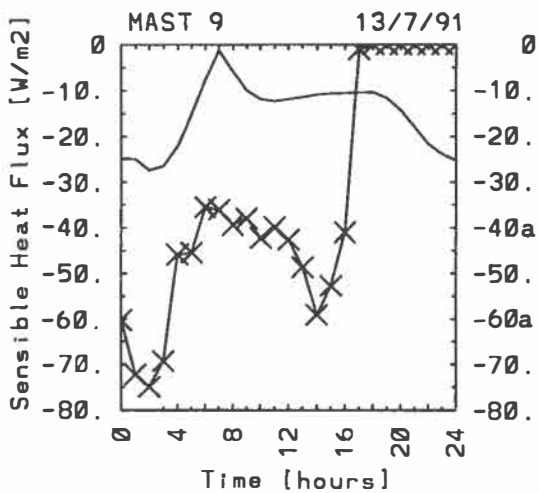
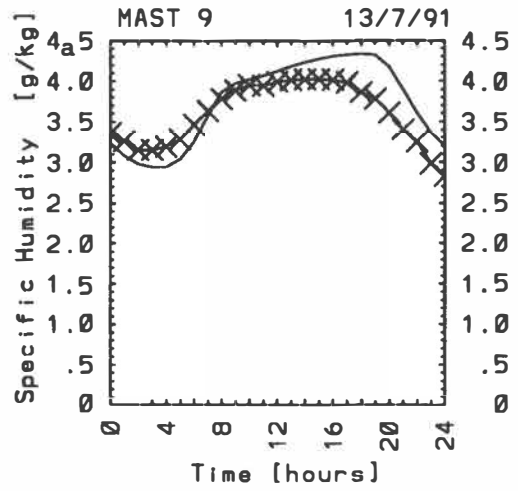
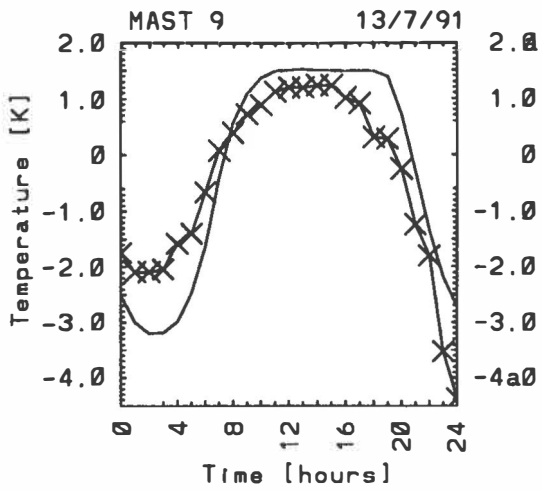
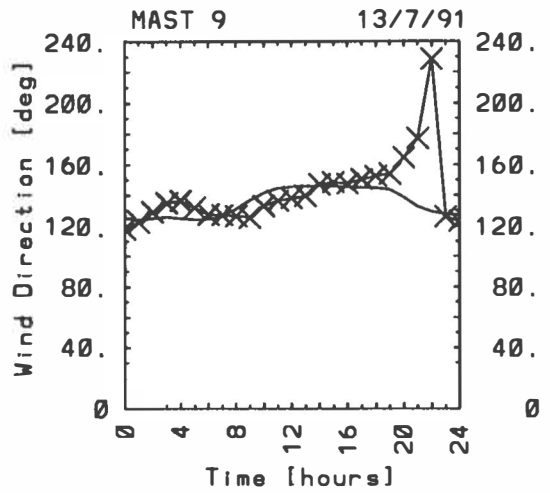
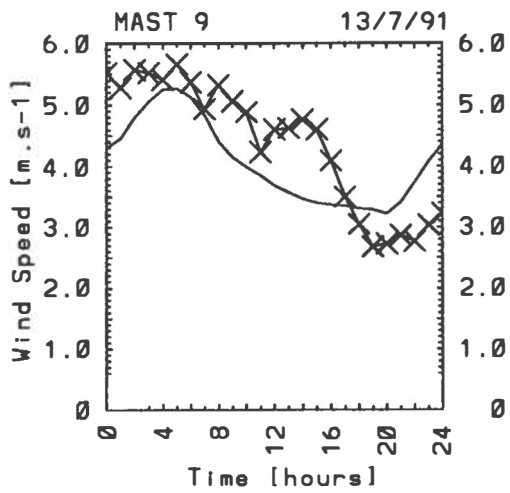
Acknowledgments

This research is sponsored by the Climate Programme of the Commission of the European Communities, under Grants EV5V-CT92-0132. H.Gallée is supported by the Belgian Scientific Research Program on the Antarctic of the Prime Minister's Science Policy Office. The authors wish to thank Prf. J. Oerlemans and Dr. M. van den Broeke for providing them the GIMEX data and for thoughtful discussions.

References

- Anthes, R.A., Kuo, Y-H, Hsie, E-Y, Low-Nam, S, and Bettge, T.W., 1989: Estimation of skill and uncertainty in regional numerical models. *Quart. J. Roy. Meteor. Soc.*, **115**, 763–806.
- Deardorff J.W., 1978: Efficient Prediction of Ground Surface Temperature and Moisture with Inclusion of a Layer of Vegetation. *J. Geophys. Res.*, **83**, 1889–1903.
- Duynkerke, P.G., 1988: Application of the E – ϵ turbulence closure model to the neutral and stable atmospheric boundary layer. *J. Atmos. Sci.*, **45**, 865–880.
- Duynkerke, P.G., and van den Broeke, M.R., 1993: Surface energy balance and katabatic flow over glacier and tundra during GIMEX-91. *Global and Planetary Change* (in press).
- Gallée, H., and Schayes, G., 1992: Dynamical aspects of katabatic winds evolution in the Antarctic Coastal Zone. *Bound.-Layer Meteor.*, **59**, 141–161.
- Gallée, H., and Schayes, G., 1993: Development of a Three-Dimensional Meso- γ Primitive Equations Model, Katabatic Winds Simulation in the area of Terra Nova Bay, Antarctica. *Mon. Wea. Rev.*, in press.
- Meesters, A.G.C.A., 1994: Dependence of the energy balance of the Greenland Ice Sheet on Climate Change: Influence of Katabatic Wind and Tundra. *Quart. J. Roy. Meteor. Soc.* (in press).
- Meesters, A.G.C.A., Henneken, E.A.C., Bink, N.J., Vugts, H.F., and Cannemeijer, F., 1994: Simulation of the atmospheric circulation near the Greenland ice sheet margin. *Global and Planetary Change* (in press).
- Oerlemans, J., and Vugts, H.F., 1993: A meteorological experiment in the melting zone of the Greenland Ice Sheet. *Bull. Amer. Meteor. Soc.*, **74**, 355–365.
- Pettré, P., and André, J.-Cl., 1991: Surface-pressure change through Loewe's phenomena and katabatic flow jumps: study of two cases in Adélie Land, Antarctica. *J. Atmos. Sci.*, **48**, 557–571.
- van den Broeke, M.R., Duynkerke, P.G., and Oerlemans, J., 1994: The observed katabatic flow at the edge of the Greenland ice sheet during GIMEX-91. *Global and Planetary Change* (in press).

Figure Caption : Comparaison between observation and simulation for mast 9 (located on the ice-sheet, 88 km from the ice-sheet margin): (1) top left panele wind speed 6 m above the surface (in m s^{-1}), (2) top right panele: wind direction (in degrees), (3) middle left panele: temperature 2 m above the surface (in K), (4) middle right panel : air specific humidity 2 m above the surface (in g kg^{-1}), (5) bottom left panel : sensible heat flux (in W m^{-2}) — positive upward), (6) bottom right panel : latent heat flux (in W m^{-2}) — positive upward). The observations are represented by the crosses.



RESOLUTION SENSITIVITY OF GREENLAND SURFACE MASS BALANCE IN A GCM

Christophe Genthon

Laboratoire de Glaciologie et Géophysique de
l'Environnement/CNRS
Saint Martin d'Hères Cedex, France

Resolution is an essential and frustrating limitation to the performances of General Circulation Models (GCMs) of the atmosphere. If GCMs have kept improving with time, it is to a fair extent thanks to the steadily increasing power of computers which has allowed ever finer grids (or larger wave numbers for spectral models) to be used. Fine resolution is particularly important for regional climate studies, and even more in topography affected regions. That is the case for Greenland.

A recently completed series of 10 year AMIP experiments carried out by MétéoFrance with the Arpège spectral GCM (FCCM 1991) with T21 (approximately 5.6° horizontal grid), T42 (about 2.8°) and T79 (about 1.5°) truncations allows to study the sensitivity of the simulated climate to resolution. The precipitation minus evaporation (henceforth called accumulation, even though run off of melt water is not included) output (see figures) over the Greenland ice sheet is presented and analyzed here.

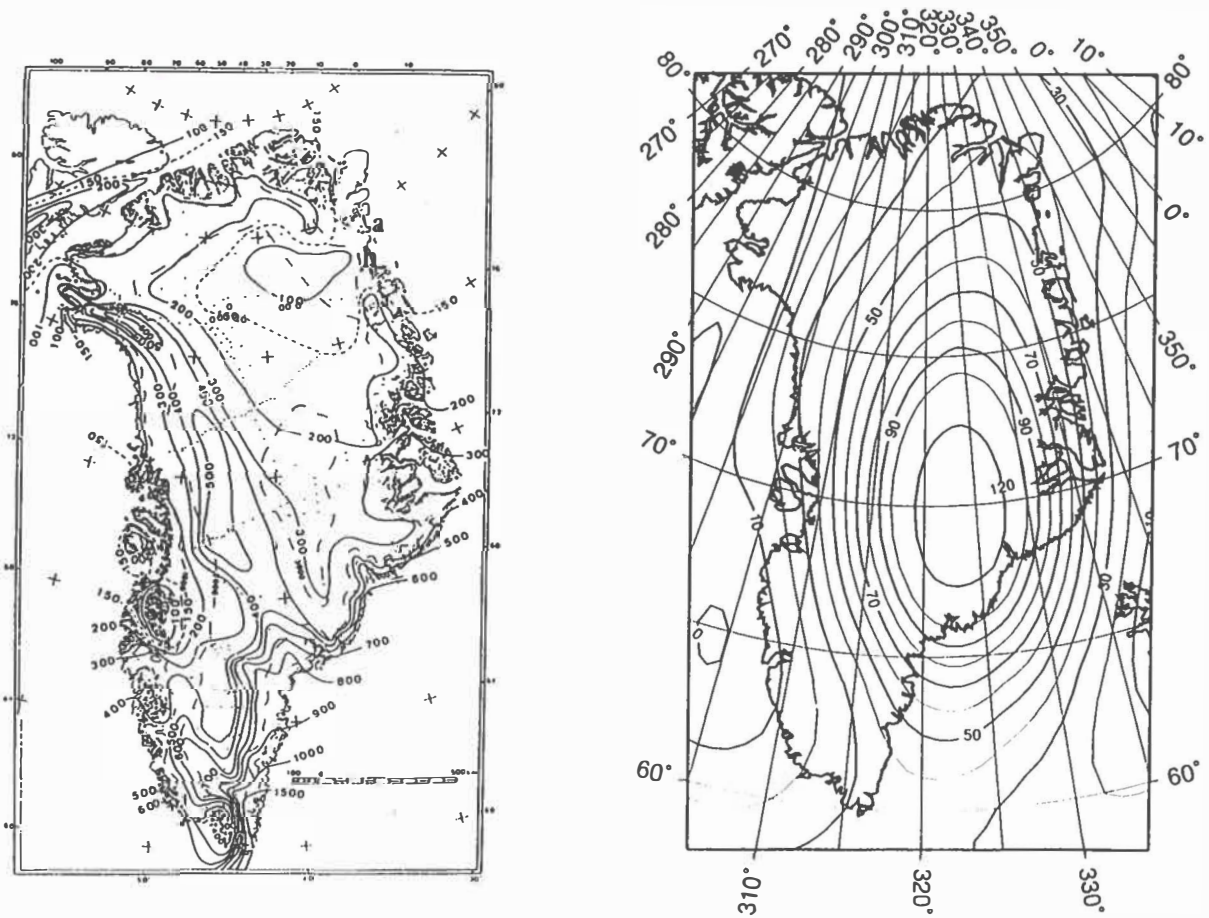
Clearly, even the largest scale features of the observed distribution of accumulation (e.g. Ohmura and Reeh 1991, see figures) are not adequately reproduced at the lowest resolution (T21). Halving the grid size (T42) brings a tremendous improvement. A region of maximum surface mass balance shows up on the east side of the southern tip, and the tongue of high accumulation along the west flank of the northern ice sheet is also broadly simulated. However, many small scale features are not captured by the model, and the area of lowest accumulation near 80°N comes out too far south.

Going to T79 brings significant additional improvement. Much of the small scale spatial structure is now outlined. There are still differences with the observation, one of the most obvious being that the region of lowest accumulation extends too far south, but the overall picture is very reasonable. At this time, the cost of running the T79 model, in terms of supercomputer resource, makes it barely manageable for climate studies. However, it is not unlikely that model quality can further improve by increasing resolution only. Embedding windows of very fine grid within standard resolution (i.e. about T42) GCMs might be a way to make regional climate modelling affordable in the nearest future. We are currently experimenting with a new "stretchable" grid GCM being developed by the Laboratoire de Météorologie Dynamique (LMD, CNRS, Paris).

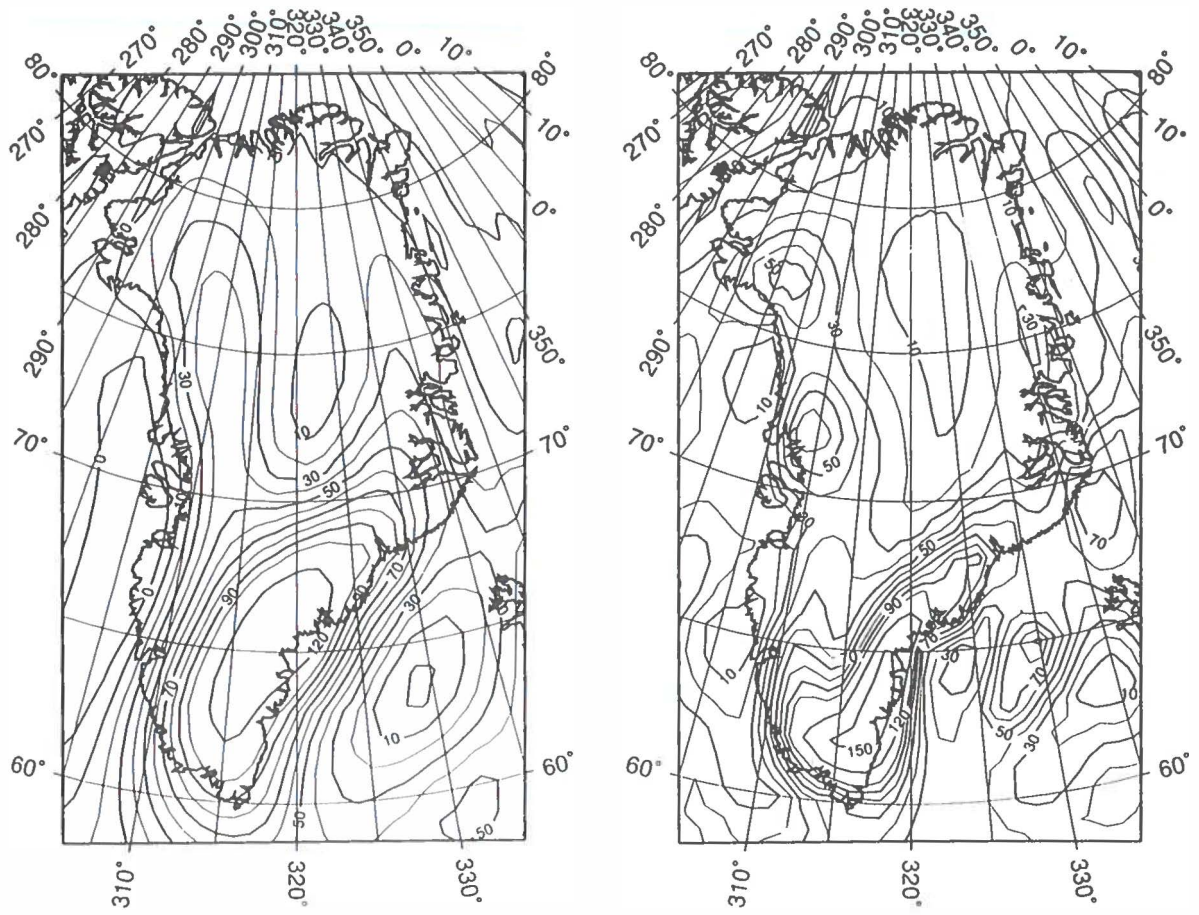
References:

- (The) French Community Climate Model, specifications. By Météo France, Les Universités and CNRS. Available from Daniel Cariolle, Météorologie Nationale, CNRM, Toulouse, France, 44 p, 1991.
- Ohmura A. and Reeh N. 1991 New precipitation and accumulation maps for Greenland. *J. Glaciol.* **37**, 140-148.

Figures:



The annual accumulation over Greenland, observed (left, in mm.yr^{-1} , by Ohmura and Reeh 1991), and simulated by the Arpège T21 GCM (right, in cm.yr^{-1}).



The annual accumulation over Greenland, simulated by the Arpège T42 (left) and T79 (right) GCM (in cm.yr⁻¹).

EGIG LINE SIMULATIONS WITH A 2-D POLYTHERMAL ICE SHEET MODEL

Ralf Greve
 Institut für Mechanik III
 Technische Hochschule Darmstadt, FRG

In natural ice sheets and glaciers two different ice phases may occur. *Cold ice* has a temperature below the pressure melting point, it can be described as an incompressible, viscous and heat-conducting one-component fluid. The temperature of *temperate ice*, however, is exactly on the pressure melting point; thus, temperate ice may contain some water. It shall therefore be described as an incompressible, viscous two-component fluid (binary mixture) [4]. Ice sheets and glaciers containing both cold and temperate regions are called *polythermal*.

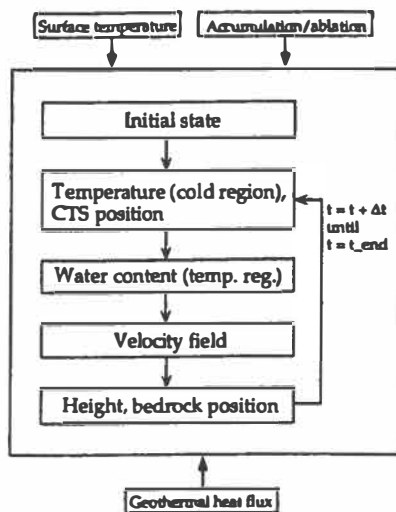


Figure 1: Iteration procedure of the 2-d polythermal ice sheet model.

The current large-scale ice sheet models deal with that problem by calculating the temperature field from the cold ice energy balance and artificially resetting temperatures above the pressure melting point on the pressure melting point. However, this is quite unsatisfactory because of two main reasons: First, it is ignored that the CTS ("cold-temperate transition surface", boundary surface between cold and temperate ice) is a phase boundary where jump conditions for the various physical quantities must hold [3]; second, the water content in the temperate region (that has a big influence on ice fluidity) is not obtained.

Here a two-dimensional time-dependent model is used that takes into account the physics of the CTS and the temperate regions [2, 5]. The iteration procedure can be seen in fig. 1, the model is driven by the climatic input quantities surface temperature and surface mass balance as well as the geothermal heat flux at the lithosphere base. Adjustment of the CTS position is conducted simultaneously with calculation of the temperature field in the cold region by vertical shifting of

the CTS until the energy jump balance at the CTS (that relates the temperature gradient on the cold side to the water content on the temperate side) is satisfied.

Two different model runs for the EGIG line carried out with this model shall be presented here. The first is a 200 ka steady state run under present conditions with no initial ice sheet; the final geometry, velocity field, homogeneous temperature field and height of the basal temperate layer are shown in fig. 2. It can be seen that this temperate layer is very thin; its maximum thickness near the western margin of the EGIG line is about 3 m, so that a very high basal resolution is necessary to find this layer.

The second run (fig. 3) is a transient one, it is driven by an "ice age sine" of the surface temperature with a period of 100 ka and a variation of the surface temperature between present conditions and 10°C below present conditions, whereas for the surface mass balance present conditions are used [1]. The steady state modelled in the first run serves as initial condition. This model experiment is conducted twice, first using the polythermal model (solid lines in fig. 3), second using a cold ice model with temperature reset as described above (dashed lines). The time series show that for the maximum surface elevation, the total transect area and the length of the temperate base (basal ice at pressure melting point) along the EGIG line the difference between the two outputs is very small, whereas for the area of temperate ice it is extremely big. The cold ice model overpredicts this area by far as compared with the polythermal model. In the ice age periods the polythermal model provides no temperate layer with non-zero thickness at all, whereas in the cold ice model there always remains a temperate layer. Since the temperate layers are very thin in both cases, the influence on the overall geometry of the EGIG line is however very small.

References:

- [1]: Abe-Ouchi, A. 1993: *Ice Sheet Response to Climatic Changes: A Modelling Approach*. Dissertation, ETH Zürich.
- [2]: Greve, R. 1993: *Thermomechanisches Verhalten polythermer Eisschilde*. Pending dissertation, TH Darmstadt.
- [3]: Hutter, K. 1983: *Theoretical glaciology, material science of ice and the mechanics of glaciers and ice sheets*. D. Reidel Publishing Company, Dordrecht, Holland.
- [4]: Hutter, K. 1993: *Thermo-mechanically coupled ice-sheet response – cold, polythermal, temperate*. J. Glac., Vol. 39, No. 131, pp. 65-86.
- [5]: Svendsen, B., Greve, R. & Hutter, K. 1993: *Classical mixture model for polythermal ice*. Submitted paper.

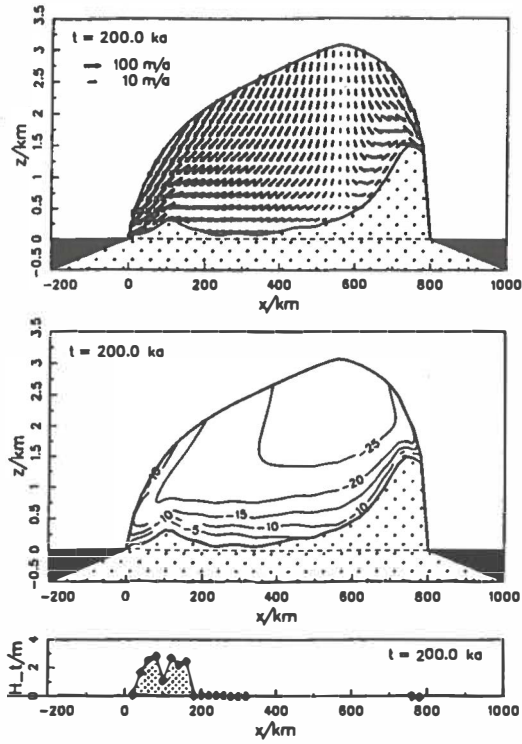


Figure 2: EGIG steady state under present conditions: Geometry, velocity field, homogeneous temperature field and height of the basal temperate layer.

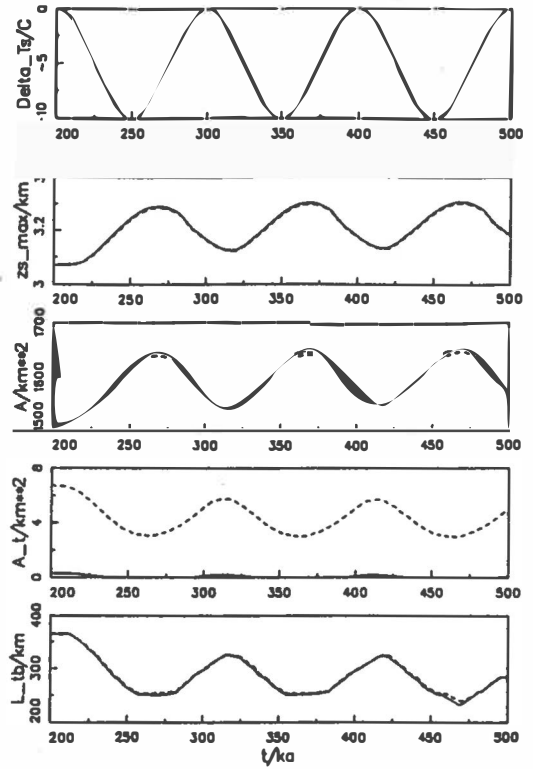


Figure 3: Transient run over three ice age cycles, idealized by the surface temperature shown in the upper plot (difference to present values). Time series for the maximum surface elevation, total transect area, area of temperate regions and length of temperate base (lower plots). Solid: polythermal model. Dashed: cold ice model.

NET RADIATION DERIVED FROM AVHRR FOR THE GREENLAND ICE SHEET- PRELIMINARY RESULTS

Marcel Haefliger
Department of Geography
Swiss Federal Institute of Technology
Zürich, Switzerland

NOAAaAVHRR

Eight clear sky scenes from NOAA 11 Advanced Very High Resolution Radiometer (AVHRR) were used to calculate the Net Radiation for the ETH Camp site on the Greenland Ice Sheet. Of the five channels on board NOAA 11 four were used for the method presented here. Channels 1 and 2 (0.57 - 0.69 μm , 0.71 - 0.98 μm , respectively) for the shortwave balance and channels 4 and 5 (10.31 - 11.30 μm , 11.49 - 12.50 μm , respectively) for the longwave balance.

Net Radiation

The Radiation Balance is:

$$NR = \underbrace{(Q + q)}_{S^*} (1 - \alpha) + \underbrace{(L^\downarrow - L^\uparrow)}_{L^*} \quad (1)$$

where NR is the net radiation, S^* the shortwave and L^* the longwave balance in Wm^{-2} . Q is the direct solar and q the diffuse sky radiation which adds up to the global radiation G . α is the surface albedo. L^\downarrow and L^\uparrow are the longwave incoming and outgoing radiation, respectively.

All the satellite sensors can measure are the radiances in their bandwidth. The general approach to estimate the net radiation and its terms, respectively, is to relate surface observations with regression models. Since there are not always enough observations available, satellite radiances can be modeled with radiative transfer models. In Haefliger et al. (1993) this approach is described in more detail.

Longwave Balance

The method of retrieving L^* is based on the surface temperature T_{ice} and the water vapor column amount WV .

Ice Surface Temperature:

$$T_{ice} = a + bT_4 + cT_5 + d((T_4 - T_5) \sec(\Theta)) \quad (2)$$

Water vapor amount along the viewing path:

$$WV(\Theta) = a + b(T_4 - T_5) + cT_5 + d \sec(\Theta) \quad (3)$$

From the above equation follows the water vapor column amount:

$$WV_e = WV(\Theta) \cos(\Theta) \quad (4)$$

T_4 and T_5 are the satellite-measured brightness temperatures in Kelvin. Θ is the viewing angle of the sensor.

L^\downarrow is a regression of T_{ice} and WV :

$$L^\downarrow = a + bT_{ice} + cWV \quad (5)$$

L^\uparrow follows from the Stefan-Boltzman equation:

$$L^\uparrow = \epsilon \sigma T_{ice}^4 \quad (6)$$

Applying the coefficients to the ETH Camp site gives following results:

Date	T_{ice} (K)		L^\downarrow (Wm^{-2})		L^\uparrow (Wm^{-2})		L^* (Wm^{-2})	
	meas.	calc.	meas.	calc.	meas.	calc.	meas.	calc.
6-21-90	271.0	271.6	231	237	306	308	-75	-71
6-23-90	271.3	271.0	236	234	307	306	-71	-72
6-24-90	271.5	271.1	239	236	308	306	-69	-70
6-27-90	271.3	270.8	231	233	307	305	-76	-72
6-28-90	270.8	271.1	231	236	305	306	-74	-70
6-29-90	270.2	270.7	221	234	302	305	-81	-71
7-1-90	271.9	271.3	243	237	310	307	-67	-70
7-2-90	271.0	271.5	232	237	306	308	-74	-71

Shortwave Balance

Albedo α is the most important term in the shortwave balance. Here an existing method to calculate α is used (Koepke, 1989):

$$\alpha_t = a + b\alpha_s \quad (7)$$

The coefficient a represents the relative amount of radiation scattered back to space by molecules and aerosol particles and the coefficient b describes the flux-transmittance of the clear-sky atmosphere. α_t is the top of atmosphere albedo, α_s the surface albedo, respectively. Koepke calculated a set of coefficients for different solar zenith angles, aerosol optical depth, ozone amount and water vapor.

In a first approach the direct solar radiation is calculated very simple with the Beer equation:

$$Q = I_0 \tau^{\sec(\Theta)} \quad (8)$$

The value for τ is set at 0.82 (Konzelmann, in press).

For the calculation of the diffuse solar radiation a linear regression was used in the form:

$$q = a + bQ \quad (9)$$

Following table shows the results of the coefficients applied to the ETH Camp site:

Date	α (%)		Q (Wm^{-2})		q (Wm^{-2})		G (Wm^{-2})		S^* (Wm^{-2})	
	meas.	calc.	meas.	calc.	meas.	calc.	meas.	calc.	meas.	calc.
6-21-90	72	74	649	655	86	101	735	755	209	200
6-23-90	71	73	642	637	85	99	727	735	211	199
6-24-90	71	72	686	686	88	104	774	790	223	220
6-27-90	70	71	681	673	87	103	768	776	229	225
6-28-90	71	72	660	667	89	102	749	769	218	218
6-29-90	70	71	676	660	87	101	763	761	228	210
7-1-90	71	69	674	684	89	104	763	788	225	242
7-2-90	71	72	633	623	82	97	715	720	209	200

Net Radiation at ETH Camp

This table shows the results of the calculation of the net radiation compared to the measured values:

Date	S^* (Wm^{-2})		L^* (Wm^{-2})		NR (Wm^{-2})	
	meas.	calc.	meas.	calc.	meas.	calc.
6-21-90	209	200	-75	-71	134	129
6-23-90	211	199	-71	-72	140	127
6-24-90	223	220	-69	-70	154	150
6-27-90	229	225	-76	-72	153	153
6-28-90	218	218	-74	-70	144	148
6-29-90	228	210	-81	-71	147	139
7-1-90	225	242	-67	-70	158	172
7-2-90	209	200	-74	-71	135	129

What remains to be done?

As in the title stated, the results presented here are preliminary results. It is a first attempt to calculate the entire radiation balance and its terms, respectively. Improvements can be done, especially for the calculation of the shortwave balance. The results, however, are very encouraging.

So far only clear-sky cases are calculated. Daily or monthly means are to be calculated and the dependence of latitude and altitude has to be investigated in order to apply corrections.

Summary and Conclusion

The net radiation for the ETH Camp site was calculated for clear sky cases and compared to field measurements. The results agree within $-13/+14 \text{ W m}^{-2}$. The method of calculating the shortwave radiative fluxes can be improved in order to get better results.

Reference

Haefliger, M., K. Steffen and C. Fowler, 1993: AVHRR surface temperature and narrow-band albedo comparison with ground measurements for the Greenland ice sheet, *Annals of Glaciology*, 17, 49-54.

Koepke, P., 1989: Removal of Atmospheric Effects from AVHRR Albedos, *J. Appl. Meteor.*, 28(12), 1341-1348.

Konzelmann, T., in press: Radiation conditions on the Greenland Ice Sheet, *Zürcher Geographische Schriften*, Heft 56, Geographisches Institut ETH Zürich, 124 pp.

DEEP RADIO ECHO SOUNDINGS IN THE VICINITY OF GRIP AND GISP2 DRILL SITES, GREENLAND

Ludwig **Hempel**
Institut für Geophysik
Westfälische Wilhelms-Universität Münster, FRG

During the EGIG expeditions from 1989 to 1992 radio echo soundings were performed along the reconstructed EGIG line and on the connection to the ice core drill sites GRIP and GISP2. The data presented was derived in the direct vicinity of the GRIP and GISP2 ice core drill sites in central Greenland.

To make these radio echo soundings as a complete data set comparable to data from ice cores it is essential to perform a conversion of the data from reflection times to real depths below surface. For this the velocity depth function of radio waves in ice has to be known very precisely. It depends mainly on the density of ice in the upper 100...200 m. These velocities were determined by high resolution Common Mid Point measurements at certain points along the profil. A Garotta-Michon velocity-analysis which stacks the tracks of the measurement along calculated reflection hyperbols with different velocities results in the desired velocity depth function. Some major reflections were picked from the dataset to calculate continuous velocity-depth-functions with polynomial fits. After the conversion these reflections which are mainly caused by acid layers in the ice can be compared to depth of layers from certain volcanic eruptions within the GRIP ice core. They are used to calibrate the velocity depth function as a whole continuous function. The continuous resampling of the data with this velocity depth function delivered the "true depth section" which can directly be compared to ice core data like the ECM record from the GRIP ice core (pers. comm. UNIVERSITY OF COPENHAGEN 1993). This comparison shows very high correlations with events found in the ECM record which are mainly due to the acid layers from volcanoes (HAMMER 1982). Because the layers in the ice core are dated precisely (JOHNSEN et. al. 1992) the reflections can be dated as well representing isochrones within the ice sheet (HEMPEL et. al., 1993).

Deep radio echo soundings show bedrock topography and internal layerings between the drill sites GISP2 and GRIP. Zones without any reflections can be found in 1900...2100 m depth which corresponds to the time interval of 20000-30000 B.P. in the last part of the Wisconsin ice age (SCHØTT et.al., 1992). The internal layerings reappear below 2100 m depth in the time interval of 30000-50000 B.P.. In general these layerings follow the bedrock topography with reduced amplitude of undulation on most of the track. However

in the area app. 5 km west of GRIP these layerings rise despite a valley at bedrock especially in the lower Wisconsin part with a slight shift of the peak position towards GRIP in the upper Holocene part. Assuming that there are no lateral bedrock structures which could have influenced the measurements this would mean that there was only snow accumulation and densification but nearly no ice flow in any particular direction to the sides in this area during the Wisconsin ice age. This might indicate that at least during the last glaciation the icedivide at the summit of the Greenland ice cap was shifted only about 5 km to the west of GRIP which is located at the present top of the ice sheet (HEMPEL & THYSSEN, 1993).

The cross-section from "Summit 74" in the south to GRIP in the north shows a mountainous area with rough bedrock relief and peak to trough amplitudes of up to 250 m. This is followed by a smooth bedrock plain with an ice thickness of about 3325 m in the south of GRIP. The GRIP drill site itself appears to be above a relatively flat rock base which means that it is located on undisturbed ice layers.

- HAMMER, C.U. 1980. Acidity of polar ice cores in relation to absolute dating, past volcanism and radio-echos. *Journal of Glaciology*, **25**(93), 359-372.
- HEMPEL, L and F. THYSSEN. 1993. Deep Radio Echo Soundings in the Vicinity of GRIP and GISP2 Drill Sites, Greenland. *Polarforschung*, **62**(1), in press.
- HEMPEL, L., F. THYSSEN and M. JONAS. 1993. Accumulation during the last 2000 years along the EGIG line and to GRIP drill site derived from radio-echo soundings.- *In*: REEH, N. and H. OERTER (ed.): *Mass balance and related topics of the Greenland ice sheet, Open File Series Grønlands Geologiske Undersøgelse*, **93**(5), 77-79.
- JOHNSEN, S. J., H. B. CLAUSEN, W. DANSGAARD, K. FUHRER, N. GUNDESTRUP, C. U. HAMMER, P. IVERSEN, J. JOUZEL, B. STAUFFER and J. P. STEFFENSEN. 1992. Irregular glacial interstadials recorded in a new Greenland ice core. *Nature*, **359**(6393), 311-313.
- SCHØTT, C., E.D. WADDINGTON and C.F. RAYMOND. 1992. Predicted time-scales for GISP2 and GRIP boreholes at Summit, Greenland. *Journal of Glaciology*, **38**(128), 162-168.

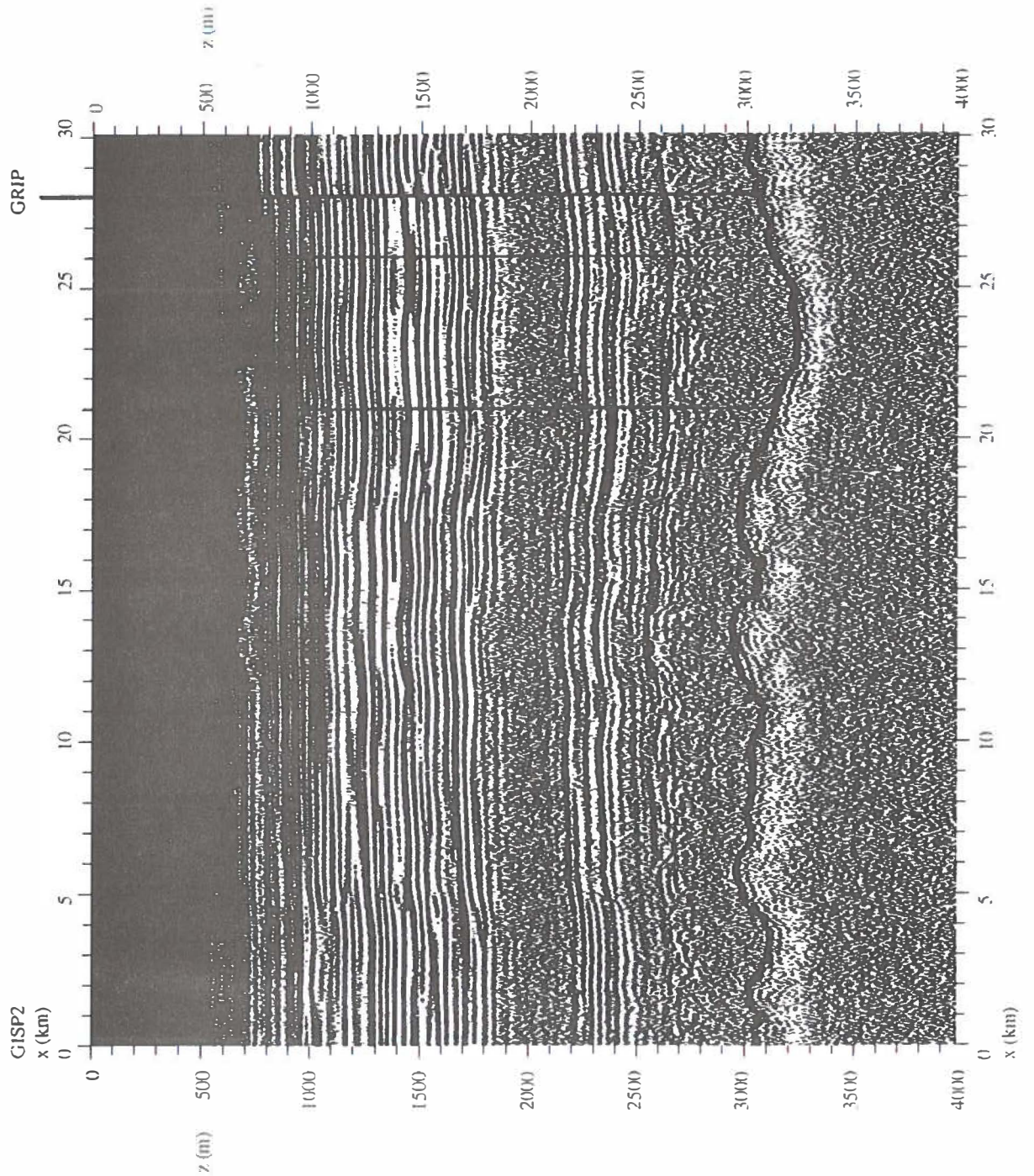


Fig. 1: Radio echo sounding between the ice core drill sites GRIP and GISP2. The reflection from the bedrock is represented by the bold line in app. 3 km depth. The marked area indicates a former ice divide 5 km west of the present summit of Greenland at GRIP.

ON THE USE OF THE PROFILE METHOD ON THE GREENLAND ICE SHEET

Edwin A.C. Henneken
Faculty of Earth Sciences
Free University, Amsterdam, The Netherlands

For the study of the behaviour of the planetary boundary layer (PBL) in general and the one over the Greenland Ice Sheet in particular, it is important to have reliable estimates for parameters like the Obukhov length, L , the friction velocity, u_* , the roughness length, z_0 , and the turbulent heat fluxes, Q_h and Q_q .

Through an eddy correlation system (sonic anemometer, Lyman- α humidity fluctuation sensor and a fast thermocouple) one is able to get such reliable estimates. If such a system is not available, an indirect way of estimating the necessary parameters is needed. The Profile Method is such a formalism; it assumes a relation between the gradient of profile quantities (like the mean horizontal wind speed, U , and the potential temperature, Θ) and the associated turbulent flux:

$$\overline{w'c'} \propto \frac{\partial}{\partial z} C(z)$$

where c' is either the fluctuating component of the temperature (θ') or the specific humidity (q'). An additional assumption is the fact that the dimensionless gradient of $C(z)$ is some universal function, ϕ_c , of stability:

$$\kappa \frac{z}{c_*} \frac{\partial}{\partial z} C = \phi_c\left(\frac{z}{L}\right)$$

where κ is the Von Kármán constant and c_* a turbulent scale for the quantity c' (see e.g. Arya, 1988).

This method has proven its value under various conditions, amongst others the nocturnal boundary layer over land surfaces; nevertheless, it is far from trivial that the stable PBL over an ice sheet should exhibit behaviour similar to that of the nocturnal boundary layer. To be specific: can ϕ -relations usually assumed for stable conditions also be used for the observations obtained on the Greenland ice sheet? Or, more fundamentally, is the Profile Method as such applicable under conditions found at the Greenland ice sheet?

Some light is shedded onto the matter by looking at the determination of the roughness length, z_o . For the dimensionless wind shear and temperature gradient we have

$$\begin{aligned}\kappa \frac{z}{u_*} \frac{\partial}{\partial z} U &= \phi_m\left(\frac{z}{L}\right) \\ \kappa \frac{z}{\theta_*} \frac{\partial}{\partial z} \Theta &= \phi_h\left(\frac{z}{L}\right)\end{aligned}$$

where the ϕ -relations have been taken from Beljaars and Holtslag (1991). Integrated from z_o to z these relations yield

$$\begin{aligned}\kappa \frac{U}{u_*} &= \ln\left(\frac{z}{z_o}\right) - \Psi_m\left(\frac{z}{L}\right) \\ \kappa \frac{\Theta - \Theta_o}{\theta_*} &= \ln\left(\frac{z}{z_o}\right) - \Psi_h\left(\frac{z}{L}\right)\end{aligned}$$

which allows us to calculate the various parameters (like z_o) for observed profiles. With the assumed ϕ -functions we get the picture in figure 1 (left panel); using 4 heights (8, 4, 2 and 1 meters) the roughness length is seen to be of the order 10^{-3} m. How sensitive is this result to choice of heights? This is shown in figure 1 (right panel). By choosing different set of heights z_o can differ by an order of magnitude.

The quantity $\kappa \frac{U}{u_*}$ can be determined from the sonic measurements together with the stability parameter $\frac{z}{L}$; figure 2 (left panel) shows the relation between both. Usually it is assumed that Ψ_m depends linearly on $\frac{z}{L}$, especially in the case of strong stable stratification. Figure 2 (left panel) is in agreement with this. A Least Squares fit of a straight line results in a z_o of about 10^{-3} m and a slope of 18.0, which differs from the one usually found (of about 5). This number 18.0 emerges again if we look at a plot of the gradient Richardson number (determined from profile measurements), Ri , versus $\frac{z}{L}$ (from eddy correlation measurements). The result is shown in figure 2 (right panel); the solid line denotes the usually assumed relation $\frac{z}{L}/(1 + 5\frac{z}{L})$, the dotted line has a coefficient 18.0 instead of 5.

General conclusions are not possible at this stage, but it is not *a priori* clear that the Profile Method can be applied in conditions found on the Greenland ice sheet. It is certain however that conditions occur under which this method cannot be applied. Under conditions when the method might be applied it may be so that ϕ -relations apply which differ from the ones normally used. It is important to investigate the role of advection, flux and radiation divergence on the ice sheet, because these quantities play a crucial role.

References

Arya, S.P.S. (1988). Introduction to Micrometeorology. Academic Press Inc., San Diego etc.

Beljaars, A.C.M. and Holtslag, A.A.M. (1991). Flux Parametrization over Land Surfaces for Atmospheric Models. J. Appl. Meteorol. 30, 327-341

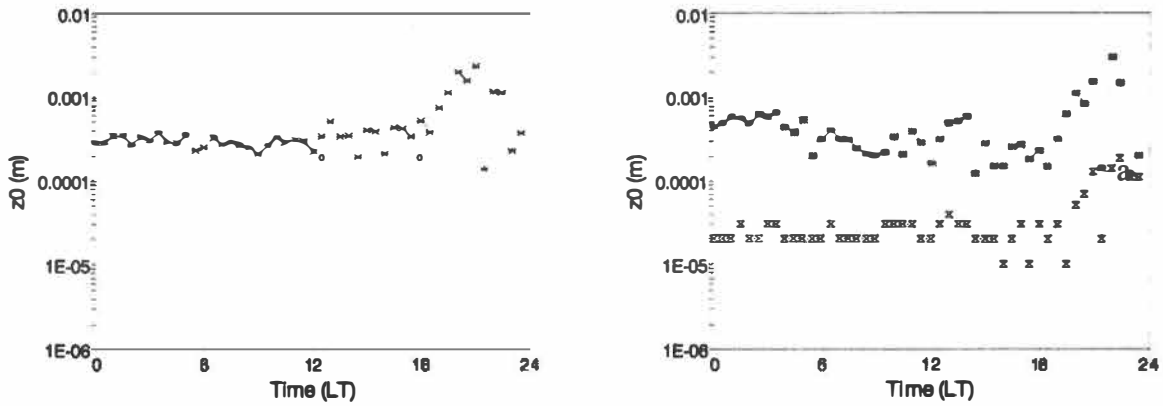


Figure 1. Left panel: roughness length as determined with the Profile Method using 4 heights (8, 4, 2 and 1 m) and the ϕ -relations specified by Beljaars and Holtslag (1991). Right panel: result of different sets of heights

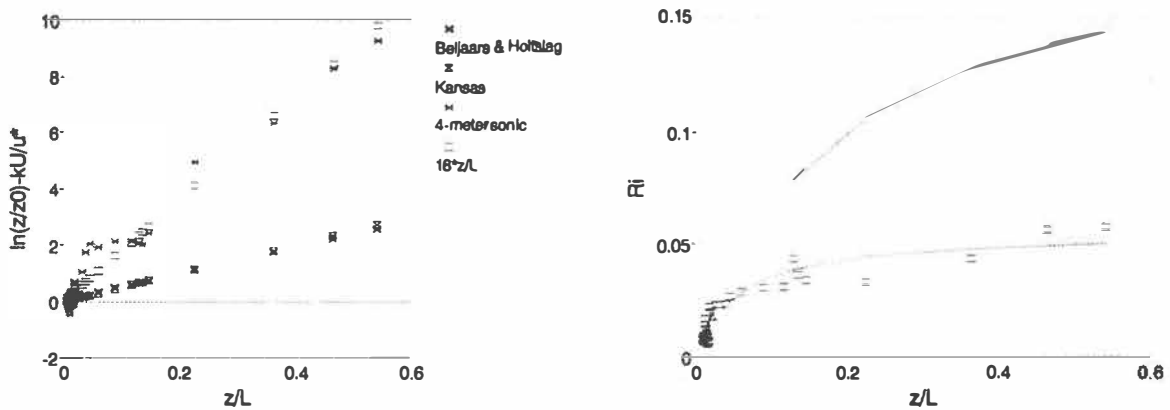


Figure 2. Left panel: roughness length as determined using the sonic observations (at 4 meters height). Right panel: gradient Richardson number, Ri , as function of stability

A MODEL STUDY OF THE GREENLAND ICE SHEET IN AN EAST-WEST TRANSECT

Hester Jiskoot¹ & Hans Oerlemans²

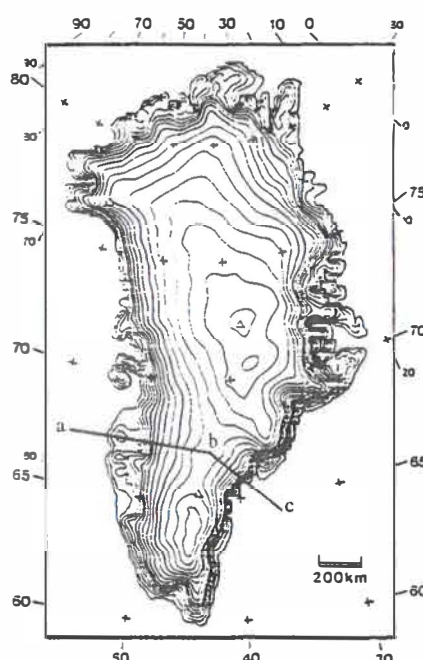
¹ Fysisch Geografisch en Bodemkundig Laboratorium
University of Amsterdam, The Netherlands

² Institute for Marine and Atmospheric Research Utrecht
Utrecht University, The Netherlands

Model

To support the interpretation of glacio-meteorological field work in west Greenland (GIMEX), a combined ice-flow mass balance model has been constructed for an east-west transect of unit width, across the Greenland ice sheet near 67°N (figure 1, after Letréguilly, 1991).

FIGURE 1



a: 67°46' N and -58°40' W

b: 66°55' N and -43°10' W

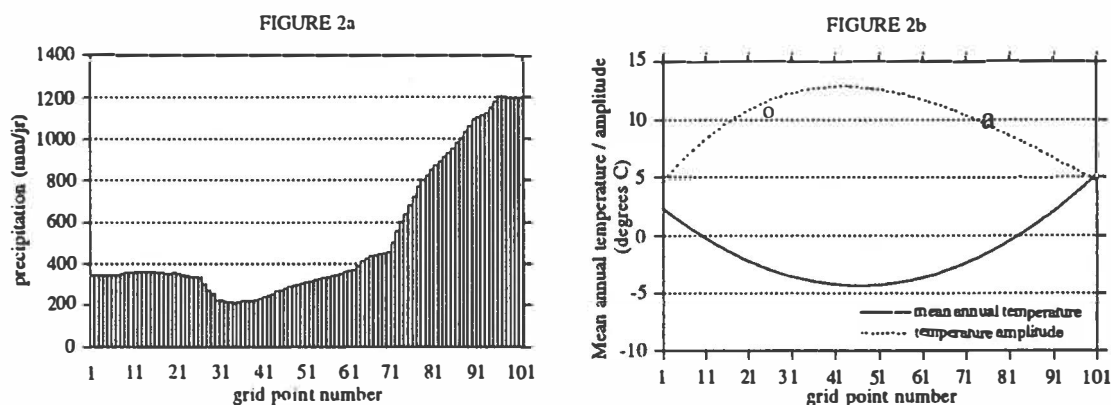
c: 64°68' N and -36°57' W

The ice flow model is of the vertically-integrated type. Both deformation and basal sliding contribute to the ice transport. Sliding is allowed when ablation takes place at the surface. Thermodynamics were not included. Ice cannot extend into the ocean due to forced calving. The bed adjusts isostatically with a 7000 yr e-folding time scale. The present bed and ice topography were taken from Letréguilly (1991) and Bindshadler (1989). Grid point spacing is 10 km.

The mass balance model is based on a calculation of the energy balance at the surface (Oerlemans, 1991). The balance is obtained by integrating

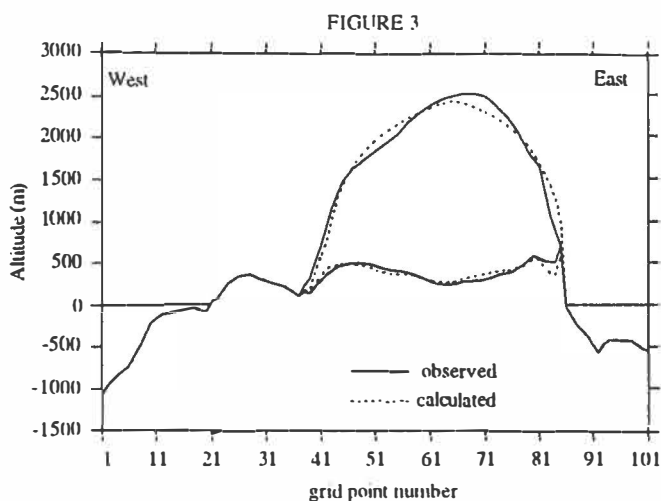
$$M = \int_{\text{year}} \left\{ (1-f) \min(0; -\Psi/L) + P \right\} dt$$

Here M is specific balance, f fraction of meltwater that refreezes, Ψ the energy balance, L latent heat of melt, P solid precipitation and t time.



Figures 2a and 2b show climate data along the transect. The ice is situated between grid points 38 and 84. Annual mean temperature and amplitude were obtained by fitting curves between data from meteorological stations on Greenland (Ohmura, 1987). Precipitation was taken from Letréguilly (1991). Insolation was calculated.

Reference case



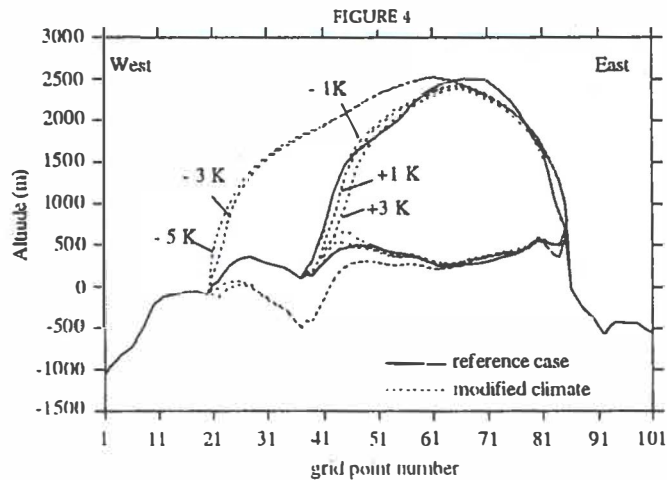
The simulated ice-sheet profile for present conditions is shown in *figure 3*. Tuning has been done by adjusting the flow parameters. Criteria used for selecting the reference case were ice topography and mean ice thickness. The reference case differs within 2 percent for ice volume, mean ice thickness and mean surface altitude from the present situation. Marked differences were found at the ice divide and the eastern ice margin. This ice margin is too steep because in the model basal sliding never takes place in the east.

Climate sensitivity

Some results of a large number of climate sensitivity experiments are explained here. *Figure 4* shows steady states for five different changes in annual mean temperature. Precipitation has been assumed to vary with 5% per degree.

For a temperature decrease of 3 K the steady-state ice volume has increased by 65 %, which is about the largest extent of the ice sheet. When temperature rises, the ice sheet retreats in eastward direction. For a 4 K temperature increase the ice sheet melts away in about 16000 years. For a 5 K increase in about 5200 years.

The difference in stability between the eastern and western margins is due to the large contrast in precipitation (see *fig. 2*), local topography, and the fact that, in the experiments, basal sliding only takes place at the western ice margin. At any change in climate the ice margins become steeper with respect to the reference case.



A further diagnosis of the model output is provided by the mass balance profiles. It should be noted that feedback mechanisms between ice surface altitude, temperature and precipitation changes and the distribution pattern of climate data control the mass balance profiles. Because specific balance is related to altitude and position along the transect, east and west Greenland have different specific mass balance curves. The western curve is in general lower than the eastern due to the large differences in precipitation. Low altitudes are more sensitive to little changes in temperature. In general the largest changes in specific balance occur at altitudes below 1200 m asl in west Greenland. As a result, the western equilibrium line altitude shifts between 800 and 1150 m asl for temperature decrease and increase of 1 K. Both profiles are effected at high altitudes with large decreases in temperature due to the effect of decreasing precipitation by more than 15 percent.

The major weak points of this study are:

- * *The choice of bed topography is very critical to the stability of the western margin.*
- * *The effect of lateral in- or outflow of ice is neglected by the assumption of a flow band of constant width.*
- * *The dependence of basal sliding velocity on ablation has no solid basis.*

Nevertheless, this study has shown that coupling of an ice-flow mass-balance model is a useful tool in studying the response of the Greenland ice sheet to imposed climate change.

References

- Bindschadler R A et al. (1989): Surface topography of the Greenland ice sheet from satellite radar altimetry. NASA SP-503.
- Oerlemans J (1991): The mass balance of the Greenland ice sheet: sensitivity to climate change as revealed by energy-balance modelling. *The Holocene* 1, 40-49.
- Letréguilly A, P Huybrechts and N Reeh (1991): Steady- state characteristics of the Greenland ice sheet under different climates. *Journal of Glaciology* 37(125), 149-157.
- Ohmura A (1987): New temperature distribution maps for Greenland. *Z.Gletscherk. Glacialgeol.* 23, 1-45.

FIRST FIELD REPORT FROM THE AWI NORTH GREENLAND TRAVERSE 1993

Friedrich Jung-Rothenhäusler, Sepp Kipfstuhl
& Thorstein Thorsteinsson
Alfred-Wegener-Institut für Polar- und Meeresforschung
Bremerhaven, FRG

This paper gives an overview of the research activities in North Greenland undertaken by the Alfred Wegener Institute in collaboration with University of Heidelberg, which were supported by the GRIP operation. The equipment used became available after the successful completion of the EGIG surveying traverse. The traverse left Dome GRIP (DG) at July 1st, 1993 and arrived at the wintering over camp (78N 37W) on July 27th. The traverse route for the 1993 and 1994 season is shown on Fig. 1.

Objectives:

The main purpose of the traverse was to obtain four deeper ice cores (100 - 150m) spaced 150km apart and the drilling of firn cores. This drilling program was supplemented by extensive geophysical measurements.

Glaciology:

- Determine the accumulation pattern of the central inland ice based on the four deep ice cores.
- Detect the variation of isotopes, ions, temperature etc. in relation to changes in latitude and elevation.
- Dating of the ice cores using: O18, D, ECM, AC-conductivity.
- Trace the history of the Arctic Haze development.
- Study of ice structure and firnification processes.

Additional Activities:

- Ground truthing of surface anomalies as seen in ERS-1 SAR images.
- Differential GPS measurements along the traverse profile.
- Gravity measurements.
- Ice radar for detecting internal subsurface horizons.

Preliminary results:

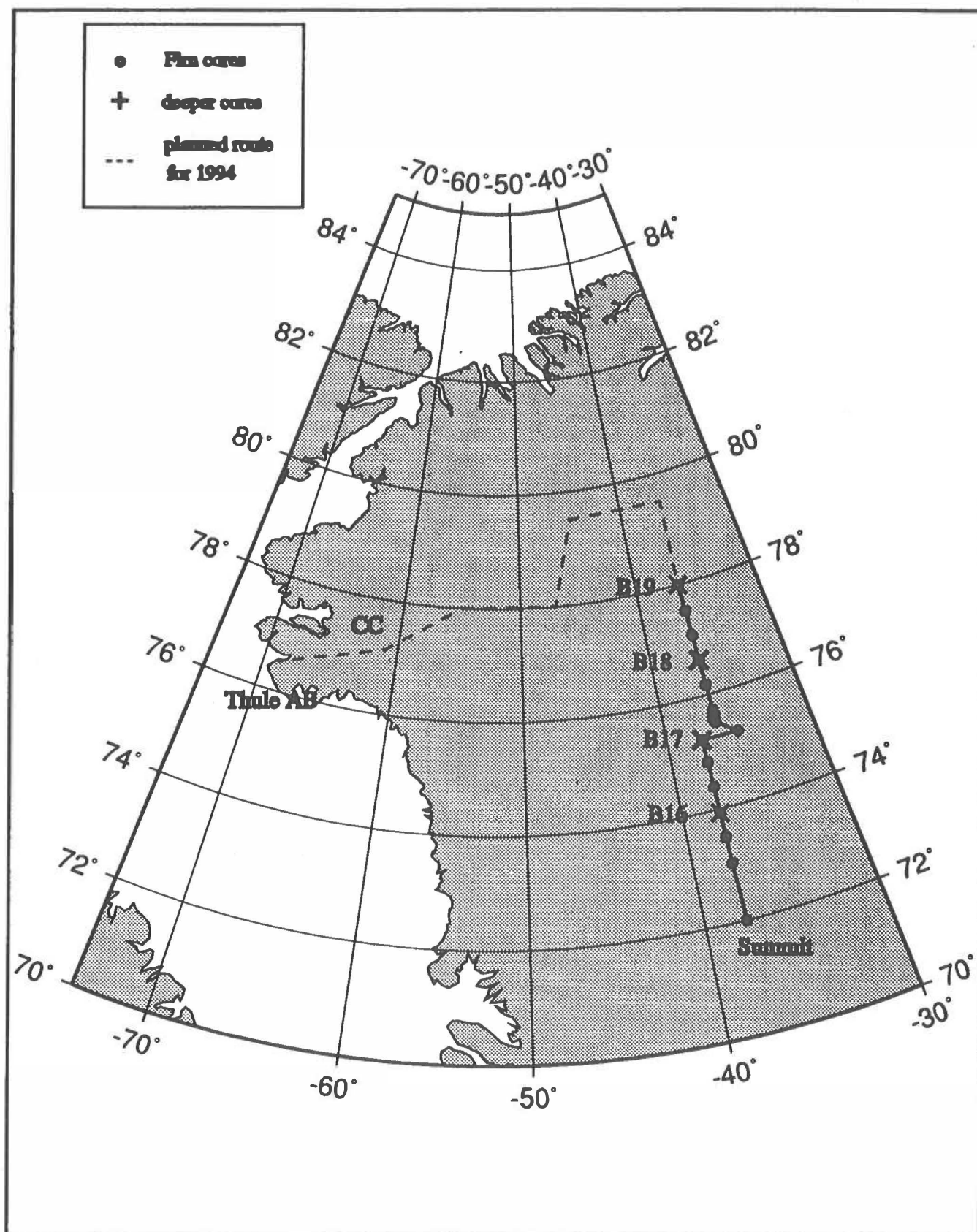
The drilling operations were successful in such as we recovered four deep ice cores. The first two from a depth of 100m the other two from a depth of 150m, representing an approximate age of 500 and 1000 years respectively. The DEP (dielectric profiling) measurements, which have been part of the core logging procedures in the field, allowed the dating of two events ascribed as volcanic events. The results as seen in Table 1 show the expected decrease of the annual accumulation with latitude.

Table 1:

Depths for dated volcanic and other events (preliminary results)							
AD	Grip	B16	B17	B18	B19		
	0 km	150km	300km	450km	600km		
1889	38.3	28.0	24.8	23.4	25.0	m	Melt layer
1816	58.8	42.7	37.8	35.3	32.7	m	Tambora
1783	67.6	49.3	43.2	40.2	37.3	m	Laki
Mean annual layer thickness (not corrected for flow)							
1889/ 1816	28.2	20.1	17.8	16.4	11.0	cm/a	
1816/ 1783	26.4	20.0	16.4	14.8	13.9	cm/a	

Additionally 15 firn cores have been drilled spaced 50km apart along with a 2m deep snow pit for snow chemistry studies. The ice radar survey produced a continuous profile along the traverse route. Differential GPS measurements have been made at all drilling locations. The GPS poles are clearly marked and are thus suitable for repeated measurements in the future.

Greenland Traverse 93/94



MASS BALANCE STUDIES AT DOME GRIP USING GPS & GRAVITY

Kristian Keller¹, Niels Gundestrup¹, Carl C. Tscherning¹,
René Forsberg² & Simon Ekholm²

¹ Geophysical Department

University of Copenhagen, Denmark

² Natural Survey and Cadastre (KMS), Copenhagen, Denmark

INTRODUCTION.

During the GRIP field seasons of 1991, 1992 & 1993 extensive gravity- and geodetic surveying were performed, using gravimeters and the Global Positioning System (GPS). The data have provided a detailed topographic map of summit of the ice sheet, covering an area of approx. 100 x 100 km. In the same area a gravity anomaly map was computed (Ekholm & Keller, 1993). These data are used as a groundtruth control for the Greenland Aero-geophysics Project (Brozena, 1991) and for ERS-1 altimeter measurements (Tscherning et al. 1992; Ekholm, Forsberg & Brozena, 1993).

At eight points poles were put up as a strain net for measuring ice movements and a reference marker was established 400 m from camp area. This reference marker was fixed 80 m down in the icesheet. Repeated observations of these poles around GRIP (25-45 km) have given information about ice movements of the top of the icecap. Due to low accuracy, the data from 1991, are not used here.

THE STRAIN NET.

In the table below positions and the measured movements are listed for the 8 poles. Also height measurements were made but due to very noisy data in 1992 these were left out. Point 47913 is the reference marker, which is kept fixed in the calculations.

position (WGS84)						horizontal movement in 1 year				
point	lat deg N	lon deg W	elev. m	dist km	az deg	ΔN cm	ΔE cm	Δr cm	err. est. cm	snow acc cm
47913	72,58	37,64	3240	0,0	-	-	-	-	-	-
47736	72,58	36,67	3210	32,1	89	8	159	159	± 20	55
47900	72,29	36,72	3189	44,6	135	-75	339	347	± 70	77
47807	72,38	37,20	3219	26,1	146	-86	152	175	± 15	68
47759	72,23	37,87	3219	39,4	192	-84	-58	102	± 50	56
47852	72,42	38,47	3210	32,2	238	-65	-196	206	± 15	54
47714	72,63	38,36	3215	25,1	284	1	-132	132	± 25	46
47828	72,80	38,32	3207	33,4	317	98	-95	136	± 15	56
47908	72,81	37,74	3216	25,7	351	118	-28	121	± 15	50

Table 1 : Position and movement of strain net, 1992-1993.

Compared to the ice surface, this reference marker moved 22 cm down in one year. The mean accumulation in the area is 23 cm of ice equivalent, corresponding to 25 cm (pers. comm. S. Johnsen) at a depth of 80 m.

The measurements were obtained using geodetic GPS receivers (dual-frequency, P-code), the observation time was limited by logistic constraints to 45 min. Later it appeared that our data from 1992 were very noisy and longer observation time might have increased the accuracy. The 1992 data are the main reason for the relatively low accuracy of 15-70 cm/year. The 1993 data's contribution to the accuracy is approx. 5 cm. In 1993 we have used better receivers (TRIMBLE 4000SSE L1PL2P instead of 4000SST L1L2P), and furthermore were six additional satellites available. The data have been processed using standard software from TRIMBLE, GPSurvey, ver. 1.10d (released oct.93). The surface velocities show a nice regular pattern and, it is seen that towards north & south the movements are slower than towards east-west, where the surface slope is somewhat larger.

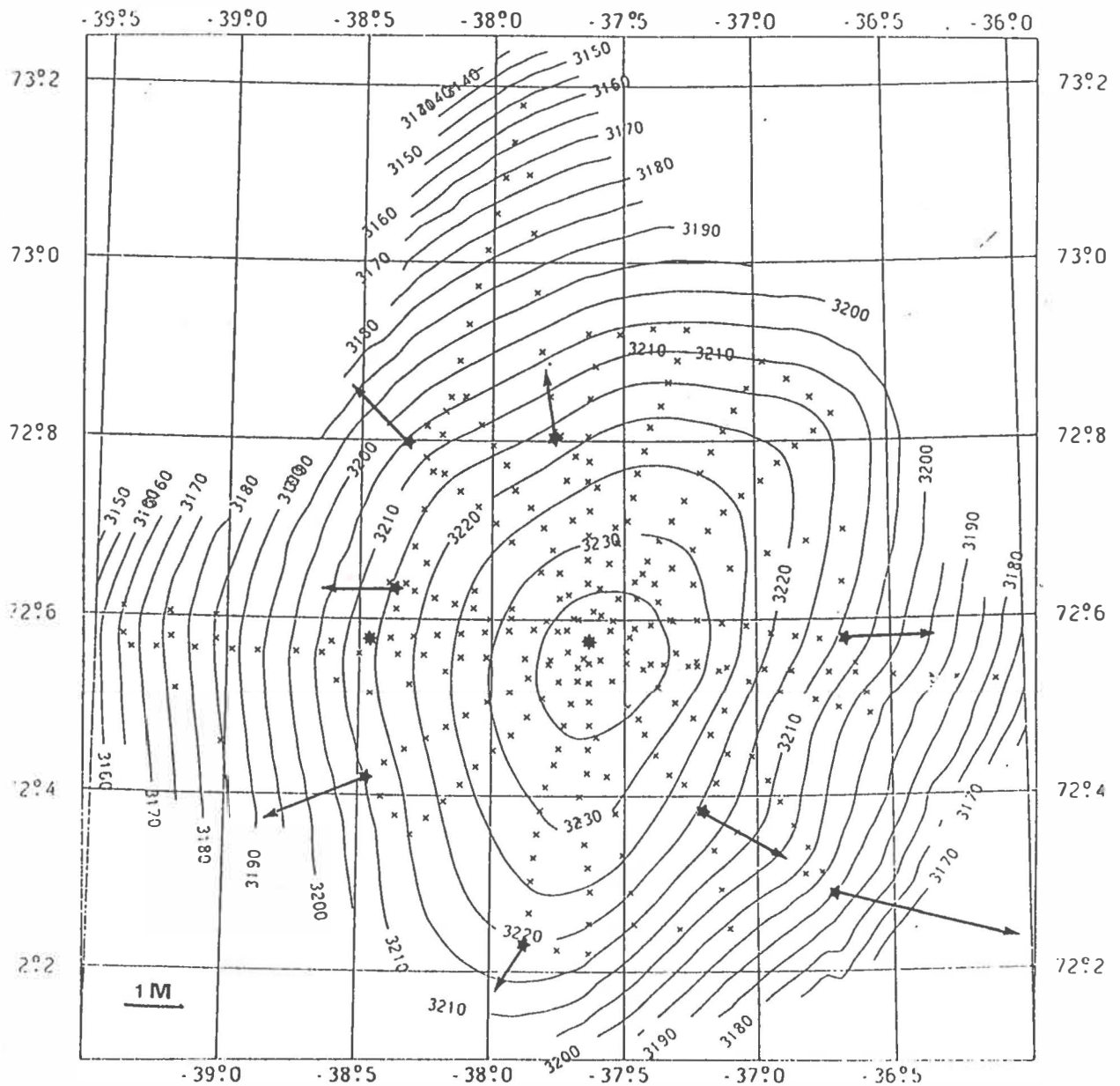


Figure 1: GRIP topography (c.i. 5 m) and ice velocities.

THE REFERENCE MARKER.

The GPS tie.

The local gravity and GPS measurements are tied to the reference marker fixed at a depth of 80 m. This reference marker in turn is referenced to the global network using a reference benchmark (No.61388) in Kangerlussuaq (Sondre Strom). This is both a precise gravity station tied to the Greenland absolute network and a precise 3-dimensional benchmark - established by KMS and tied into the global ITRF92 system by the GAP project. Several observations were made both in 1992 and 1993.

The three sessions in 1992 shows a good accuracy of approx. 20-40 cm, when precise orbit information are used. When the broadcast ephemerides are applied, the accuracy decreases two or three times. In 1993 the precision is even better than above mentioned. Using precise ephemerides this year as well, the mean error drops roughly to 15 cm.

Even though not all the processing is finished, the results for such a long baseline (796.5 km) are quite satisfactory. In table 2 the GPS-measurements indicate that the reference marker at GRIP is sinking. The expected sinking rate in the depth of 80 m is 25 cm/year.

year	latitude	longitude	ell.height	surface height
1992	72°34'31.2776" N	37°38'41.4390" W	3282.16 m	3279.63
1993	72°34'33.2801" N	37°38'41.4541" W	3281.83 m	3279.52
diff.	+ 8 cm N	+ 14 cm W	- 33 cm	- 11 cm

Table 2: Position(WGS84) and movement of the top of the reference marker at GRIP, 1992-1993. The geoid height at GRIP is approx. 42 m. Point 61338 in Kangerlussuaq is used as fixed reference: ITRF92 coordinates: 67° 00' 21.635" N, 50° 42' 11.465" W, h = 67.88 m

The Gravity tie.

Measuring the gravity at top of the reference marker in successive seasons, can in principle resolve the vertical movement of the ice at a depth of 80 m. The expected sinking of the pole is 25 cm, sufficiently to be seen 'in the noise' of the gravity surveys under ideal conditions.

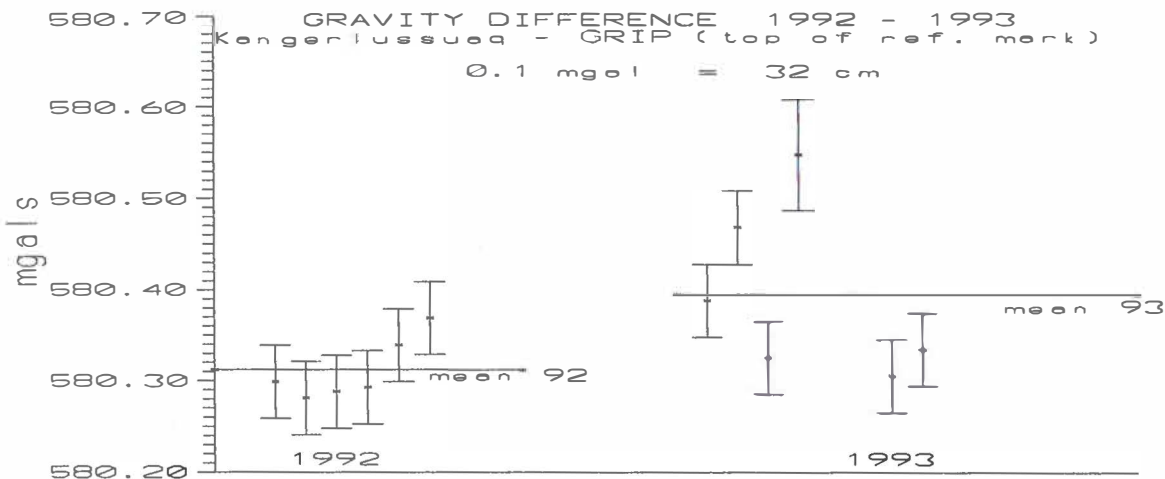


Figure 2: Gravity difference (raw measurements), Kangerlussuaq - GRIP, 1992 & 1993.

The change of gravity is due to ice movements of the reference marker relative to sea level. The vertical free-air gradient of gravity is 0.3086 mgal/m. This is applied to determine height changes due to the fact that gravity is considered constant in time, and on the assumption that the ice sheet is in equilibrium.

Both in 1992 and 1993 two LaCoste & Romberg gravimeters were used. In 1992 10 observations were made but because of a big 'bump' all four observations from instrument G-69 were out of range and not used at all. In 1993 6 observations were made, all are used. Figure 2 presents the gravity differences between Kangerlussuaq and GRIP in 1992 and 1993. It shows that in spite of the rather noisy data there is a signal of gravity increase of approx. 96 μ gal (result of adjustment) which is equivalent to a 31 cm descent of elevation.

Successive gravity observations have also been performed at the strain net points, for similar analysis, but they turned unfortunately out much too noisy due to the 'rough' transportation (plane or skidoo) of the gravimeters.

CONCLUSION.

Local gravity and surface topography were measured in a 50 km network around GRIP. The accuracy of the surface topography is comparable to the height of a sastruga.

Repeated GPS observations at the eight pole strain net 45 km around GRIP has provided surface velocities in the area. The accuracy of the latest observations is ± 5 cm and the estimated error of the velocity is approx. 25 cm/year.

Long GPS baselines from GRIP to Kangerlussuaq has indicated an ice sinking rate in agreement with the present accumulation.

The vertical ice velocity has also been measured by gravitational means. The gravity results confirm the GPS measured sinking rate, although the gravity measurements are somewhat more inaccurate than the GPS measurements.

Repeating the measurements in 1994 can further improve the accuracy of the results.

ACKNOWLEDGEMENTS.

This work is a contribution to the Greenland ice core project (GRIP), a European Science Foundation Programme with eight nations collaborating to drill through the central Greenland ice sheet.

REFERENCES.

- Brozena, J.M.: The Greenland Aerogeophysics Project: Airborne Gravity, Topographic and Magnetic Mapping of an Entire Continent (IUGG General Assembly, Vienna, August 1991).
- Ekholm, S., R. Forsberg, J.M. Brozena: Accuracy of Satellite Altimeter Elevations over the Greenland Ice Sheet (1993).
- Ekholm, S. & K. Keller: Gravity and GPS Survey on the Summit of the Greenland Ice Sheet 1991-1992 (National Survey and Cadastre, Geodetic Division, Technical Report no. 6, 1993).
- Tscherning, C.C. P. Knudsen, S. Ekholm & O. Baltazar Andersen: An Analysis of the Gravity Field in the Norwegian Sea and Mapping of the Ice Cap of Greenland using ERS-1 Altimeter Measurements (ERS-1 Symposium, Cannes, 1992).

ENERGY BALANCE OF DRY AND WET SNOW COVERS AT ETH CAMP

Thomas **Konzelmann**
Department of Geography
Swiss Federal Institute of Technology
Zürich, Switzerland

Periods with completely dry and wet-snow conditions in spring and summer 1991 are used to compare the energy-balance situation at ETH Camp.

Global, diffuse sky, shortwave reflected, allwave outgoing and allwave sky radiation (diffuse sky and longwave incoming radiation) were measured directly, and the radiation balance was calculated as the sum of shortwave net ($GL - \alpha GL$) and longwave net radiation ($L\downarrow - L\uparrow$). Sensible heat (H) and latent heat fluxes (LE) derived by the gradient method on the high tower (J. Forrer and M. Rotach, personal communications) were used for wet-snow conditions. Cold content (C), conductive heat flux at the top of the snow cover (G_0) and ground heat flux G (A. Abe-Ouchi, personal communication) were obtained using temperature profiles in snow and ice, respectively. For the premelt season (dry-snow conditions) the sum $H+LE$ was treated as a residual of the the energy balance by assuming melting heat (M) to be zero. For a wet snow cover, G_0 is equal to zero and melting heat M is treated as a residual. However, Ohmura et al. (in press) show that the calculated and measured mass balance are in good agreement. Additionally, radiation penetration into the snow was measured between 400 and 1150 nm in six different spectral ranges. A general overlook of the ETH Greenland expedition is given in Ohmura et al. (1992), while a detailed description concerning all the radiative fluxes is presented in Konzelmann (in press).

In Figures 1 and 2 the estimated energy balance of the dry snow cover (May 13 to 28, 1991) and of the wet snow cover (June 10 to July 10, 1991) are presented, respectively. The height of the snow cover was at least 50 cm. Therefore, no influence of the ice layer beneath the snow due to higher absorption can be expected. The total energy balance of the snow cover was estimated using the approach given in Ohmura (1981, p. 321).

In May 1991 (Fig. 1) the average energy balance at the surface shows large global radiation and a high albedo. Therefore, the shortwave net radiation is minimal. The loss of energy at the surface due to the longwave net radiation is partly compensated for by the turbulent fluxes. The net radiation in the snow cover is only about 1% of global radiation, while the amount of conductive heat flux from the top of the snow cover (G_0) is much smaller and negligible. The energy of the penetrating radiation is the main source for heating up the snow cover (C), while the heat flux (G) into the ice is very small.

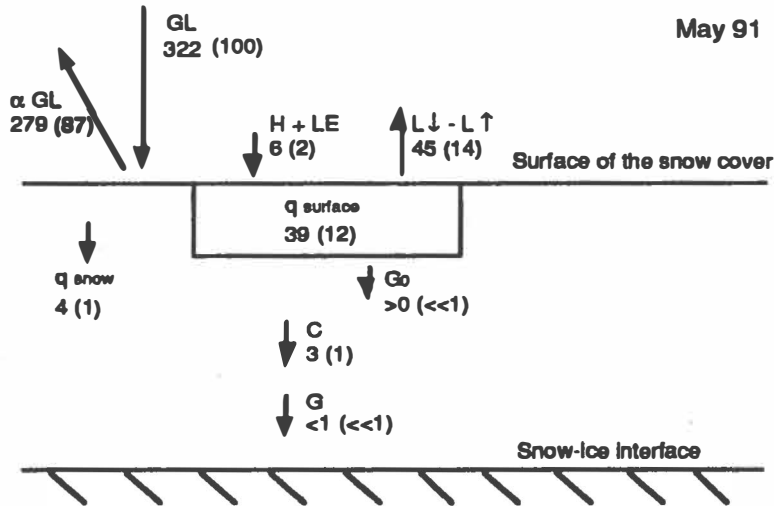


Fig. 1 Daily mean energy balance for the dry snow cover (May 13 to 28, 1991). q_{surface} is the absorbed radiation by the surface of the snow cover and q_{snow} is the net radiation in the snow cover. The values given in brackets are a percentage of the global radiation. Unit: W m^{-2} .

The average energy balance at the surface for wet-snow conditions (Fig. 2) is similar to the dry-snow situation considering global radiation, longwave net radiation, sensible and latent heat fluxes and surface absorptivity (q_{surface}). Due to the lower reflectivity at the surface the shortwave net radiation is double compared to dry-snow conditions and the net radiation in the snow cover (q_{snow}) is much larger and shows an amount of 13% of global radiation. This energy is mainly used for melt (M) and less for heating the ice (G) beneath the snow cover.

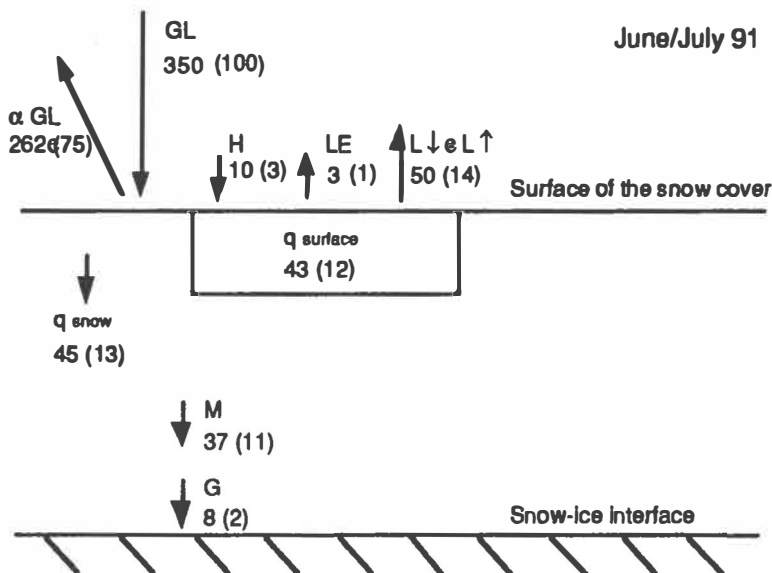


Fig. 2 Daily mean energy balance for the wet snow cover (June 10 to July 10, 1991) with a snow height larger than 50 cm. q_{surface} is the absorbed radiation by the surface of the snow cover and q_{snow} is the net radiation in the snow cover. The values given in brackets are a percentage of the global radiation. Unit: W m^{-2} .

References

- Konzelmann, T., in press. Radiation conditions on the Greenland Ice Sheet. Zürcher Geographische Schriften, Heft 56, Geographisches Institut ETH Zürich, 124 pp.
- Ohmura, A., 1981. Climate and energy balance on arctic tundra. Zürcher Geographische Schriften, Heft 3, Geographisches Institut ETH Zürich, 448 pp.
- Ohmura, A., Steffen, K., Blatter, H., Greuell, W., Rotach, M., Konzelmann, T., Forrer, J., Abe-Ouchi, A., Steiger, D., Stober, M. and Niederbäumer, G., 1992. Energy and mass balance during the melt season at the equilibrium line altitude, Paakitsoq, Greenland Ice Sheet. ETH Greenland Expedition Prog. Rep. No.2, Dept. of Geogr., Swiss Fed. Inst. of Technol., Zurich, 1992, 94 pp.
- Ohmura A., et al., in press. Energy balance on the equilibrium line of the Greenland Ice Sheet. IAHS Publ., Proceedings of the fourth scientific assembly of the IAHS, Yokohama 1993, Symposia J2 and J5.

MODELLING THE MASS BALANCE OF ICE SHEETS. LONG-TERM SIMULATION WITH A SIMPLE CLIMATE MODEL

Isabelle Marsiat

Institut d'Astronomie et de Géophysique G. Lemaître

Louvain-la-Neuve, Belgium

Past experiments in paleoclimatology showed that the energy balance on the ice sheet surface was of primary interest in representing the 100,000 years cycle. In particular, modelling of the net mass-balance function is an important part of the coupled ice-sheet-climate models. In this work (Marsiat, 1994), we have coupled a fine grid horizontal (latitude, longitude) model (CIM, Continental surface and Ice sheet Model) allowing to represent the inception, the waxing and the waning of the ice sheets at the Earth's surface to the two-dimensional LLN-model (latitude, altitude) representing in zonal mean the different parts of the climate system for the northern hemisphere (atmosphere, ocean, sea ice, continental surface covered or not by snow) (Gallée et al, 1991). The horizontal model (CIM) we developed involves three parts: a model representing the ice dynamics, a model representing the depression of the asthenosphere under the weight of the ice and finally, the mass balance evaluation over the ice sheets and over the continents.

The annual mass balance is defined as the difference between snow accumulation and snow ablation during a whole year. In our model, in each continental point, the evaluation of the temperature and precipitation seasonal cycles at the real altitude of the surface, allow to compute the seasonal evolution of a possible snow layer and the annual snow and/or ice mass balance. Although based on the present observed precipitation rate, the parameterization of the snow or rain precipitation rates differs slightly from those generally used. In paleoclimatic simulation, a desert altitude-effect is generally used to limit the precipitation rates at high altitude where the cold air contains less precipitable water. We use here the explicit evaluation of the variations of the water vapor pressure as a function of the local temperature.

We introduced also the annual cycle of precipitation and take into account the upslope precipitation effect. The snow ablation rate is computed from the annual cycle of surface temperature. When the balance between atmospheric heat fluxes and heat conduction in the soil (snow or ice) leads to a surface temperature higher than 0°C, this temperature is lowered to 0°C and the excess of energy is used to melt the snow or the ice. The evaluation of atmospheric heat fluxes requires to use the solar and I.R. downward fluxes and the 500 mb temperature computed by the LLN-model. The coupling between a horizontal (latitude-longitude) model of continental surfaces like the CIM model and a zonal vertical model (latitude-altitude) like the LLN-model is not easy. We assume that at the 500 mb level, vertically to the points situated at the same latitude, the atmosphere is similar to the zonal mean computed by the LLN-model. The local radiation fluxes are also interpolated from the zonal mean taking into account local characteristics such as altitude, surface temperature, soil water availability and soil albedo.

Previous experiments showed the importance of the snow albedo parameterization in the deglaciation processes. This parameterization, which is also dependent on the vegetation cover but principally on the surface temperature and the snow precipitation frequency will be used here. We distinguish two types of vegetation cover: the tundras or low vegetation

cover, like steppes and the taïga or high vegetation cover, of forest type. Because snow rarely covers the threetops, the albedo of the forest covered by snow is much lower than the albedo of the snow-covered fields. The constant value $\alpha_s = 0.4$ is chosen. Over tundras and ice sheets, the snow surface albedo is a function of snow precipitation frequency and of snow surface temperature. Subsequently, we will distinguish the very cold areas where the surface temperature is lower than -10°C , the temperate areas where the surface temperature is equal to 0°C and the cold areas where the surface temperature is intermediate. The snow precipitation frequency is characterized by the number of days since the last snowfall ≥ 0.3 cm. The snow albedo over tundras vary then from 0.4 to 0.85.

When running paleoclimatic simulations, the CIM model computes the annual snow and/or ice mass balance over the northern hemisphere continents covered or not by ice sheets, using the climatic equilibrium computed by the LLN-model. Snow accumulation during thousands of years allows the inception of ice sheets without help of small start glaciers or initial snow cover. Inversely, the CIM model gives to the LLN-model the spatial extension of the ice sheets and their mean altitude. The coupling between both models is asynchronous, an equilibrium climatic state of the LLN-model is computed every 1000 years. In the CIM model, we do not restrain the growth domain of the ice sheets, and we are taking into account the sea level variations. The one and only limitation to the extension of the ice sheet is the presence of a deep ocean: ice breaks when it floats. The sea level lowering subsequent to the ice growth allows the ice sheets to extend on the continental shelf.

The present day climate of the northern hemisphere is quite well represented allowing the relative simplicity of the model. In particular, the January snow field extension which is close to the maximum extension of the snow during the year and the July snow field extension which is representative of the permanent snow field persisting along the whole year are well computed. The Greenland simulated snow mass balance (fig. 1) is in good agreement with the data. Simulated low accumulation rates (0 to 40 cm ice/yr) are observed north of 76° N and at the eastern part of Greenland. High accumulation rates are encountered at the south point and at the south western part of the ice sheet. Ablation by melting is more important on the western side of the inlandsis. On the northwestern side of Greenland the simulated high ablation rates are in contradiction with the high accumulation rates deduced from observations. This is probably due to the lack of high precipitation rates in the Jaeger's precipitation data (1976) which are used for this simulation. If days having a mean temperature $T_s > 0$ are said to be ablation days, their number equals to 96 at 400 m height (49° W , 69° N) and to 60 at 1130 m height (47.3° W, 69° N) can be compared to those given by Ambach (1985) for the west coast (Jakobshavn station).

During the last glacial to interglacial cycle, total ice volume and sea level variations (fig. 2) are well simulated. This suggests that the physical mechanisms that have been included in the model are sufficient to explain ice sheets building and terminations that are such a striking feature of individual ice age cycle. Due to the zonally averaged character of the atmospheric forcing, ice repartition between the different ice sheets differ from the geological reconstructions. Improvement of the glaciation pattern must be expected in the future using 3-D climate models.

References

- Gallée, H., van Ypersele, J.P., Fichefet, Th., Tricot, Ch. and Berger A., 1991. Simulation of the last glacial cycle by a coupled sectorially-averaged climate ice-sheet model. I. The climate model, *J. Geophys. Res.*, 96, D7, 13139-13161.
- Marsiat I., 1994. Simulation of the northern hemisphere continental ice sheets over the last glacial-interglacial cycle: experiments with a latitude-longitude vertically integrated ice-sheet model coupled to a zonally averaged climate model, *Palaeoclimates, Data and modelling*, in press.

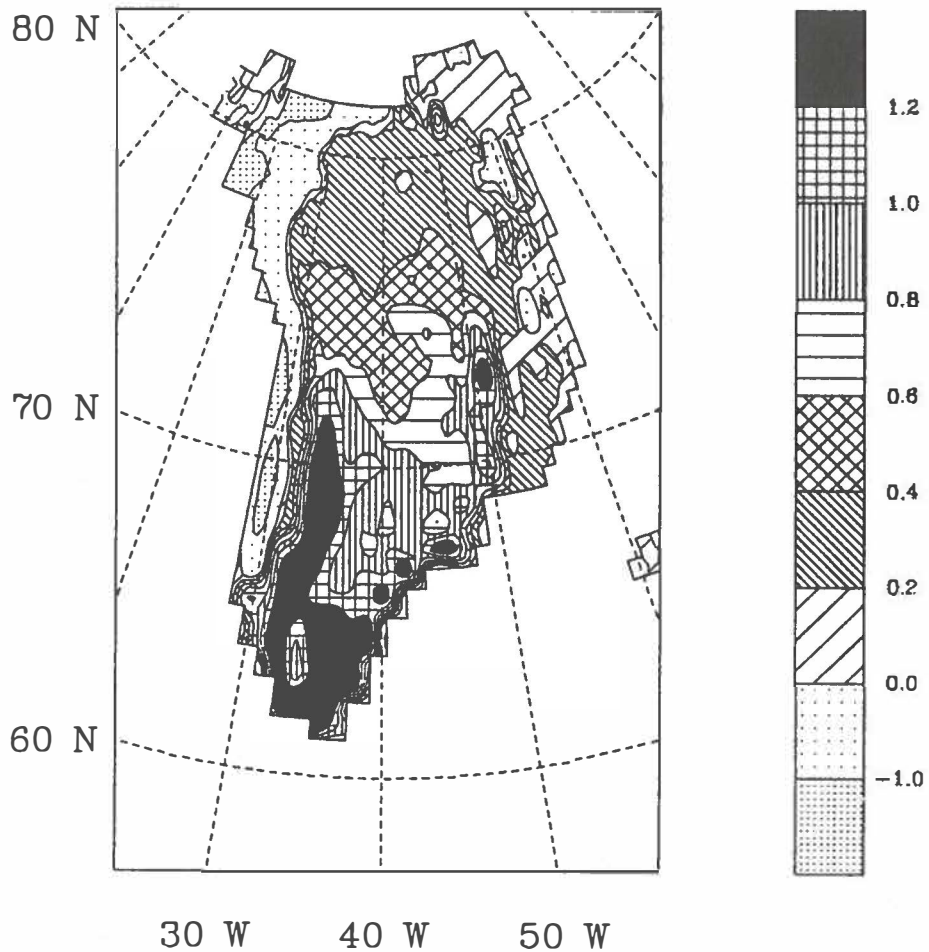


Fig. 1. Simulated present-day Greenland mass balance (m ice/year).

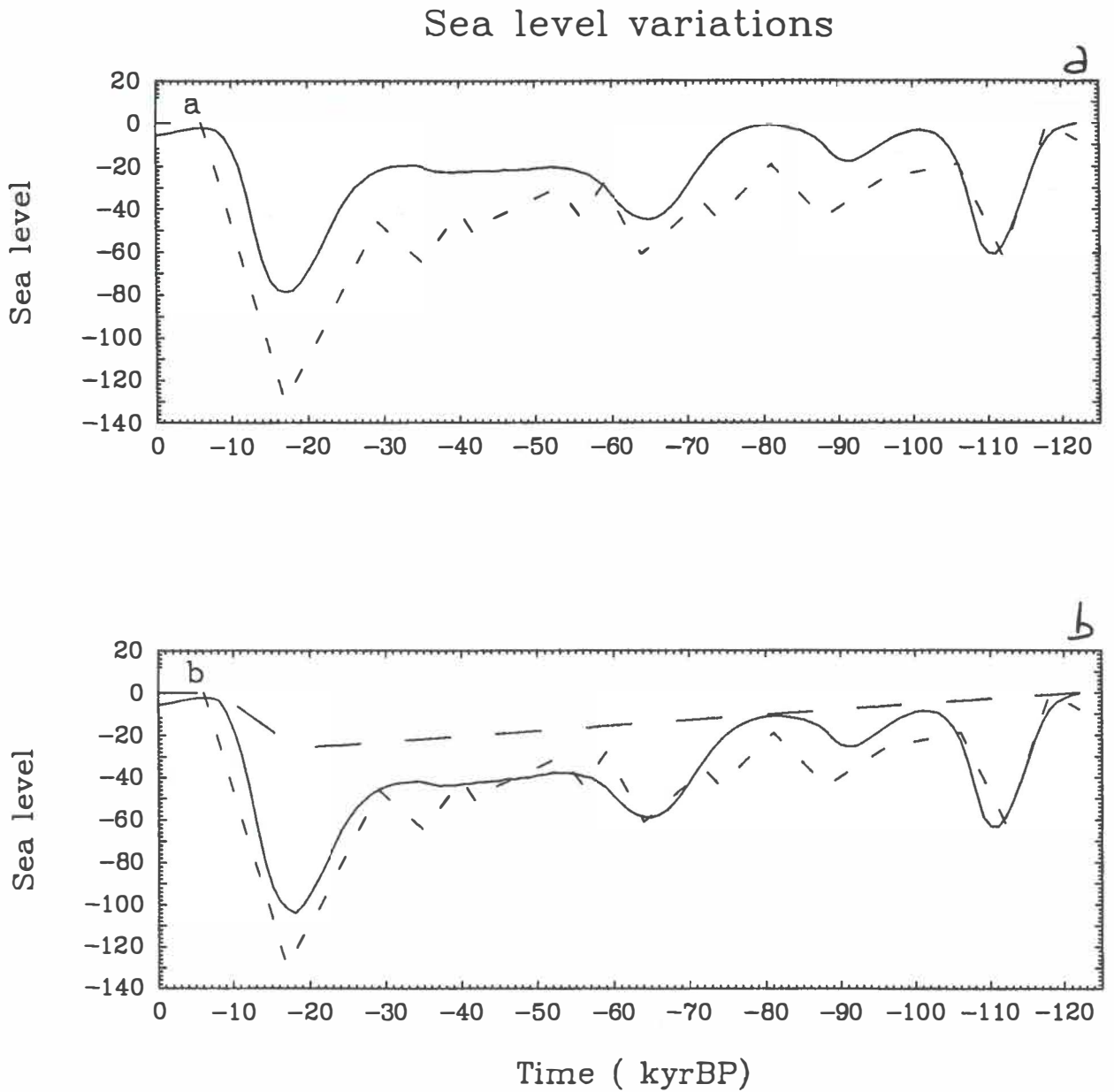


Fig. 2. (a) Variation of the sea-level simulated (full line) by the model (related to the variations of the ice-sheet volume of the Northern Hemisphere) compared with the data of Chappell and Shackleton (1986) (short dashed line).

(b) Variation of the sea-level (full line) including a reconstruction of the Antarctic ice-sheet contribution (long dashed line) based on the estimation at the LGM (-26 m) from Tushingham and Peltier (1991).

DATING DEGLACIATION AND ITS AFTERMATH IN SØNDRE STRØMFJORD/SANDFLUGTDALEN

Jaap J.M. van der Meer¹, Klaas van der Borg², Cees Laban³
& Frank G.M. van Tatenhove¹

¹ Fysisch Geografisch en Bodemkundig Laboratorium
University of Amsterdam, Amsterdam, The Netherlands

² Subatomaire Fysica, Utrecht University, The Netherlands

³ Mariene Geologie, Rijks Geologische Dienst, Haarlem,
The Netherlands

In the context of the Dutch GIMEX programme the University of Amsterdam research group is responsible for recording Holocene deglaciation of the Søndre Strømfjord/Sandflugtdalen area. For the area Kangerlussuaq to the inland ice this is achieved e.g. by detailed geomorphological mapping (van Tatenhove, 1991). For the fjord area the main inventory has been done by the Geological Survey of The Netherlands, Marine Geology Division, (in close cooperation with the Amsterdam research group) during the 1992 GIMEX-MAR cruise (Oele, 1992). Since maps of former glacial extent are of limited use, unless these extensions have been fixed in time, dating is a major part of the research programme.

Given the great extent of organic deposits in the area it has been clear from the beginning that dating by ¹⁴C, using the AMS technique, would be the most profitable. The more so, because the same technique can be applied to shells in marine deposits. Using standard ¹⁴C dating techniques would have meant that samples from marine deposits (e.g. cores), would simply be too small to allow dating.

Here we will discuss some preliminary results of dates obtained so far for different parts of the research area. Details on the dates can be found in table 1.

1. Dating the Ørkendalen moraines.

A widespread cluster of moraines relatively close to the present-day ice margin has been mapped as the Ørkendalen phase by ten Brink (1975) and dated by him between 700 and 300 B.P. In the field this date creates problems, because too many geomorphologic events have to be squeezed in the time remaining until the present. Dating the base of peat sequences on both sides of, as well as in between the Ørkendalen phase moraines, thereby bracketing this phase, resulted in dates between 6400 - 3000 B.P. The age of this phase could further be confined by dates of over 5000 B.P., obtained on organic material included in the top of a delta at the W end of lake Sanningasoq (fig. 1). This delta formed in a lake dammed by the inland ice when it occupied the position set by the Ørkendalen moraines. The consequence of these latter dates is that the Ørkendalen moraines must have formed between 6000 and 5000 B.P. This leaves ample time to allow all observed geomorphologic events like peat development, polygon formation, deposition and erosion of loess, deglaciation of unknown extent, and ice sheet expanse with formation of existing ice-cored moraines. Further details will be discussed by van Tatenhove in his PhD thesis in 1994.

2. Dating of marine terraces at Kangerlussuaq.

Marine terraces at Kangerlussuaq have provided several dates (e.g. Ten Brink, 1975) which have been used to reconstruct isostatic recovery for the fjord area. Because data for isostasy of the Kangerlussuaq area and the Sanningasq/Ajuitsup tasia area do not seem to be compatible (van der Meer et al 1993) we have looked in detail at the marine terraces near the airport. A shell recovered in life position from ca. 7 m below the surface provided a date of 6930 ± 70 B.P., which fits well with existing dates.

The problem is not so much to find and to date shells; in our study we sampled over forty shells in a vertical sequence, all in life position. As most shell species have a certain tolerance to waterdepth and to other ecologic values (like salt content), it is much more difficult to translate such dates to former sea-level. In our recording of the sedimentary sequence of the Kangerlussuaq terraces we noticed sedimentary structures indicative of former sea-level. As such we can mention disturbance by floating (winter-)ice and sets of dessication cracks. Both form at sealevel or just several dm below it. Combining sedimentological observations with dates to be obtained on the shells will allow a very accurate reconstruction of sea-level and hence of isostatic recovery.

3. Dating of fjord material.

Figure 1 shows the position of some of the cores obtained during the 1992 GIMEX-MAR cruise as well as some dates found in literature (Sugden, 1972). On the basis of on-board description and on X-ray observations we selected four cores for preliminary dating, two in Itivdleq and two in Søndre Strømfjord. For dating purposes shells and plant material were collected from different levels in these cores (table 1). The cross-sections in figure 1 give the relative positions of the resulting dates. From these dates some conclusions can be drawn:

- the marine dates obtained sofar are not suitable for fixing former glacier extent along the fjord
- as the dates are not in the right chronostratigraphic order, the organic material must be mainly derived by erosion, not by in situ growth
- sedimentation in Søndre Strømfjord is active, and seems to involve only recent material
- sedimentation in Itivdleq involved older deposits as exposed in raised deposits in the drainage basin and has stopped after ± 4000 B.P.

The consequence of the last conclusion is that the col between the two fjords has last acted as an overflow before ± 4000 B.P. Because reconstructions of local isostasy for the area indicate 20 to 30 m recovery since that date, the col stood only 15 m above sea-level. As a consequence blocking of Søndre Strømfjord leading to overflow of the col, as postulated by van der Meer et al (1993), is even more easily reached. Full appreciation of this hypothesis will only be possible after further analyses of the isostatic history of the area.

References

- Brink, N.W. ten 1975 Holocene history of the Greenland ice sheet based on radiocarbon-dated moraines in West Greenland. *Grønlands geol. Unders. Bull.* 113.
- Meer, J.J.M. van der, F.G.M. van Tatenhove, C. Laban & E. Oele 1993 Glaciation and isostasy in the Søndre Strømfjord-Itivdleq system. In: N. Reeh & H. Oerter (eds) *Mass balance and related topics of the Greenland ice sheet*. GGU Open File Series 93/5, 84-86.
- Oele, E. 1992 Cruise report GIMEX-MAR '92. Marine Geology Division, Rijks Geologische Dienst, Haarlem.
- Sugden, D. 1972 Deglaciation and isostasy in the Sukkertoppen ice cap area, West Greenland. *Arctic and Alpine Research* 4, 97-117.
- Tatenhove, F.G.M. van 1991 A geomorphological branch on the GIMEX tree. In J.J.M. van der Meer (ed) *GIMEX '91*. *Circumpolar Journal* 6, 34-41.

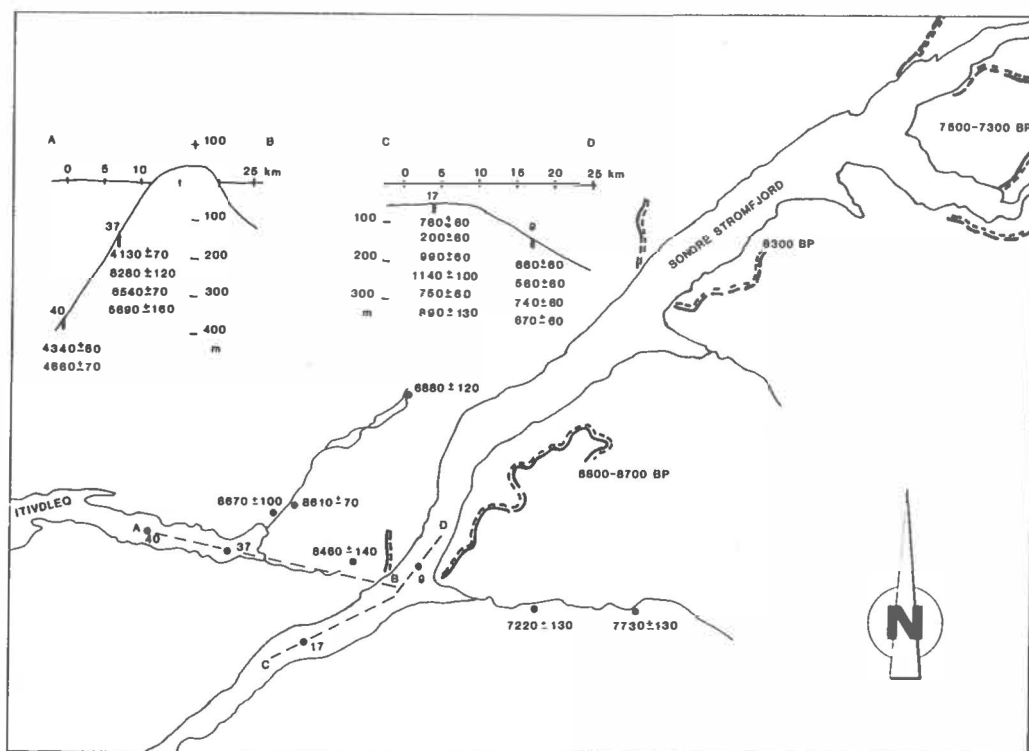


Fig. 1: Dates obtained on fjord cores collected by GIMEX-MAR '92, plotted on cross-sections AB and CD. Dates on land have been taken from literature; double lines trace older Holocene moraine systems.

Table 1. New dates from the Søndre Strømfjord area

<u>location</u>	<u>number</u>	<u>date</u>	<u>material</u>	<u>cm depth</u>	<u>m. asl</u>
<u>GIMEX dates</u>					
Russellg. site 11	GrN18576	3015+ <u>35</u>	peat	150	150
Russellg. no. 2B	Utc2034	4060+ <u>60</u>	peat	156	180
Russellg. no. 29	Utc2033	3890+ <u>50</u>	peat	160	355
Sandfl.d. no. 18A	Utc2035	3950+ <u>60</u>	peat	93	180
Sandfl.d. no. 28	Utc2036	5360+ <u>70</u>	peat	86	175
Sandfl.d. no. 28A	Utc2037	4430+ <u>60</u>	peat	113	175
Leverett no. 44	Utc	modern	wood	380	230
Leverett no. 30	Utc	2010+ <u>80</u>	wood	90	230
Sanningas	Utc	5090+ <u>70</u>	org.	130	235
ibid	Utc	5280+ <u>130</u>	org.	365	235
Raventer.	Utc2533	6930+ <u>70</u>	shell	600	25
			unident. (Mya ?)		
<u>Dates by GIMEX-MAR</u>					
SoSPCM9	Utc2527	880+ <u>60</u>	wood	20	-151
ibid	Utc2528	580+ <u>60</u>	shell	429	
ibid	Utc2529	740+ <u>60</u>	shell	754	
ibid	Utc2530	670+ <u>60</u>	Cardium psilate shell	877	
			unident.		
SoSGDW17	Utc2526	780+ <u>60</u>	shell	10	-50
ibid	Utc2525	200+ <u>60</u>	Yoldiella sp. wood	179	
ibid	Utc2524	990+ <u>60</u>	org.	233	
ibid	Utc2523	1140+ <u>100</u>	shell	233	
ibid	Utc2521	750+ <u>60</u>	Astarte sp. shell	337	
ibid	Utc2522	890+ <u>130</u>	Yoldiella sp. shell fr.	357	
			unident.		
ItvPCM37	Utc2520	4130+ <u>70</u>	shell fr.	128	-138
ibid	Utc2519	8280+ <u>120</u>	unident. shell fr.	280	
ibid	Utc2518	6540+ <u>70</u>	unident. shell fr.	474	
ibid	Utc2517	5890+ <u>160</u>	unident. shell	673	
			Astarte triolanta ?		
ItvPCM40	Utc2531	4340+ <u>80</u>	shell	566	-367
ibid	Utc2532	4680+ <u>70</u>	unident. shell	617	
			Yoldiella sp.		

ENERGY BALANCE OF THE ABLATION ZONE: INFLUENCE OF TUNDRA AND KATABATIC WIND

Antoon Meesters

Institute for Earth Sciences, Free University, Amsterdam,
The Netherlands

The katabatic wind is driven by the negative buoyancy force that is caused by the cooling of the air as it touches the ice sheet. At daytime in summer, the wind at the margin of the ice sheet is enhanced by thermal forcing if ice-free land areas are present there. This is confirmed for the Søndre Strømfjord area by GIMEX measurements (Van den Broeke et al. 1994).

The katabatic wind influences the energy balance of the ablation zone by advecting heat (the potential temperature increases if one goes upstream) and by promoting turbulent exchange of sensible (and latent) heat at the ice surface.

A 2-dimensional atmospheric model has been set up for the western margin of the Greenland ice sheet. The model corresponds to a vertical section through the GIMEX transect, extending from the sea to the center of the ice sheet. The relief of the area between the ice sheet and the coast (160 km) is neglected for convenience. For each ice or tundra surface point, the model contains a multi-level box. The atmospheric part of the model has been set up along the usual lines for meso-scale models. Infrared radiation is calculated from temperature and moisture profiles. The turbulent exchange depends on the Richardson number, and is calculated along traditional lines.

In the following, results of 4 runs (A-D) with the model will be discussed. A full treatment is given by Meesters (1994). For run A, conditions for 12 July 1991 are used: the sky is clear, the large-scale wind is still, the area between the coast and the ice sheet is ice-free. The resulting katabatic wind causes an appreciable sensible heat flux for the ablation zone.

The set-up of the other 3 runs differs from run A in only one respect in each case. For run B, the tundra is snow-covered. As a consequence, both the katabatic wind and the

sensible heat flux for the ablation zone are strongly reduced. This happens because a stable boundary layer above the ice sheet is present now. Similar situations are observed at the coast of Antarctica (Gallée and Schayes 1992). It is concluded that ice-free surroundings stimulate ablation, and so enhance the sensitivity of the ice sheet to climate change.

For run C, the tundra is again ice-free, but now the initial air temperatures are all increased by 5 K to mimic a warmer climate. As a result, the katabatic wind becomes stronger because both the negative buoyancy and the thermal forcing at the margin are increased. As is to be expected, the sensible heat flux for the ablation zone also increases. The increase is larger than what would be the case if the katabatic wind speed was kept constant (as is usual in current models). The increase would probably not be so large if the ice-free surroundings were lacking.

It is also found that the incoming long-wave radiation is strongly increased for the ablation zone, whereas the increase in the air temperature at reference height is relatively weak. This happens because the temperature at reference height remains close to the surface temperature, which cannot rise above 0 °C. Hence, parametrizing the long-wave radiation in terms of the temperature at reference height appears not very useful above a surface with melting ice.

For run D, a weak western large-scale wind is stipulated. In our simulation, this leads to the genesis of a front at the ice sheet margin, where the western wind encounters the south-eastern katabatic wind. In the frontal zone, a rather strong southern wind develops over the ablation zone, causing strong enhancement of the sensible heat fluxes. Since frontogenesis requires considerable thermal gradients, one would expect the effect to be much weaker if no ice-free surroundings were present.

References

- Gallée, H.G. and Schayes G. (1992). Dynamical aspects of katabatic winds in the Antarctic coastal zone. *Boundary Layer Meteorology* 59, 141-161.
- Meesters A.G.C.A., Henneken E.A.C., Bink N.J., Vugts H.F., Cannemeijer F. (1994). Simulation of the atmospheric circulation near the Greenland ice sheet margin. *Global and Planetary Change* 9 (in press).
- Meesters A.G.C.A. (1994). Dependence of the energy balance of the Greenland ice sheet on climate change: influence of katabatic wind and tundra. *Quarterly Journal of the Royal Meteorological Society* (accepted).
- Van den Broeke M.R., Duynkerke P.G., Oerlemans J. (1994). The observed katabatic flow at the edge of the Greenland ice sheet during GIMEX-91. *Global and Planetary Change* 9 (in press).

**SYNOPTIC OBSERVATION DURING TWO YEARS
FROM AUTOMATIC WEATHER STATION AT ETH CAMP**

Gunthard **Niederbäumer**
Department of Geography
Swiss Federal Institute of Technology
Zürich, Switzerland

Measurements

At the end of the field season 1991 an automatic weather station has been installed at the ETH Camp (Ohmura et al., 1992). Measurements were started Sept. 1, 1991. Data were read first time in summer 1992 and again in summer 1993. Snow and ice temperatures are measured once the day (00:00 UTC). The snow sensors are 0.3 m, 0.6 m and 0.9 m above the ice horizon and the ice sensors in 0.25 m, 0.75 m, 1.25 m, 2 m, 3 m, 4 m, 5 m, 6 m, 8 m and 10 m depth. Wind speed was measured in 2 m and 10 m heights every ten minutes. Every three hours the average was computed and stored in a data logger. In addition, the maximum ten minutes value was also stored. Wind direction in 10 m height and two air temperature sensors in 2 m height were measured eight times a day. The data are stored in two data loggers. One has been working without any problems during the two years. So the snow-, ice- and air temperatures and the wind speed in 10 m height are available from 1. 9. 1991 to 7. 6. 1993. The second data logger did not work the first year and failed in mid-winter of second year. So, wind direction, wind speed at 2 m height and one air temperature at 2 m height are available only from 18. 6. 1992 to 13. 11. 1992. But the station is still running, so there will be more data available next year.

Results

The mean monthly values of air temperature are summarised in Table 1. For 1992 the mean annual temperature was - 15.5 °C. Data shows that June 1992 was 6 °C colder then the two previous years and that the whole summer was colder. In winter 1993 temperature values for January and March were 7 - 8 °C colder then in 1992.

Tab. 1: Monthly mean air temperature 2 m above the surface at the ETH Camp from June 1990 to May 1993, unit: °C.

month	1	2	3	4	5	6	7	8	9	10	11	12
1990						-0.9	0.6	-1.8				
1991						-0.5	0.5	-3.5	-8.1	-14.0	-24.1	-20.5
1992	-22.4	-31.3	-24.0	-18.3	-14.2	-7.0	-1.0	-4.0	-9.0	-9.0	-22.6	-24.6
1993	-30.0	-27.2	-31.0	-18.2	-9.8							

Results of the wind speed measurements (Table 2) show for monthly mean values only small variation between the different years. The maximum was found for September 1992 and 1993 with a difference of 3.2 m s^{-1} . Mean wind speed shows in summer only small variations. The annual mean wind speed in 1992 was 8.9 m s^{-1} .

Tab. 2. Monthly mean wind speed 10 m above surface at the ETH Camp from June 1990 to May 1993, units: m s^{-1} .

month	1	2	3	4	5	6	7	8	9	10	11	12
1990						8.2	6.8	7.5				
1991						6.9	6.8	7.0	7.4	8.2	9.1	10.8
1992	10.4	9.0	8.3	10.2	6.7	7.1	6.8	7.4	10.6	8.1	11.2	11.0
1993	9.9	9.9	8.8	8.5	8.0							

Measurements of the snow temperature show two similar annual cycles (Fig. 1). The sensor installed 0.9 m above the ice horizon was not covered by snow from September to November 1991. This is the reason for the strong fluctuation of this temperature. In summer 1992 the snow level did not sink under 0.9 m and so the upper sensor did not melt out.

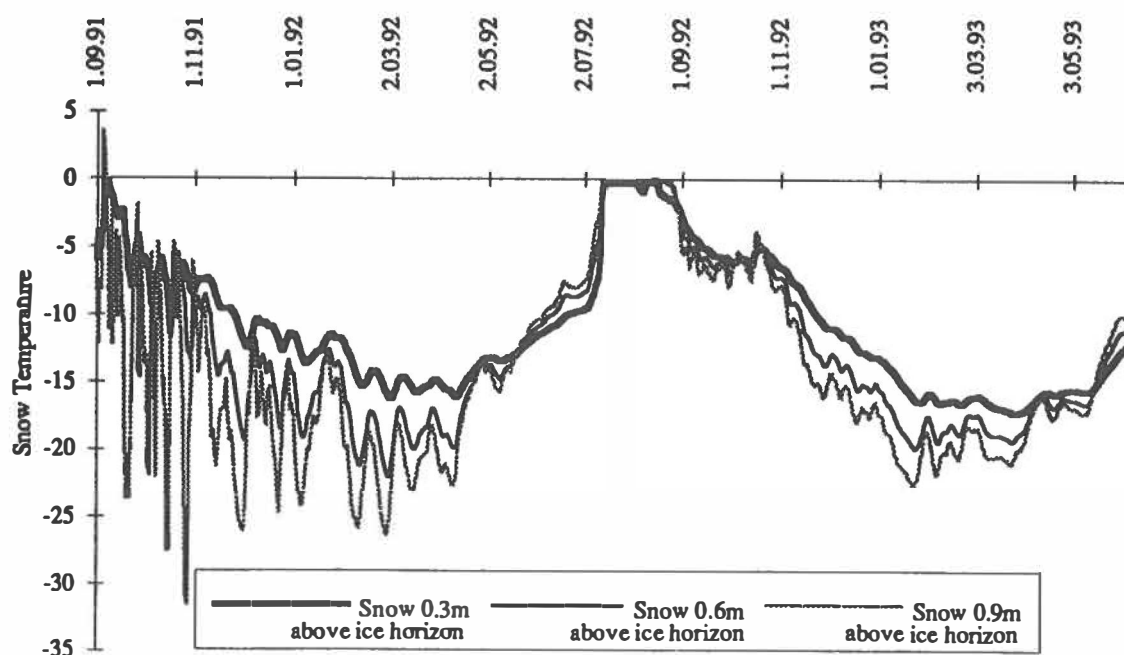


Fig. 1: Snow temperature at 0.3 m, 0.6 m and 0.9 m above the ice horizon in $^{\circ}\text{C}$. The values are measured once a day from Sept. 1, 1991 to May. 31, 1993. Unit: $^{\circ}\text{C}$.

The ice temperature at ten different depths is shown in figure 2. In summer 1992 the maximum of the 0.25 m temperature was recorded end of August, while the 10 m temperature shows a time lag of about seven month.

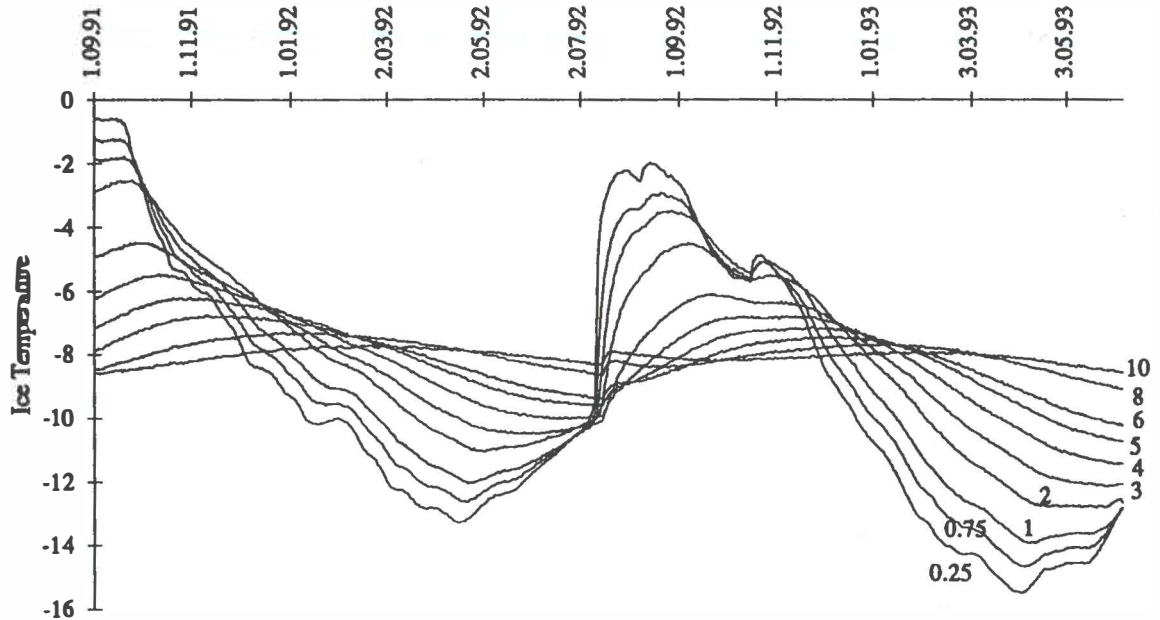


Fig. 2: Ice temperature measured at 0.25 m, 0.75 m, 1 m, 2 m, 3 m, 4 m, 5 m, 6 m, 8 m and 10 m depth below the ice horizon. from Sept. 1, 1991 to May. 31, 1993. Unit: °C.

Reference

Ohmura A., Steffen K., Blatter H., Greuell W., Rotach M., Stober M., Konzelmann T., Forrer J., Abe - Ouchi A., Steiger D. and Niederbäumer G. (1992): ETH Greenland Expedition, Progress Report No. 2, Department of Geography Swiss Federal Institute of Technology, Zürich, pp. 94.

GLACIOLOGICAL FIELDWORK IN 1993 AT THE ICE MARGIN IN KRONPRINS CHRISTIAN LAND, NE GREENLAND

Hans Oerter¹, Niels Reeh² & Carl E. Bøggild³

¹ Alfred-Wegener-Institut für Polar- und Meeresforschung,
Bremerhaven, FRG

² Dansk Polar Center, København, Denmark

³ Grønlands Geologiske Undersøgelse, København, Denmark

Introduction

Ablation studies have been carried out in Northeast Greenland since 1989 on Storstrømmen, one of the largest outlets of the northeastern part of the Greenland ice sheet. These studies have been continued at the beginning and the end of the summer field season 1993. Inbetween the authors went further north to Kronprins Christian Land, and shared logistics with the Geological Survey of Greenland who started up a geological programme there which is planned to last for the next two summer seasons. This is also within the time frame for our glaciological studies. The location of both catchments is shown in Fig. 1.

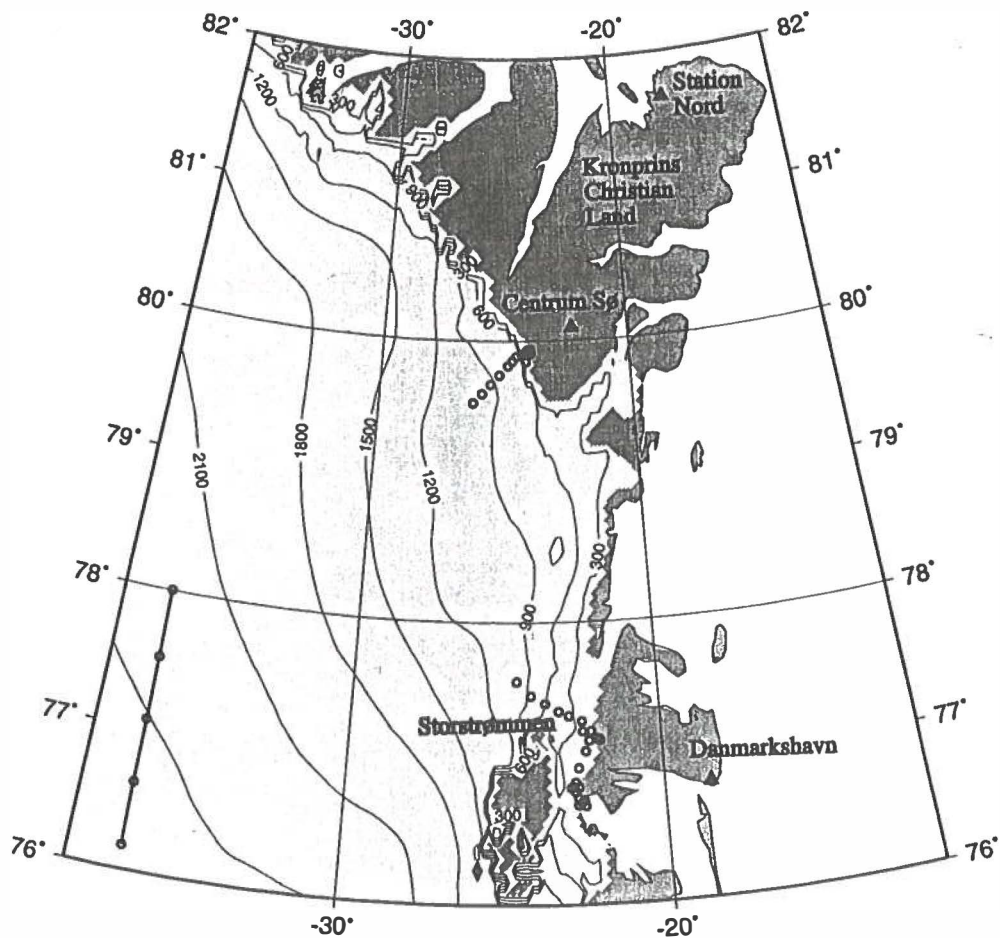


Figure 1: Map of Northeast Greenland showing the area under investigation at Storstrømmen and in Kronprins Christian Land. The circles indicate stake positions.

Measurements

In 1993 a stake net consisting of 18 main stakes was drilled in. The stakes extend over a length of 60 km covering an elevation range from 180 m a.s.l. to 1060 m a.s.l. They are used for ablation readings and velocity measurements.

At 418 m a.s.l. at a distance of about 1.4 km from the ice margin a meteorological station ($79^{\circ} 54' 53''$ N, $24^{\circ} 07' 32''$ W) was set up on the ice for measuring air temperature and wind speed as well as direction appr. 2 m above the ground. The barometric pressure is also recorded. This station is supposed to run at least until 1994, recording the data on a Campbell data logger. During the field season global radiation was also measured (8.7.-26.7.1993).

The ice surface at this part of the ice margin shows a highly variable pattern of light and dark areas. To get an idea of the albedo changes due to the varying dirt and dust content at the surface albedo spot measurements were carried out along the main stake line.

The 18 main stakes were positioned by means of GPS measurements, the intermediate stakes were surveyed from a fixed rock point beside the ice margin. The same point was also used as the fixed point for the GPS measurements and referred to an earlier triangulation point at Centrum Sø.

In addition surface ice sampling was done along two profiles, profile KS 450 m long (end point at $79^{\circ} 51' 13''$ N, $24^{\circ} 11' 58''$ W; spacing 2.5 m) and profile K1000 m long (end point at $79^{\circ} 54' 40''$ N, $24^{\circ} 06' 21''$ W; spacing 1 m), respectively, as well as along 20 m profiles at each of the main stakes. The marking poles for the 1000 m profile put in every 50 m were read for ablation purposes several times during the season.

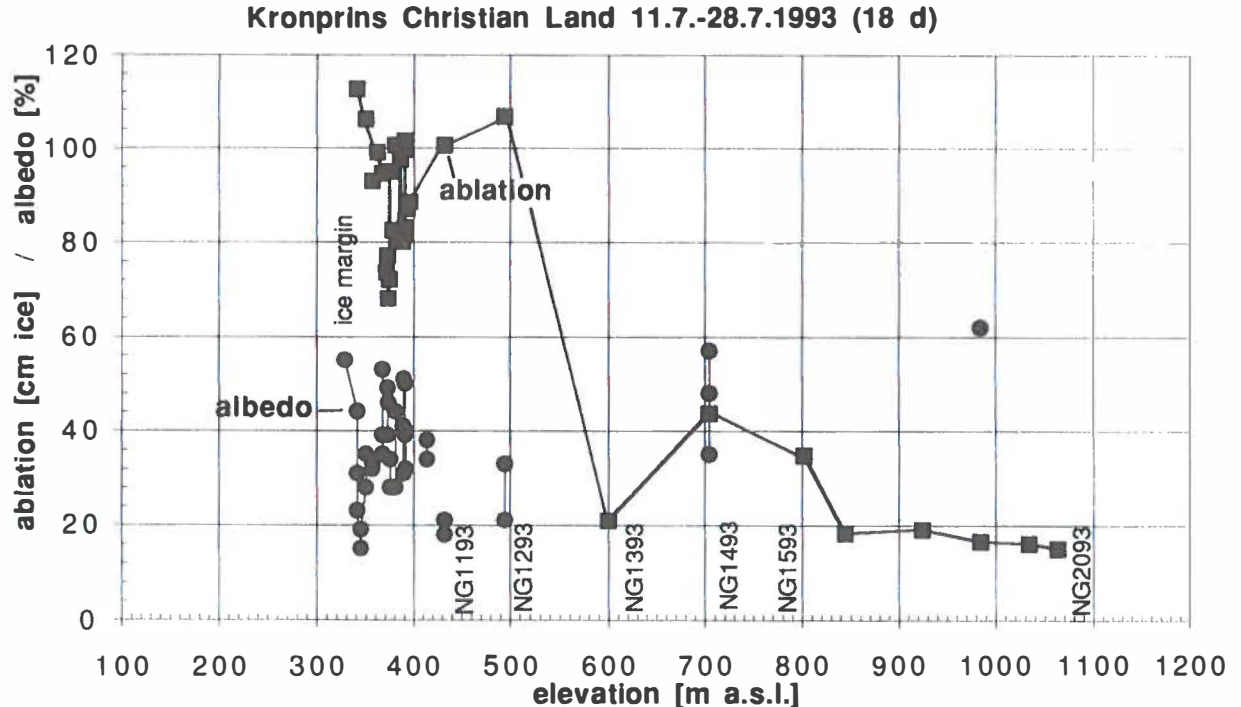


Figure 2: Ice margin Kronprins Christian Land: Results of ablation and albedo measurements in the summer season 1993 along the main stake line, extending from stake NG0293 at $79^{\circ} 54' 34''$ N, $24^{\circ} 03' 32''$ W to stake NG2093 at $79^{\circ} 33' 38''$ N, $26^{\circ} 17' 40''$ W (see figure 1).

First results

Figure 2 summarizes the ablation and albedo measurements along the main stake line. One can easily recognize the high variability of both ablation and albedo in the elevation interval 340-400 m, where ablation readings were done at distances of 50 m. There the mean albedo was $36.7 \pm 9.8 \%$ and in the period 11.7.-27.7.1993 (17 d) the mean ice ablation was $842 \pm 122 \text{ mm}$ ($758 \pm 110 \text{ mm we}$). For the corresponding time the mean air temperature at 2 m level at the meteorological station was $3.66 \pm 0.79 \text{ }^\circ\text{C}$. Using a temperature gradient of $0.7 \text{ K}/100 \text{ m}$, in total 67.2 degree days were available for melting, resulting in a degree-day factor of $11.2 \text{ mm we d}^{-1} \text{ K}^{-1}$. In the elevation interval 400-600 m, corresponding to a distance of 1-6 km from the ice margin, in general a very dark ice surface is exposed causing an increase in ablation due to albedo values which are there between 20 and 35 %. With the same corrections as above one obtains degree-day factors of $14.1 \text{ mm we d}^{-1} \text{ K}^{-1}$ and $17.5 \text{ mm we d}^{-1} \text{ K}^{-1}$ for the stake NG1193 (431 m a.s.l.) and NG1293 (494 m a.s.l.), respectively. At the end of the season we realized that stake NG1393 (600 m a.s.l.) was drilled just at a location where a local firn patch remained. Between the stakes NG1493 and NG1593, at appr. 750 m elevation and 12 km inland from the margin the zone with visible surface runoff starts. From this altitude upwards the ablation is decreasing.

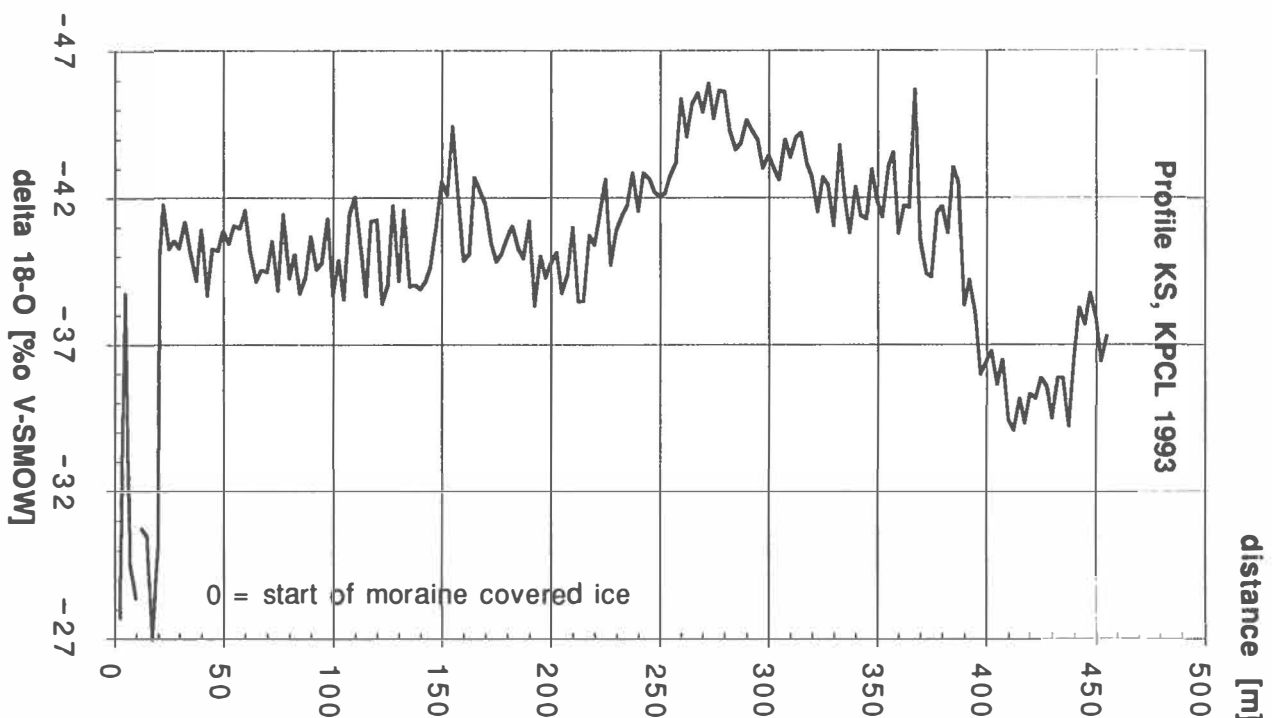


Figure 3: Ice margin Kronprins Christian Land: $\delta^{18}\text{O}$ values of southern profile KS. The sampling started (zero point) just above the moraine covered ice. At 20 m there was a very distinct transition from dirty lineated ice to lighter but dust covered brownish ice. There was a step of about 20-40 cm at the ice surface, obviously caused by the large albedo differences. Sampling was stopped where the brownish band was not clearly recognizable at the surface any longer.

The outermost brownish band along the ice margin extends at the southern profile KS over appr. 420 m inland from a sharp dirty boundary some 20 m above the moraine covered ice. Starting from the same boundary at the northern profile K this band extends over 640 m. Figure 3 shows the results of the $\delta^{18}\text{O}$ analyses of the samples of profile KS. By comparing this $\delta^{18}\text{O}$ profile with earlier measurements carried out in Pakitsoq, West Greenland (Reeh et al. 1991) or with ice core profiles one can clearly identify this brownish band as originating from ice-age ice. It is interesting to see that apparently ice from the last interglacial is missing. The sharp increase at 20 m is too large to count for Eemian ice. Most probably this ice belongs to a bottom ice layer.

References

Reeh, N., Oerter, H., Letréguilly, A., Miller, H., Hubberten, H.W. A new, detailed ice-age oxygen-18 record from the ice sheet margin in central West Greenland. *Palaeogeography, Palaeoclimatology, Palaeoecology (Global and Planetary Change Section)*, **90**, 373-383 (1991)

ETH GREENLAND CLIMATE PROGRAMME - BALANCE OF FOUR YEARS' FIELD EXPERIMENT

Atsumu Ohmura
Department of Geography
Swiss Federal Institute of Technology
Zürich, Switzerland

During the summer of 1993, our group carried out the last comprehensive field programme. With this season we have for the time being completed all of the initially planned experiments. This contribution is intended as a review of the past four years' achievements and of future activities.

The ETH Greenland Climate Programme has four main objectives:

1. Investigation of the relationship between climate and mass balance. This branch has three subprojects:
 - a) precipitation climatology,
 - b) surface energy balance with hydrology and
 - c) investigation of the mechanism of calving.
2. Modelling of the ice sheet and the climate. This subproject has two directions:
 - a) modelling of the ice sheet and
 - b) modelling of the Greenland climate within the GCM.
3. Application of satellite information especially for surface and cloud processes.
4. Understanding the climate of Greenland.

To Achieve the above objectives our group was engaged in both field and laboratory work. The field work was organised to investigate the surface energy balance together with the structure of the boundary layer not only for the sake of Point 1, but also with a hope of providing the GCM with a more realistic formulation of the boundary layer over ice surfaces. The work was also intended to obtain basic information on the surface features of the ice sheet and high quality radiative fluxes to use for calibrating the satellite data. Laboratory work were done in the areas of computation of the field of the atmospheric moisture budget, modelling of the ice sheet, the GCM and further updating of the climate data bank for Greenland, in addition to the evaluation of the field data.

The analyses of the field data on the surface energy fluxes, including the individual radiative components and net radiation, 30 m-tower and radiosonde observations for 1990 and 1991 were completed and used currently for further topic oriented studies, such as the structure of the boundary layer on the ice sheet and katabatic wind. The complete list of observed fluxes and climatic elements was presented in Ohmura (1993). The surface radiation fluxes and especially the processes for the radiative heating of the snow cover are included in the dissertation by Konzelmann (in press). The surface mass balance for the same years was also fully analysed. The data from the automatic weather station was successfully recovered for two consecutive winters, 1991/92 and 1992/93 and the station was fitted for another winter (Niederbäumer, 1994). The modelling of the ice sheet reached the first stage of completion with the two dimensional model along the EGIG line in the form of a dissertation by Abe-Ouchi (1993). The GCM works were concentrated on the investigation of the ability to reproduce the present climate jointly with Prof. L. Bengtsson's group at the Max-Planck-Institut für Meteorologie at Hamburg using the ECHAM3 with T-106 resolution. The means of the five years simulation reproduce very well the surface temperature, longwave radiation (both incoming and outgoing) and precipitation. Shortwave incoming radiation for the melt period is seriously underestimated mainly owing to the overestimation of the cloud amount. For the validity of the formulation of the surface turbulent fluxes, it was found that the GCM greatly overestimates sensible heat flux. Fig. 1 shows the relationship between the GCM computed and the sonic anemo-thermometer measured sensible heat flux during the Special Observing Periods in 1991. In addition the overestimation in the model, it seems that the range of the variation in the model computation is larger than the observed. The main cause of the overestimation is for one reason due to the small values in the Monin-Obukhov function which is currently used, but for the second reason, due to the strong departure of the wind and temperature profiles from the classic log-linear profile for the layer above 20 m. The lowest atmospheric layer in the model being about 31 m, the computation is done for the layers for which the present micro meteorological law is no longer valid. Between 20 m and 100 m, that is lower part of the katabatic wind, the profile becomes almost linear whose relationship to the vertical exchange processes is currently being investigated in our group.

To substantiate the ground-truth for the satellite, a special investigation was carried out in the summer of 1993, by observing the surface radiation and the atmospheric profile with radiosondes during the satellite overhead crossings. At the same time our partner group from the University of Colorado carried out the further measurements of the detailed bi-directional spectral reflectance of the snow cover. These data are going to be used for

charting the radiative components, global radiation, longwave incoming and outgoing radiation and the radiative characteristics such as albedo for the entire ice sheet (Haefliger, 1994).

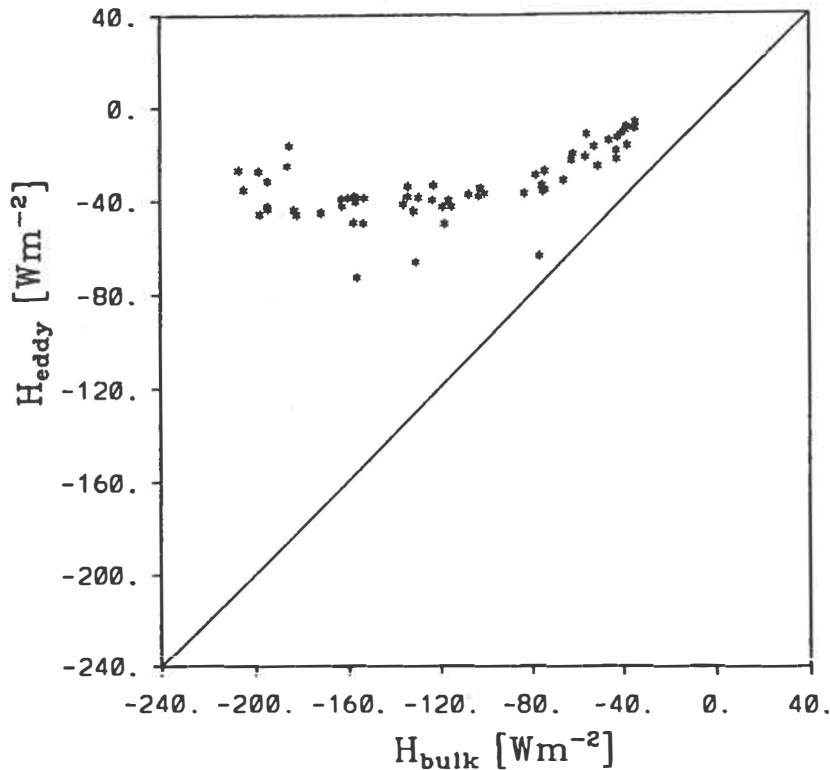


Fig. 1: Comparison of the sensible heat fluxes measured by a sonic anemo-thermometer (30 min. means) in summer 1991 and computed by a code in ECHAM 3. The observation periods were chosen from the runs with the surface at the melting point. The ECHAM 3 code for the surface sensible heat flux was activated with the observed temperature and wind speed for 30 m above the surface which closely approximates the lowest height of 31 m in the model.

The moisture flux field and the related quantities such as the divergence were investigated by Calanca (1993) to understand the transport mechanism of water vapour and the distribution of precipitation for the ice sheet. The ECMWF analyses proved to be extremely useful for this investigation. One of the possible applications is the computation of monthly or seasonal precipitation over the ice sheet, which is presently not available from the observation.

All observational data obtained during these activities outlined above are currently inserted into our Greenland Climate Programme data archive and will be used for updating the picture of the climate of Greenland.

The author takes the opportunity to thank the GCM group of Max-Planck-Institut für Meteorologie in Hamburg, especially Prof. L. Bengtsson and Dr. E. Reckner for providing valuable expertise for the ETH group. The computations was made in the Swiss Federal computing Centre at Manno. The project was financed by the grants from the Swiss National Foundation, Grant No. 21-27449-89 and 20-32648-91 and the Research Funds of the ETH Zürich No. 0-20-004-90, 0-40-040-90, 0-15-003-90, 0-15-150-90 and 0-43-018-91.

References

- Abe-Ouchi, A., 1993: Ice Sheet Response to Climate Changes. A Modelling Approach. Zürcher Geographische Schriften, Heft 54, Geographisches Institut ETH Zürich, 134 pp.
- Calanca, P., 1993: The Atmospheric Water Vapour Budget over Greenland. Dissertation ETH Zürich, pp 119.
- Haefliger, M., 1994: Radiation balance, derived from AVHRR for the Greenland Ice Sheet - preliminary results, in this issue.
- Konzelmann, T. in press: Radiation conditions on the Greenland Ice Sheet. Zürcher Geographische Schriften, Heft 56, Geographisches Institut ETH Zürich, 124 pp.
- Niederbäumer, G., 1994: Synoptic observation during two years from automatic weather station at the ETH camp, in this issue.
- Ohmura, A., 1993: ETH Greenland Ice Sheet Climate Programme: An Overview. In Reeh, N. and Oerter, H. (editors): Mass balance and related topics of the Greenland ice sheet. Open File Series 93/5, Grønland Geologiske Undersøgelse, Kopenhagen, p. 30-33.

**THE ROLE OF INFREQUENT HYDROLOGICAL EVENTS
IN GLACIFLUVIAL SEDIMENT TRANSPORT
FROM THE WESTERN MARGIN OF THE GREENLAND ICE SHEET,
NEAR KANGERLUSSUAQ (SØNDRE STRØMFJORD)**

Andrew J. Russell

School of Geography, Kingston University, U.K.

Aims

This paper examines processes and rates of glacial sediment transport along the northern flank of the Russell Glacier, Kangerlussuaq (Søndre Strømfjord) (Fig. 1). Attention is focused both on the transfer of sediment to a river channel subject to periodic jökulhlaups, and on the role of such floods in transporting sediment from the glacier margin.

Rationale

Although there have been previous studies of sediment yield from smaller alpine glaciated catchments, few studies have examined the capacity of larger ice sheet catchments to generate sediment. Knowledge of sediment transport from present ice sheets is essential for the interpretation of the Quaternary sedimentary record and for an assessment of the role of ice sheets in landscape modification. It is therefore essential that present ice sheet catchments are studied.

The field area (Russell Glacier)

Channel change resulting from a jökulhlaup in 1987 was examined within a river system along the northern flank of the Russell Glacier (Russell 1987,1991) (Fig. 1). Flood powers, sediment supply and channel resistance to erosion were found to vary considerably between channel reaches. Consequently, amounts of channel change and the character of the sedimentary record showed extreme variation (Russell, 1991). In addition, parts of the jökulhlaup channel which experienced backwater effects may have experienced two sediment transport peaks. Variations between the character of deposits found within each channel type reflect local differences in sediment supply, stream power and channel resistance to erosion.

Flow magnitude and frequency

Jökulhlaups from the large ice-dammed lake stand out as distinctive events within this catchment (Russell 1989,1993) (Fig. 1). The longer-term magnitude

and frequency of jökulhlaups from the large ice-dammed lake are difficult to determine as there is no record of such events other than from the downstream geomorphological and sedimentological evidence.

Sediment supply to the proglacial fluvial system

Glacial sediment is supplied to the main river channel both directly and indirectly. Englacial and subglacial meltwater transports sediment via conduits to the main proglacial rivers at several locations along the Russell Glacier. Where the river undercuts the ice-margin, sediment melts out directly into the river channels. In some locations the meltout and erosion of ice-cored moraine ridges supplies the bulk of sediment to the proglacial fluvial system. Supraglacial meltwater washes over debris covered areas of the glacier and ice-cored moraine ridges, resulting in the formation of debris or talus aprons comprising fluvial and debris flow sediment. Once sediment is expelled from the ice margin both 'normal' and jökulhlaup flows play a part in its removal. Although the relative roles of different flow magnitudes are not known, information is available regarding the transport of sediment during a jökulhlaup in 1987.

Jökulhlaups and sediment transfer

1987 jökulhlaup flows had the capacity to suspend coarse-sand and fine-gravel through most of the fluvial system on the northern side of the Russell Glacier. In places, material of up to gravel-size was capable of being suspended.

Ice-cored moraine ridges near the mouth of jökulhlaup conduit were undercut and eroded over a distance of 454m during the 1987 jökulhlaup, releasing 4704m³ of sediment (Fig. 1). Distinctive erosional trimlines marked the jökulhlaup limits on nearby moraine ridges. Moraine composition above the wash limits was dominated by material finer than sand or fine gravel-size (Fig. 2), while sediment below the trimline showed a greater concentration of larger clasts (Fig. 2). After the jökulhlaup, ice-cored moraines were subject to heavy ablation as the protective mantle of surface debris was removed, forming distinctive, sediment-rich meltwater plumes, releasing large clasts, and generating debris flows. moraine slumping, collapse, and flow were observed after 2-3 days of heavy rain during the 1988 field season. Nearly all of this material will be available for entrainment during the next jökulhlaup.

Small outwash fans were re-generated by supraglacial meltwater within the 1987 jökulhlaup wash limits within one meltseason. Rates of fan development were judged to be highest during periods of high discharge. These fluvial deposits are much better sorted than those derived directly from ablation and slope processes.

Jökulhlaups and sediment storage

Jökulhlaups increase sediment storage by preserving otherwise transportable sediment in high relief amplitude bars with armoured surfaces out of reach of normal flows (Russell, 1987). Following a jökulhlaup, sediment is deposited by fluvial and debris flow processes generated by ablation. The effectiveness of 'normal' processes will in turn determine the degree of channel change during the next jökulhlaup, resulting in a change in the volume of stored sediment.

Role of 'normal' flows in sediment transfer

Normal flows were only capable of reworking the finest jökulhlaup deposits, mainly in reaches subject to backwater conditions. Sand and gravel-sized material appeared to travel through most reaches within the main channels. Suspended and dissolved loads are likely to be highly significant but are as yet unquantified.

Applicability of results to downstream reaches and nearby catchments?

Where glacial sediment is relatively abundant the frequency of jökulhlaups will have less impact on rates of sediment transport. As the fluvial system on the northern flank of the Russell Glacier is sediment-limited rather than transport-limited, slower sediment re-stocking between jökulhlaups will result in lower rates of channel reworking. Examination of jökulhlaup routeways may therefore provide information about temporal and spatial variations in sediment availability. Both Leverett and Ørkendalen fluvial systems are fed by major subglacial conduits and have markedly different flow regimes (Fig. 3). It is therefore likely that sediment transport characteristics (magnitude and frequency) of these systems will differ both from each other and from the those within the Russell catchment.

Implications for future research

Proposed fieldwork involves hydrological measurement, during the summers of 1994 and possibly 1995, at several locations on rivers draining into the head of the Søndre Strømfjord (Fig. 3). River stage, water temperature, turbidity, and electrical conductivity data will be logged automatically using Squirrel data loggers (Fig. 3). Suspended sediment samples will be obtained at regular intervals at each reach and at a number of meltwater portals. This will allow the relationship between meltwater flow regime and sediment concentration (suspended and dissolved) to be compared between these different systems.

References

Russell, A. J. 1987. Bar sedimentology and morphological change following a jökulhlaup in West Greenland. (Abstract) In Abstracts of the 26th Annual Meeting of the British Sedimentological Research Group (December 1987). *University of Aberdeen, Department of Geology, Occasional Paper.*

Russell, A. J. 1989. A comparison of two recent jökulhlaups from an ice-dammed lake, Søndre Strømfjord West Greenland. *J. Glaciol.*, 35(120), 157-162.

Russell, A. J. 1990. The geomorphological and sedimentological effects of jökulhlaups. *PhD thesis.*, University of Aberdeen, 135pp.

Russell, A. J. 1993. Obstacle marks produced by flows around stranded ice blocks during a jökulhlaup in West Greenland. *Sedimentology.*, 21pp.

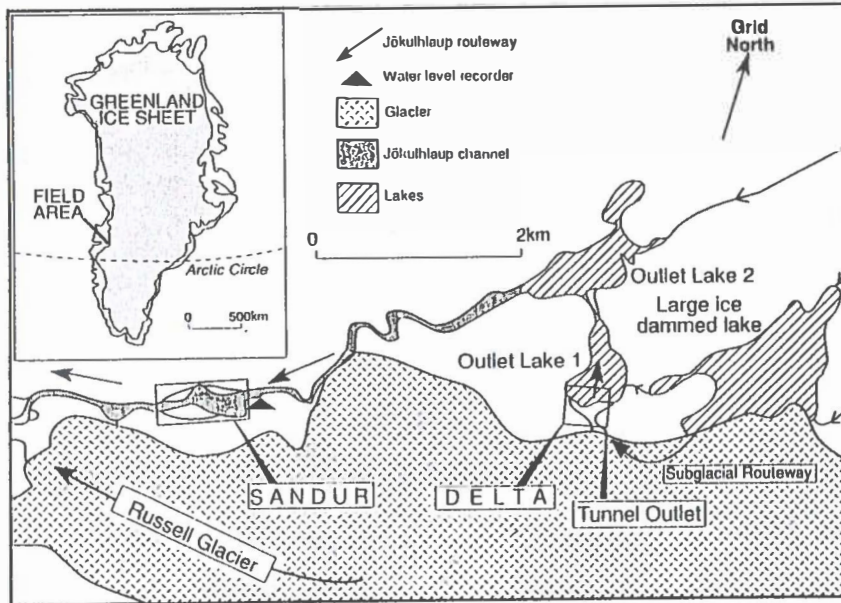


Figure 1

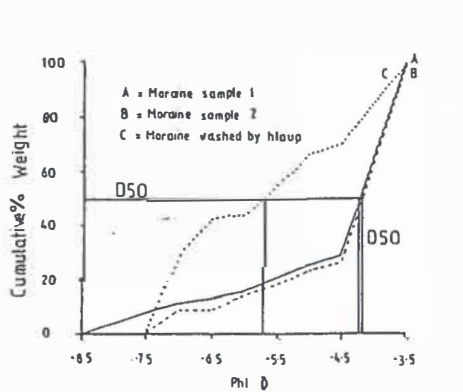


Fig. Cumulative % grain size distributions of two moraine samples taken above maximum flood wash limits downstream of Sandur 1 (Fig. 2.20). Third plot (c) represents material below the jökulhlaup trimlines.

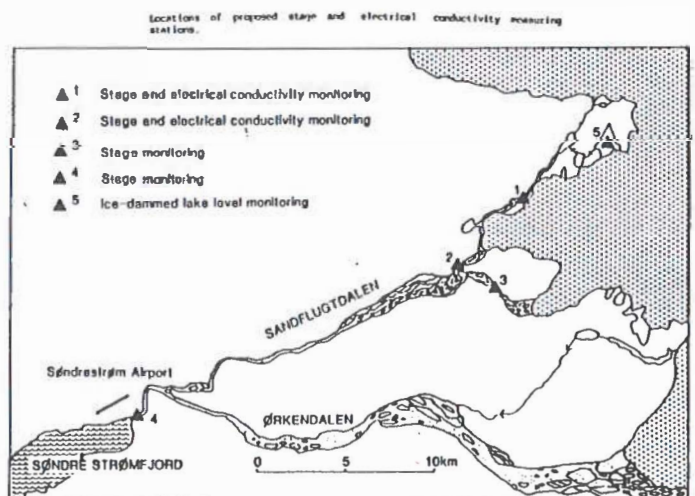


Figure 3

MASS BALANCE CALCULATIONS AROUND GRIP, CENTRAL GREENLAND

Christine Schøtt Hvidberg, Kristian Keller & Niels Gundestrup
 Geophysical Department
 University of Copenhagen, Denmark

Introduction.

Recently two deep drilling projects have been completed to bedrock in the Summit region in Central Greenland, the European GRIP (Greenland Icecore Project, 72,58 °N, 37,64 °W) and the U.S. GISP 2 (Greenland Ice Sheet Programme, 72,58 °N, 38,47 °W). In connection with the GRIP project several glaciological surface programs were carried out in the Summit region. These programs include observations of surface elevations and velocities, and preliminary data are now available (Keller, this publication). Observations of accumulation rate and ice thickness are furthermore available in the area (Clausen et al., 1988, Dahl-Jensen et al., 1993, Hodge et al., 1990, Alley et al., 1993).

These observations together with velocity-depth profiles derived from ice core analyses lead to a preliminary estimate of the global mass balance in the Summit region. Also sufficient data are available for a preliminary estimate of the local mass balance at the GISP 2 bore hole location.

Global mass balance.

The global continuity for an area A can be expressed as

$$A \frac{\partial H}{\partial t} = Q_{acc} - Q_{ice} = \int_A a \, dA - \int_L u_m H \, dL$$

where H is ice thickness, t is time, $\partial H/\partial t$ is the global rate of ice thickness change, Q_{acc} is the total accumulation flux in the area A , a is accumulation rate, Q_{ice} is the total ice flux out of the area, L is the boundary of the area A , and u_m is the depth averaged horizontal velocity component normal to the boundary. A shape factor, $f = u_s/u_m$ is introduced, where u_s is the surface velocity.

The surface topography and surface velocities has been measured around GRIP by using Global Positioning System (GPS, Keller, this publication). The horizontal surface velocity has been measured at 8 positions at distances from GRIP of 25-45 km. The horizontal velocities are in the order of 1-3 m/yr, with an error of about 15-20%. In this study, the global mass balance in the area within a radius of 30 km from the GRIP location will be investigated.

The average accumulation rate in this area is to a first order the accumulation rate at GRIP. At GRIP the mean accumulation rate through the last appr. 1000 years is 0.23 m of ice equiv./year (Dahl-Jensen et al., 1993). The recent accumula-

tion is 0.228 ± 0.003 m of ice equiv./year (Sigfus Johnsen, pers. comm.).

The ice thicknesses in the region have been measured by airborne ice radar survey (Hodge et al., 1990). The thickness in the area is relatively constant at about 3000 m of ice equiv., however decreasing to about 2700 m of ice equiv. in the eastern part. The error of the ice thickness is ± 50 m.

The shape factor f is determined by assuming an analytic horizontal velocity profile, which is constant in the upper layers and decreasing linearly to zero at the bottom. A best fit of the annual layers derived from this analytical profile to the observed annual layers along the deep ice cores determines the shape of the horizontal velocity profile (Dahl-Jensen et al., 1993), and a value of $1/f = 0.79 \pm 0.01$ is obtained.

The total ice flux, Q_{ice} is calculated by integrating $u_m H$ over the boundary of the area within a radius of 30 km around GRIP. $u_m H$ is integrated piecewise, by assuming a linear variation between the directions pointing from GRIP to a position, at which the surface velocity is observed.

The result for the global mass balance within 30 km from GRIP is

$$\partial H / \partial t \text{ (global)} = 0.5 \pm 4.3 \text{ cm of ice equiv./yr}$$

The error of this result is largely dominated by the error of the velocity observation, which contribute with about ± 3.3 m of ice equiv./yr to the error of the global mass balance. More accurate observations will be obtained after the 1994 field season.

Alternatively, f was calculated with velocity profiles given by a finite element model (Hvidberg, unpublished). The model calculated the steady state ice flow and temperatures along a flow line with a horizontal bed, and considered the divergence of the ice flow. With the flow law parameters assumed uniform in the ice, $1/f = 0.88$ was calculated. If this is taken into account by increasing the error of f to ± 0.1 , the resulting error of the global mass balance increases to ± 7.3 cm of ice equiv./yr.

Local mass balance at GISP 2.

By introducing a horizontal (x, y) -coordinate system with the x -axis in the direction of the flow, the local continuity can be expressed as (Reeh and Gundestrup, 1985)

$$\frac{\partial H}{\partial t} \text{ (local)} = a - \frac{1}{f} \left(H \left(\frac{\partial u_s}{\partial x} + \frac{\partial v_s}{\partial y} \right) + u_s \frac{\partial H}{\partial x} \right)$$

where u_s and v_s are the surface velocities in the x and y direction respectively, and f is assumed constant along the flow line. Surface strain rates are not yet available, therefore the transverse strain rate is assumed to be $\partial v_s / \partial y = u_s / R$, where R is the radius of curvature of the surface contour lines.

At the GISP 2 bore hole site, which is located 28 km west of GRIP, R is determined to 24.3 ± 3.5 km (Keller, this publication), the ice thickness gradient is estimated to 0.001 ± 0.010 (Hempel and Thyssen, In press), the ice thickness $H = 3029$ m of ice equiv., $a = 0.248 \pm 0.003$ m ice equiv./yr (Alley et al., 1993),

and u_s is 1.32 ± 0.25 m/yr (position close to GISP 2; see Keller, this publication).
The local mass balance is estimated to

$$\partial H/\partial t \text{ (local)} = 0.4 \pm 7.6 \text{ cm of ice equiv./yr}$$

Conclusion.

This mass balance study indicates that the Summit region of the Greenland Ice Sheet is close to mass balance at present. However, the error of the calculated mass balance is large, about 25% of the annual accumulation. This is mainly due to the uncertainty of the surface velocity data, which will be improved in 1994. The long term effects contributing to a surface elevation change, from the slow thinning of the layer of soft Wisconsin ice, and from the increase of basal temperatures due to the warmer temperatures since the termination of the ice age, should be considered, when interpreting the mass balance result. However, simulations of these effects give a surface elevation change at present of -0.4 cm of ice equiv./yr (Abe-Ouchi, 1993), which is below the detection limit.

Acknowledgements. This work is a contribution to the Greenland Icecore Project (GRIP), a European Science Foundation Programme with eight nations collaborating to drill through the Central Greenland Ice Sheet.

References.

- Abe-Ouchi, A. 1993. Climatic impact on the Greenland Ice Sheet: A modelling approach. Mass balance and related topics of the Greenland Ice Sheet., eds. N. Reeh and H. Oerter, Open File Ser. Grønlands geol. Unders., 93/5, 20-21.
- Alley, R. et al. 1993. Abrupt accumulation increase at the Younger Dryas termination in the GISP 2 ice core. *Nature*, 362(6420), 527-529.
- Clausen, H.B. et al. 1988. Glaciological Investigations in the Crête Area, Central Greenland: A search for a new deep-drilling site. *Annals of Glaciology*, 10, 10-15.
- Dahl-Jensen, D. et al. 1993. Past accumulation rates derived from observed annual layers in the GRIP ice core from Summit, Central Greenland. Nato Advanced Research Workshop Publication, workshop held in Aussois, France.
- Hempel L. and Thyssen, F. In press. Deep radio echo soundings in the vicinity of GRIP and GISP 2 drill sites. *Polarforschung*, 62(1).
- Hodge, S. et al. 1990. Determination of the surface and bed topography in Central Greenland. *Journal of Glaciology*, 36(122), 17-30.
- Hvidberg, C. S. Unpublished. A thermo-mechanical ice flow model for the centre of large ice sheets. Phd-thesis submitted to University of Copenhagen, 1993.
- Keller, K. et al. Mass balance studies at Dome GRIP using GPS and gravity. This publication.
- Reeh, N. and Gundestrup, N. 1985. Mass balance of the Greenland Ice Sheet at Dye 3. *Journal of Glaciology*, 31(108), 198-200.

INVESTIGATIONS ABOUT REFRACTION INFLUENCES IN TRIGONOMETRIC LEVELING ON THE GREENLAND ICE SURFACE

Manfred Stober
Fachhochschule für Technik, Stuttgart, FRG

1. Introduction

The error budget of the trigonometric leveling is mainly dominated by influences of vertical refraction. Therefore in 1991 a geodetic research program took place on the Greenland ice surface at the Swiss station (Department of Geography of ETH Zürich, Prof. Dr. A. Ohmura). The program was financially promoted by the Deutsche Forschungsgemeinschaft (DFG)

In this paper the following questions should be mainly investigated:

- What is the amount of the refraction coefficient above ice depending on different atmospheric conditions ,
- Is it possible to calculate the refraction coefficient by using meteorological dataa?
- Which sytematic errors can we expect in the measured height differences.

2. Theoretical background

From simultaneous reciprocal zenith angles between two points 1 and 2 we obtain the height difference Δh

$$\Delta h = S/2 * (\cos Z_1 - \cos Z_2) - S^2/(4R)*(k_1 - k_2) . \quad (1)$$

with S = slope distance,
 Z_1, Z_2 = zenith angles on stations 1 and 2 ,
 k_1, k_2 = efficient refraction coefficients in 1 und 2,
 definition of the refraction coefficient $k = R/r$.
 R = earth radius (about 6384 kma) ,
 r = radius of beam of light

Only if the efficient refraction coefficients are equal in both stations ($k_1 = k_2$), the height difference is free from systematic refraction errors. Under this condition we obtain the true height difference

$$\Delta h = S/2 * (\cos Z_1 - \cos Z_2) . \quad (2)$$

and the mean efficient refraction coefficient k for the whole line from

$$k = 1 + R/S * (200 - Z_1 - Z_2) * \pi/200 \quad (3)$$

If the true height difference Δh_t between two stations is known, the efficient refraction coefficient k_1 in station 1 is to be calculated from

$$k_{1a} = 1 + (S \cdot \cos Z_1 - \Delta h_t) \cdot 2 R / s^2 \quad (4)$$

Local refraction coefficients can be calculated from vertical temperature and humidity profiles. If we accept an atmosphere with globe-symmetric stratification we obtain with the refractive law of SNELLIUS

$$n \cdot \sin Z = \text{const}$$

the local refraction coefficient by

$$\kappa = R / r = - \sin Z / n \cdot (dn/dh) \quad (5)$$

with Z = zenith angle ,
 n = refractive index ,
 dn/dh = vertical gradient of the refractive index.

From the relationship of BARRELLA+ SEARS for the refractive index as a function of absolute temperature (T) air pressure (p) and partial water vapor pressure (e) we find the local refraction coefficient

$$\kappa = 501,525 \cdot \sin Z \cdot p/T^2 \cdot (0,034 + dT/dh) + 79,135 \cdot \sin Z/T \cdot de/dh \quad (6)$$

Applying this method we have to determine the gradients

dT/dh = vertical temperature gradient
 de/dh = vertical water vapor pressure gradient

and from those calculate the local refraction coefficient κ .

3. Results from simultaneous reciprocal zenith angles

The refraction coefficient above snow is generally positive (tabel 1) The beam of light has a curvature in the same SENSE as the earth. The refraction coefficient is depending on the topography. Under almost every weather conditions the refraction coefficient on line A2-C2 is essentially greater (mean $k = 1,06 \pm 0,12$) than on the lines A2-B2 and B2-C2 (mean $k = 0,27 \pm 0,06$). The topography on line A2-C2 is convex (curvature in same SENSE as the earth), so the beam of light has in the middle of the line only a distance of about 0,5 m to the snow surface. Against that, the topography of lines A2-B2 and B2-C2 has a concave curvature, so the distance between the light path and the ground is greater (about 2,5 m) in the middle of the line.

4. Interdependence of the refraction coefficient on meteorological data

For this purpose the observations were grouped in series of constant meteorological conditions, these mainly are those measurements from the same day. At first we want to examine whether there will be a dependence from k on only one single meteorological parameter such as

- velocity of wind
- global radiation
- direct sun radiation

- net radiation
- difference between global and direct sun radiation

4.1 Dependency on velocity of wind

The refraction coefficient is increasing with the wind speed (fig. 1). At all the three test areas, the regression line has the same angle of inclination, although the values of k are varying considerably from area to area. This result might be astonishing, because in the lowest layers there was a stable atmosphere during most of the days, which apparently could not be changed in spite of stronger wind speed.

4.2 Dependency on radiation

The best (negative) correlation between k and various kinds of radiation are found to the relative radiation difference, which is defined here as the difference between global and direct sun radiation divided by the global radiation (fig. 2) a Increasing k is corresponding with decreasing relative radiation difference. In this case the global radiation is approaching the direct sun radiation, that means free sky without clouds.

The refraction coefficient k is contrarily effected by global radiation and direct sun radiation. While k is increasing with increasing sun radiation, it is decreasing with global radiation, probably caused by different parts of long wavelength radiation

The relationship between k and net radiation has the form of a parabola with the minimum of k when net radiation is near zero. All the three test areas show the same behaviour.

All these statements cannot give more than a trend, because of the standard deviations of k and because of the dependency on the various test areas So the significance level is only 80 - 90 % .

4.3 Dependency on time

In this evaluation all mentioned times are the local standard camp time (LCT) a which is related to GMT with

$$\text{LCT} = \text{GMT} - 4 \text{ h} .$$

The station is situated in geographic longitude $\lambda=49,3^\circ$ West, so the local time would better correspond to GMT - 3,3 ha and the used LCT is displaced 0,7 h against the mean sun time.

At two of three test areas we see a dependency of the refraction coefficient on a function of local camp time with a minimum of k at 10 h (fig. 3). The sorting of the data in sunny days with wind (k big) and overcast days without wind (k small) is clearly confirmed.

Summarising we see that the refraction coefficient is influenced by wind speed and radiation, but it is not possible to predict the refraction coefficient from only one single meteorological parameter.

Only the combination of the two most evident parameters -- velocity of wind and relative difference between global and sun radiation -- show the relationship a little better. If weather conditions with relative difference of radiation $< 0,5$ are called as mainly "overcast", k is decreasing from "sunny with wind", "sunny without wind", "overcast with wind" to "overcast without wind". The smallest values of k we find during "overcast without wind" (average $k = 0,04 \pm 0,05$), especially when the beam of aiming has a larger distance from the snow surface.

5. Refraction coefficients calculated from vertical temperature and humidity profiles

From formula (6) local refraction coefficients K_1 could be calculated with the ETH-data (30-meter tower), and they could be compared to the efficient refraction coefficients k from simultaneous reciprocal zenith angles (fig. 4). At all the three test areas the values resemble very good each other, but sometimes greater differences ($k - K_1$) up to about 0,6 are apparent. If the various distances between the line of sight and the snow surface are taken into account and if we calculate an integral refraction coefficient K , the differences ($k - K$) become even better (fig. 5).

The remaining differences ($k - K$) may have several causes :

- the vertical temperature profile at only one station (starting point of a line) is not a representative one,
- refraction is not symmetrically in both ending points of a line, and therefore k from reciprocal zenith angles cannot be correct.

Further investigations will be carried out for this topic.

6. Refraction coefficients from zenith angles in one station and true height differences

True height differences Δh_t are known from trigonometric leveling with short sides and from a long observation period of the test areas. So it is possible to calculate refraction coefficients at one station by formula (4), efficient in only one direction. In case of reciprocal observations we are able to calculate one-side refraction coefficients (k_1, k_2) in each station independently, and we can compare the differences ($k_1 - k_2$). As we see from figure 6, the refraction coefficients k_1 and k_2 are not always equal and so they indicate unsymmetric refraction in both stations. In test area C2-A2 the differences ($k_1 - k_2$) rise up to 0,55, corresponding to a systematic error in height of 14 mm (last term in formula (1)).

7. Systematic refraction errors in simultaneous reciprocal observations

Using formula (2), the calculated height differences should be free from refraction errors, if they are symmetrically in both stations. In order to test his hypothesis, we compare them against their true values Δh_t (fig. 7). In test area C2-A2 the mean values of the groups 4,6,7,11, and in test area C2-B2 of the groups 1 and 2 are significantly biased up to 12 mm. In spite of simultaneous reciprocal zenith angles, we did not succeed in eliminating the whole influence of unsymmetrical refraction errors. This statement is corresponding to the results from chapter 6.

8. Summary

The refraction coefficient over the snow surface in Greenland arises up to $k \approx 2$, so it is about one order bigger than in usual central European conditions. k is varying with meteorological parameters, small values can be found when sky is overcast without wind. It is not possible to derive a functional dependency of k on single meteorological parameters.

In order to determine k , the crucial point is the vertical temperature gradient. Local refraction coefficients agree well with those derived from simultaneous reciprocal zenith angles, even better, when the actual distance between sight line and snow surface is considered along the whole range.

In spite of simultaneous reciprocal zenith angles, however, remaining systematic refraction errors occur up to about 2 cm for a height difference over a range of 1 kilometera

REFERENCES

- BROCKS, K.:** Die Lichtstrahlkrümmung in Bodennähe.
Deutsche Hydrographische Zeitschrift, Band 3, Heft 3/4, 1950
- DODSON, A.H. und ZAHER, M.a**
Refraction Effects on Vertical Angle Measurementsa.
Survey Review Vol. 28, 217, July 1985a.
- STOBER, M.:** The Geodetic programme 1990/1991 .
Ina: OHMURA et al.: ETH Greenland Expedition,
Progress Report No. 2,
Department of Geography, ETH Zürich, October 1992.
- WEBB, E. K.a** Temperature and Humidity Structure in the Lower Atmosphere.
Ina: BRUNNER, F.K. (Editor)a Geodetic Refractiona,
Springer-Verlag 1984.

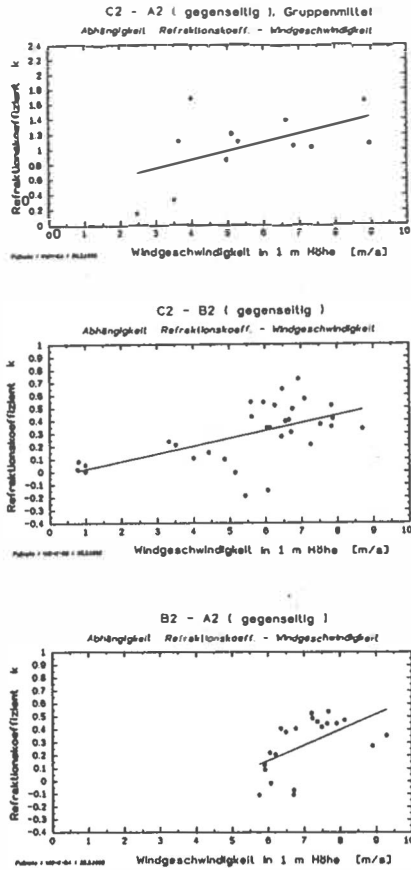


Fig. 1: Interdependence from refraction coefficient on velocity of wind at three different test areas

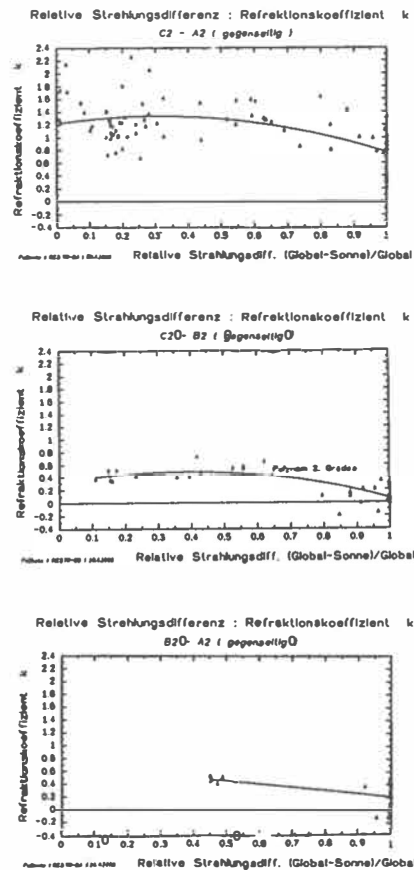


Fig. 2: Interdependence from refraction coefficient on relative difference between global and direct sun radiation at three different test areas

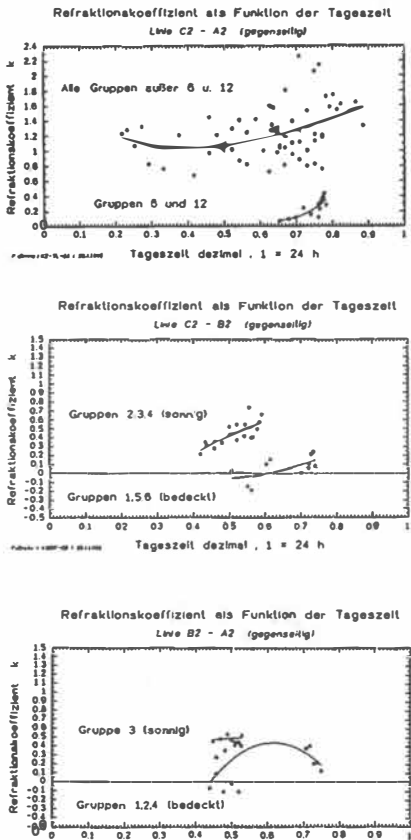


Fig. 3: Refraction coefficient as function of local camp time

line	group	date	time	atmospheric conditions			
				rel. diff. global-sun radiation			
				< 0,5 sunny		> 0,5 overcast	
				with wind	without wind	with wind	without wind
		1991	standard				
			camp time				
			= GHT - 4 h				
A2 - C2	1	30.07.	14.00 - 19.30	1.65			
	2	31.07.	11.00 - 13.30			1.03	
	3	31.07.	15.40 - 18.33			0.87	
	4	1.08.	10.00 - 13.30	1.11			
	5a	1.08.	16.00 - 17.30	1.21			
	5b	1.08.	18.00 - 18.30			1.21	
	6	4.08.	15.50 - 18.45				0.11
	7	5.08.	14.30 - 18.30	1.03			
	8	6.08.	15.40 - 16.00		1.12		
	9	6.08.	18.20 - 21.30		1.68		
	10	8.08.	5.10 - 9.20			1.08	
	11	15.08.	15.00 - 15.40			1.37	
	12	16.08.	18.15 - 18.40				0.36
A2 - B2	1	11.08.	17.00 - 18.00				0.27
	2	14.08.	11.00 - 12.40				0.39
	3	15.08.	10.48 - 12.50	0.49			
	4	16.08.	10.35 - 12.30			-0.02	
B2 - C2	1	10.08.	12.00 - 17.45				0.03
	2a	11.08.	10.00 - 11.30				
	2b	11.08.	12.00 - 13.30	0.47			0.26
	3	13.08.	10.25 - 13.00	0.39			
	4	15.08.	13.20 - 14.15	0.54			
	5	16.08.	13.00 - 14.45			-0.003	
	6	16.08.	17.20 - 17.45				0.18

Table 1: Efficient refraction coefficients k from simultaneous reciprocal zenith angles, arranged at relative difference between global and direct sun radiation and velocity of wind

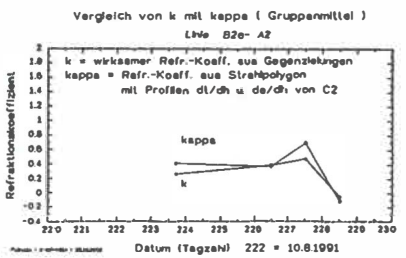
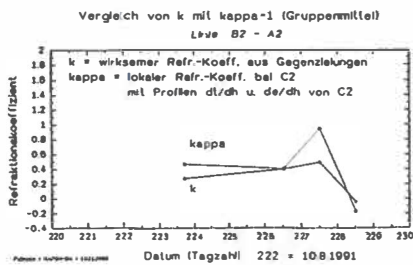
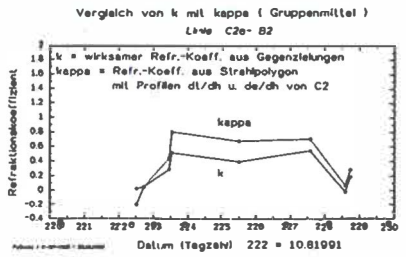
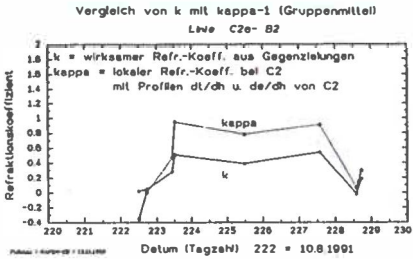
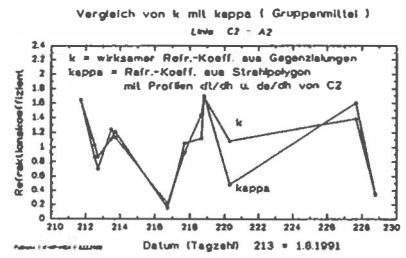
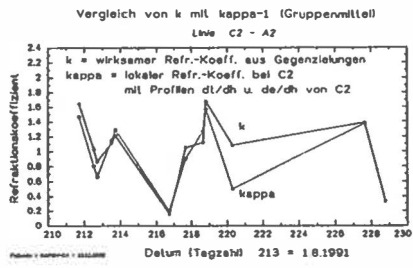


Fig. 4: Comparison between efficient refraction coefficients (k) from reciprocal zenith angles and local refraction coefficients (K1) from vertical temperature and humidity profiles at station C2.

Fig. 5: Comparison between efficient refraction coefficients (k) from reciprocal zenith angles and local refraction coefficients (K) from vertical temperature and humidity profiles with variable distances to the snow surface along the whole range.

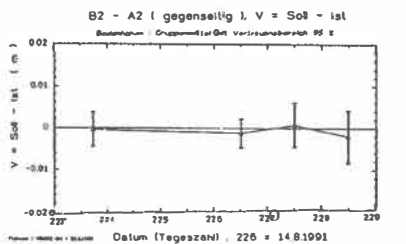
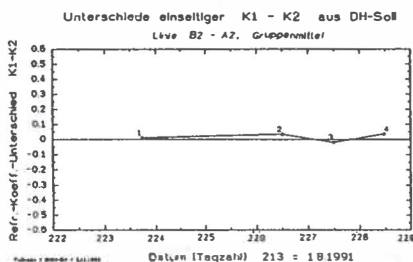
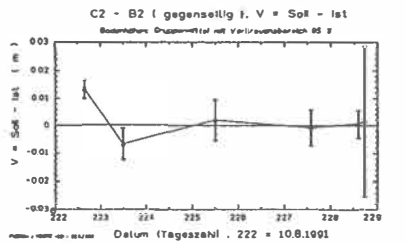
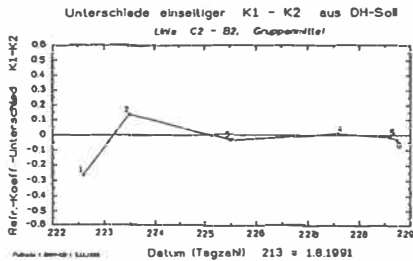
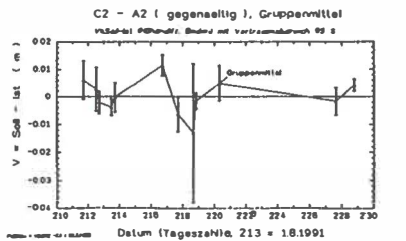
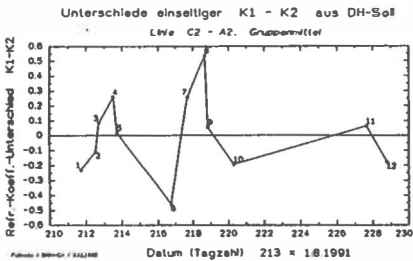


Fig. 6: Differences (k1-k2) of one - side refraction coefficients from true height differences

Fig. 7: Discrepancies of height differences from simultaneous reciprocal zenith angles and true height differences

**CHANGE IN POSITION AND ALTITUDE
OF A SMALL OUTLET GLACIER DURING THE PERIOD 1943-1992,
LEVERETT GLACIER, WEST GREENLAND**

Frank G.M. van Tatenhove¹ & Chris M. Roelfsema²

¹ Fysisch Geografisch en Bodemkundig Laboratorium
University of Amsterdam, Amsterdam, The Netherlands

² Faculty of Geodesy, Technical University Delft,
The Netherlands

Within the study on the Holocene deglaciation dynamics of a part of the western margin of the Greenland ice sheet special attention is given to recent, i.e. historical, fluctuations of the ice sheet. Fluctuations in position and surface altitude of the Leverett glacier are determined from a photogrammetrical analysis.

The Leverett glacier in west Greenland is a small outlet glacier draining the main ice sheet. Its area encompasses approximately 161 km². Within glacier inventory of west Greenland glaciers, the Leverett glacier has been coded 1DG03002 (Weidick et al, 1992, GGU report 158). That part of the glacier surrounded by mountains is ± 7 km². These mountains have a maximum altitude of 582 m.a.s.l. From large parts of the western margin of the Greenland ice sheet, aerial photographs are available from the fourties, sixties and eighties. In the Leverett area, the aerial photographs are from 1943, 1968 and 1985. With the use of these photographs a detailed reconstruction of glacier fluctuations and changes in ice marginal morphology is possible.

In 1992 a glacial geological expedition was held to the Leverett glacier. This expedition was part of the Dutch research effort in west Greenland, known as the GIMEX-project. A geodetic net around the Leverett glacier was erected to enable a quantitative analysis of aerial photographs and to measure transverse and longitudinal profiles on the glacier and several points on moraines. Results of the analysis of the moraines will be reported in a separate paper.

During the GIMEX 1992 expedition 6 controlpoints were measured in the surrounding of the Leverett glacier with the use of a distancemeter (AGA 220 Geodimeter) and theodolite (Wild T2). The position of the controlpoints was based on the recognizability of the points on 3 sets of aerial photographs. The maximum standard deviation of the controlpoints are

$$\sigma_x = 0.03 \text{ m}; \quad \sigma_y = 0.03 \text{ m}; \quad \sigma_z = 0.10 \text{ m}$$

A longitudinal and transverse profile on the glacier and 15 points on ice marginal moraines were measured using the same equipment. The accuracy of these points is less than the accuracy of the control points, but is estimated to be better than the accuracy of the most distant point on the longitudinal profile. The accuracy of this point (± 1500 m from control-point 1) is given by

$$\sigma_x = 0.05 \text{ m}; \quad \sigma_y = 0.05 \text{ m}; \quad \sigma_z = 0.11 \text{ m}$$

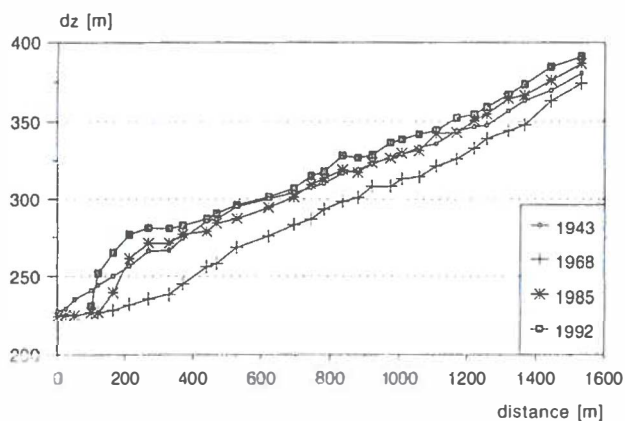
Photogrammetrical measurements were carried out on a Zeiss Planicom C100 at the faculty of Geodesy of the Technical University in Delft. The altitude of points could be measured with an absolute accuracy of $\sigma_z < 0.86 \text{ m}$. This figure includes the errors introduced by the identification of control points on the areal photographs, the size of the stereographical overlap, photoscale, filmdeformation, camera distortion, flight height, measuring errors and errors in terrestrial measurements.

Results.

During the period 1943 - 1968 the average amount of wasted ice on the Leverett glacier was $15.1 \pm 0.1 \text{ m}$. A thickening is registered in the period 1968 - 1985 of $18.8 \pm 0.2 \text{ m}$. This thickening continues during the period 1985 - 1992. In this period the average altitude increased with $7.0 \pm 0.5 \text{ m}$. Before 1985, these figures are based on the digital terrain model which has been measured on a 25 m grid. After 1985 the altitude changes is determined from the longitudinal profile. The associated fluctuations of the ice margin are: retreat of 200 - 350 m during the period 1943 - 1968; an advance of 150 - 200 m in the period 1968 - 1985 followed by an advance of $\pm 175 \text{ m}$ from 1985 to 1992.

The recent thickening of the Leverett glacier is regarded as real within the light of measurement error and year to year variability in ablation. Similar advances of the ice margin can be observed along the Russell glacier to the north and have been observed in the Ørkendalen to the south. Although a quantitative evaluation in the latter areas is not possible, we think that thickening and advances of the ice margin are a regional phenomena in the central part of west Greenland.

LONGITUDINAL PROFILE 1943 : 1968 : 1985 : 1992



TRANSVERSE PROFILE 1943 : 1968 : 1985 : 1992

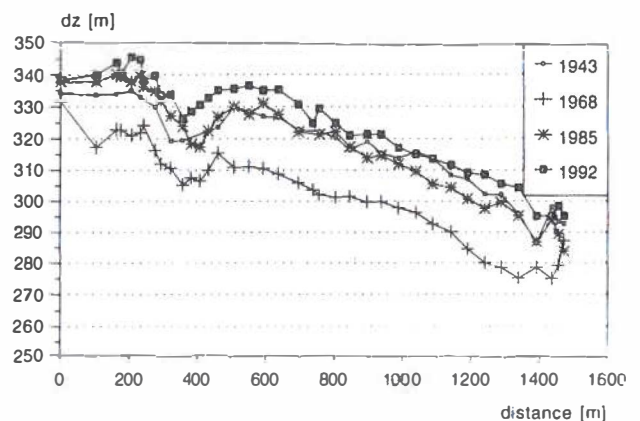


Figure 1: Longitudinal and transverse profiles over the Leverett glacier illustrating the change in surface altitude and frontal position.

GREENLAND ICE SHEET THICKNESS CHANGES MEASURED BY LASER ALTIMETRY

R. Thomas¹, W. Krabill², S. Manizade³ & K. Jezek⁴

¹ Code YS, NASA HQ, Washington, USA

² NASA/Wallops Flight Facility, USA; ³ EG&G, USA

⁴ Byrd Polar Research Center, USA

INTRODUCTION

We do not currently know whether the ice sheets of Greenland and Antarctica are growing larger or smaller. Available glaciological data suggest that they are in balance to within an equivalent sea-level rise or fall of about 3 mm per year. This large uncertainty is partly because the ice sheets are very large and very remote, but also because mass-balance is generally computed by comparing estimates of total snow accumulation with estimates of total loss, by both melting and ice discharge - the comparison of two very large numbers, each of which has significant errors. A more direct indication of ice-sheet mass balance can be obtained by comparing precise, repeat measurements of many surface-elevation profiles across the ice sheets. However, conventional surveying techniques are time consuming and costly, and to date only one profile across the Greenland ice sheet has been optically levelled (Seckel, 1977) and none has been attempted across the Antarctic ice sheet.

Surface-elevation profiles can also be estimated from satellite radar-altimetry data, but only over surfaces with slopes of less than about one degree. Moreover, errors are introduced by surface slopes and undulations within the large beam-limited radar footprint and by radar penetration into the surface snow. Nevertheless, by comparing data obtained at points where orbit tracks from one survey cross those from an earlier survey, Zwally et al (In preparation) conclude that central parts of the Greenland ice sheet south of 72° north thickened between 1978 and 1987 by 1.3 meters - an average of 15 cm/year.

Many of the problems in the interpretation of satellite radar altimeter data can be overcome by using a laser altimeter with a footprint, from satellite orbit, of a few tens of meters. Unfortunately, the earliest satellite laser altimeter to orbit the Earth is currently planned for launch early next century as part of NASA's EOS program. Meanwhile, in September 1991, in April 1992, and in June/July 1993 NASA conducted airborne laser-altimeter missions over Greenland in an attempt to determine whether ice-surface elevations can be measured from an aircraft to the accuracy needed to detect ice thinning or thickening over periods of a few years. Here, we present results from repeated flight lines over the Jakobshavn Glacier, and from flights over locations on the ice sheet where earlier precise position fixes had been obtained from Doppler satellite measurements.

RESULTS

The results presented here are preliminary. The accuracy of 1991 data is limited, primarily by the number of GPS satellites then available for tracking. The impact is to degrade the accuracy of derived ice topography with increasing flight time. In 1992 and 1993, this aspect of the experiment progressively improved as more GPS satellites were launched. Moreover, we have continued to discover small corrections that can be applied to the data to effect further improvements. However, we believe that this stage of the experiment is complete, and that we have detected all the significant sources of error. Comparison between the 1991 airborne measurements and data from an optically-levelled traverse along the flight track suggest that the airborne data are consistent to better than 20 cm, and repeated 1993 airborne measurements over a carefully surveyed runway show consistency at the 10-cm level. The results presented here are probably accurate to a few tens of cm. The elevation changes suggested by the data are far larger than this.

Change detection over Jacobshavn Glacier

In September, 1991 and again in April, 1992 we overflew a route down the Jacobshavn Glacier (Figure 1). In its lower reaches, the Jacobshavn Glacier moves approximately 8 km every year, making it the world's fastest glacier. It drains a very large area of Greenland into a fjord that is only 5 km wide. Within the Jacobshavn drainage basin, at surface elevations lower than about 1400 m, there is considerable surface melting in summer, with fast-flowing melt streams cutting into the ice and large lakes of melt water forming in more level areas. The intense melting thins the ice and lowers the surface elevation to reach a minimum at the end of the melt season. In winter, heavy snow accumulation, and advection of the steeply-sloping ice, raises the surface elevation to reach a maximum at the beginning of the melt season. Because Jacobshavn Glacier is so active, we expect this seasonal thickening and thinning to be quite large, providing an opportunity to test the ability of the airborne altimetry system to detect changes in surface elevation.

Figure 2 shows elevation profiles over the lower reaches of Jacobshavn Glacier, derived from airborne data collected in 1991 and 1992, with the elevation change during the interim also plotted. At the time of writing this paper, data from a third repeat flight in 1993 have not yet been processed. The most obvious change between the 1991 and 1992 profiles is the advance of the glacier front, by about 2 km. This does not fully reflect the glacier speed because there was probably significant calving of icebergs during the interim. Thickness change near the ice front is obscured by noise in the data associated with movement of ice pinnacles along the profile, but the glacier appears to have thickened by several meters between September, 1991 and April, 1992. This was probably balanced to some extent by melting later in 1992 which, however,

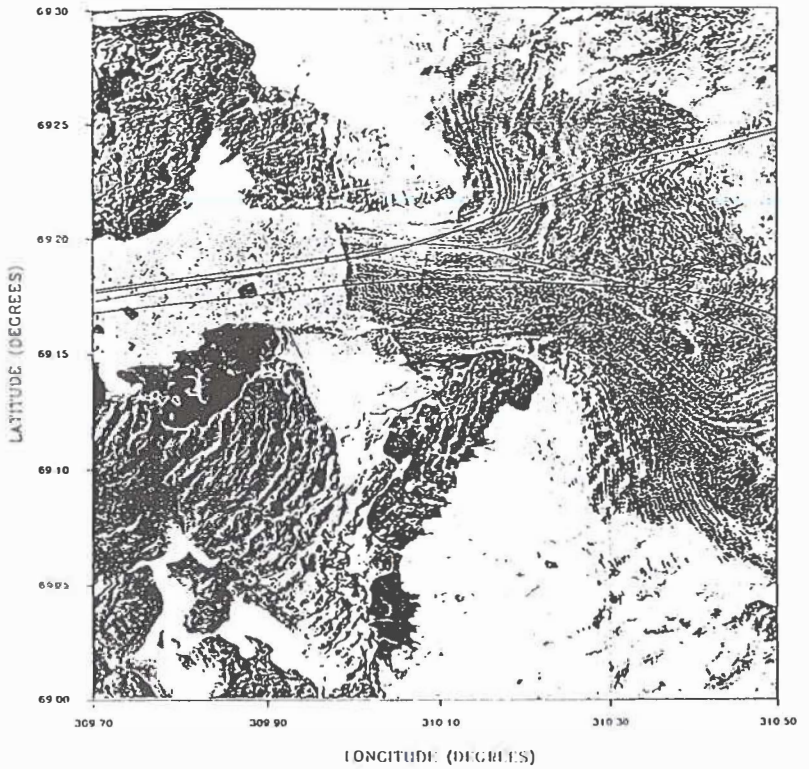


Figure 1. Photomap of Jacobshavn Glacier, showing routes of aircraft laser-altimetry flights.

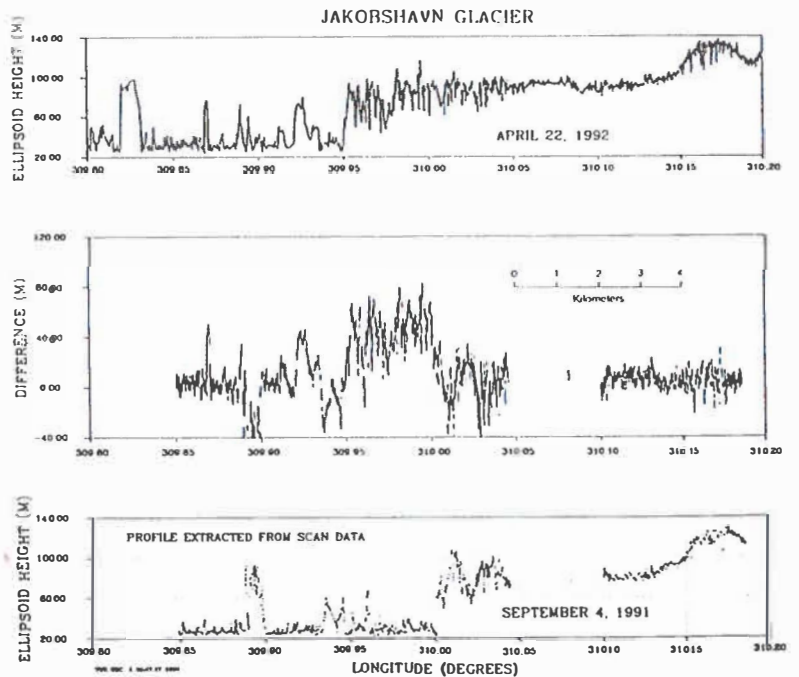


Figure 2. Surface profiles of Jacobshavn Glacier derived from the 1991 and 1992 laser-altimetry flights, with a plot of elevation differences at locations where 1992 flights were coincident with 1991 measurements. The calving front of the glacier was at Longitude 310° East in 1991, and at 309.95° East in 1992.

had a very cold summer. By contrast, the summer of 1993 was very warm, with record melting in many parts of the ablation zone. Clearly, measurements over short periods have to be interpreted with caution.

Figure 3 shows elevation profiles and elevation changes further upstream, where the glacier surface is free of crevasses and pinnacles. Here, the ice has thickened by about 3 meters, but the thickening is cyclic along the profile, caused apparently by 600-meter wavelength undulations in the glacier surface moving forward with the glacier (Figure 4).

Change detection over the ice sheet

In 1980 and 1981, at three positions in the southern part of the ice sheet, large stake arrays were carefully surveyed by a group from the Ohio State University using "Geociever" Satellite Doppler techniques (Drew, 1983). The locations of these stake clusters are shown in Figure 5. This work yielded precise estimates of latitude, longitude, and snow-surface elevation above the ellipsoid at each of the stakes. In 1993, several of these stake locations were included in the laser-altimetry flight lines, and here we present results from two flight lines that passed directly over 14 of the 1980 "cluster" stake locations.

In 1980 the Geociever survey yielded differential solutions using stations on the coast as control points. In 1993, we reoccupied, with a GPS receiver, one of the coastal control stations, situated on bedrock, in order to compare solutions from the 1980's and 1990's. This comparison required conversion of the 1980 solutions from the WGS-66 ellipsoid to the WGS-84 ellipsoid used for solution of the GPS surveys. Nevertheless, the comparison is remarkably good; the 1993 solution is 36 cm northwest of the 1980 solution, and 23 cm higher in elevation - consistent with isostatic uplift!

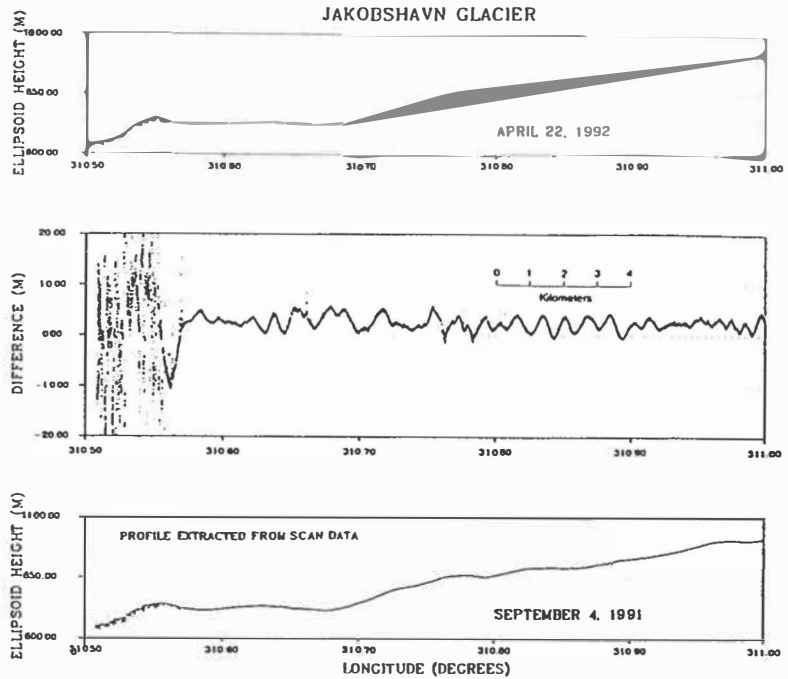


Figure 3. 1991 and 1992 surface profiles of Jakobshavn Glacier inland of those shown in Figure 2. Most of this region is crevasse-free, and the elevation-difference plot clearly shows a thickening trend of about 3 meters, but with a strong cyclic variation in thickening rate.

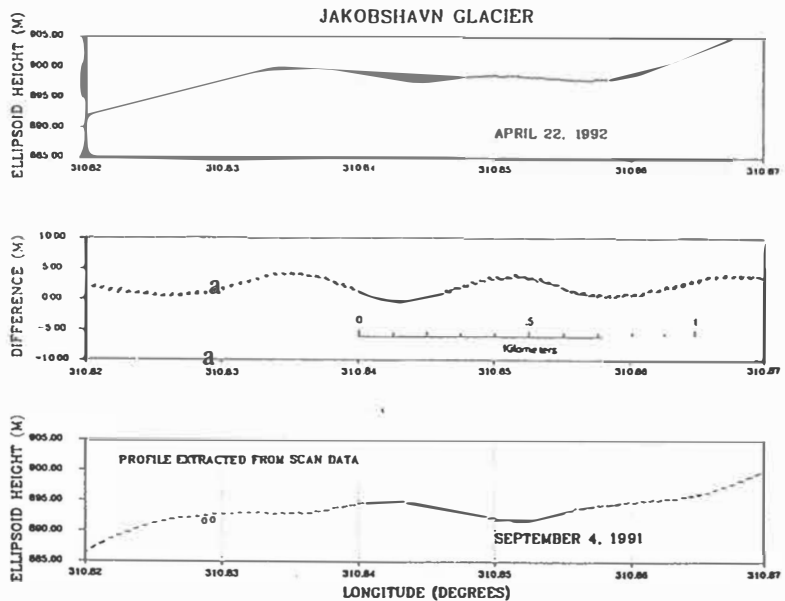


Figure 4. Expanded section of the surface elevation profiles shown in Figure 3. Surface undulations, of wavelength 600 meters and waveheight of about 3 meters, appear to be moving with the glacier, causing the cyclic variation in the plot of elevation difference.

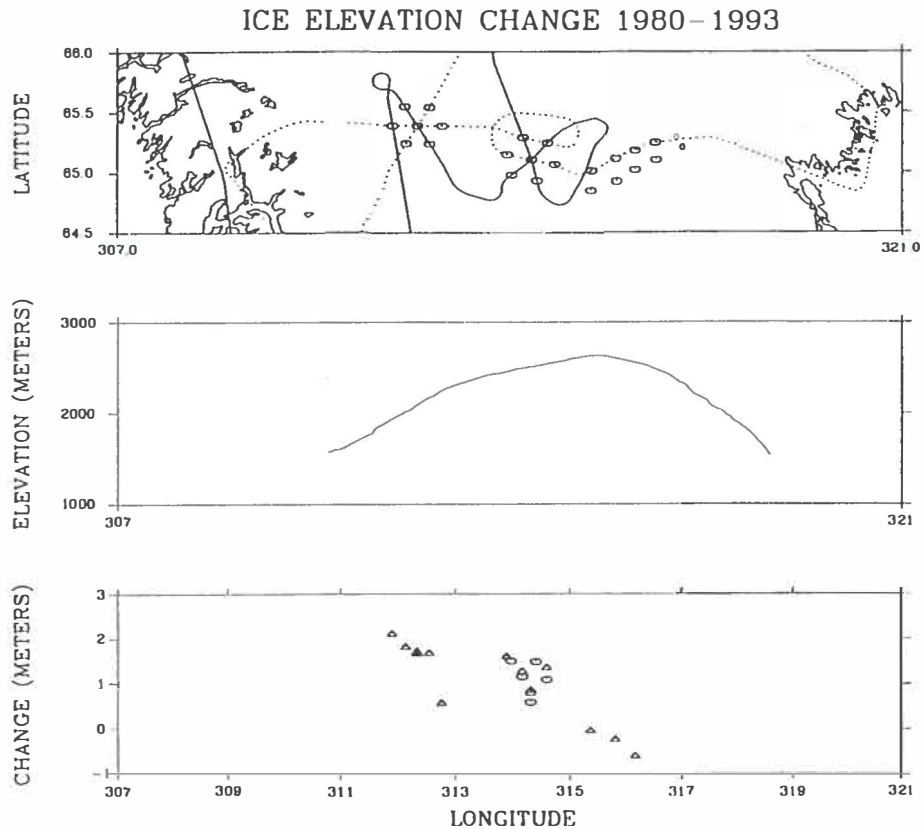


Figure 5. Southern Greenland, showing 1993 laser-altimetry flights over Ohio State University stake clusters that were surveyed in 1980. Also shown is a plot of the elevation change derived by comparing the 1980 measurements with those from 1993.

The changes in surface elevation between 1980 and 1993 at the overflow cluster locations are included in Figure 5, where they are plotted against Longitude of the cluster location. There appears to be a clear thickening trend in the west, progressively decreasing towards the east, possibly to thinning on the eastern side of the ridge summit. These results are broadly in agreement with those of Zwally et al (In preparation) from comparison of Seasat and Geosat measurements. However, we should stress that they refer only to the cluster locations, at approximately 65° latitude.

In 1991, and again in 1993, we overflow parts of the EGIG survey line. Our results for 1993 have not yet been analysed, and the data will be difficult to compare directly to those obtained from the surface-levelling traverse because they are referenced to the Ellipsoid, whereas the surface data are referenced to the Geoid. We plan to repeat the EGIG overflights periodically to monitor thickening/thinning rates along this traverse. In 1993, we made extensive flights over the southern part of the ice sheet, including all the major drainage basins. We plan to complete a similar mission in 1994, and then to repeat all flight lines at intervals of approximately 5 years in order to monitor ice thickening/thinning over the entire ice sheet.

Acknowledgements

We thank all who helped to obtain, and to process, the aircraft-altimetry measurements; they are too numerous to identify, but they did most of the work. Funding support was provided by the NASA Polar Research Program

References

- Seckel, H., 1977. Hohenänderungen im Grønlandischen Inlandeis zwischen 1959 und 1968. *Medd. Grønland*, Bd. 187, Nr. 4.
- Drew, A.J.R., 1983. Glacial movements in Greenland from Doppler satellite observations. *Ohio State University, Institute of Polar Studies*, Report No. 82, 66 pp.
- Zwally, H.J., T. Seiss, A. Brenner, and R.A. Bindshadler, In Preparation. Growth of the Greenland Ice Sheet: seasonal and interannual variations. To be submitted to *Science*.

NEOGLACIAL CHANGES OF THE INLAND ICE MARGIN

Anker Weidick

The Geological Survey of Greenland
Copenhagen, Denmark

This concerns an improved determination of Inland Ice marginal changes during the last part of the Holocene. The determinations serve as a calibration for modelling of ice margin response to climatic change, and is carried out by GGU in collaboration with DPC (Denmark) and AWI (Germany).

The early Holocene recession of the Inland Ice and its related glacio-isostatic emergence is documented by the ice margin deposits and marine deposits of the coast land. However, the margin retreated beyond the present position and major parts of information on most recent glacial events are concealed under the present ice margin.

The present position was reached essentially between 8 and 6 ka ago and the subsequent period must be characterized as the altithermal hiatus where continued recession and subsequent neoglacial readvances of the ice margin imply other procedures than of conventional mapping and dating of ice margin features and related marine shore lines.

Key areas for determination of duration and extension of altithermal hiatus

Requirements for key areas are optimally:

- Abundant organic material for ¹⁴C-dating (conventional as well as AMS) brought to the ice margin from its base. Already existing collections from the key sites have facilitated this part of the task. All AMS-datings on the mentioned collected material are performed by the Svedberg Institute (Uppsala, Sweden) and all conventional datings by the ¹⁴C-dating laboratory of the National Museum (Copenhagen, Denmark)
- knowledge of the mass balance and other physical conditions of the nearby Inland Ice margin
- knowledge of the preceding Holocene development

The following areas have been selected:

- a) Qagssimiut area at 61°N on the southern slope of the Inland Ice. The foreland area is characterised by a fast recession of the Inland Ice margin, and present position was reached already at or prior to c. 8 ka B.P. (Kelly, 1980).

The datings now performed extend the period of altithermal hiatus up to c. 3 ka B.P. Minimum recession of the ice margin during this period is estimated to be at least 15 km.

The period of c. 3 ka to c. 0.2 ka B.P. is not represented by datings. A local readvance (the Narssarssuaq stage) east of the locality exceeded the present ice margin position and might have occurred at around 2.5 ka B.P. whereas in general the termination of the altithermal hiatus can be put to c. A. D. 1750 or 1850.

- b) Kangersuneq area between 64° and 65°N at the west slope of the Inland Ice where present position seems to have been reached prior to c. 6 ka B.P. and the performed datings of subfossils extend this period up to c. 4 ka B.P. Events of the following 3 millenia are not known. For the last millenium records of Norse ruins buried under advancing ice appear in the 1700s (Weidick, 1982) indicative of the culmination of the neoglacial maximum around 1750. Also the submergence of the nearby area of c. 6 m throughout the last millenium can only be explained as a glacioisostatic effect off the increasing ice load during the neoglacial time.
- c) Jakobshavn Isfjord area at 69°N on the west slope of the Inland Ice where the present position presumably was reached at around 6 ka B.P. and where the gradual readvances in general reached a neoglacial maximum at around A.D. 1850-1890 (Weidick et al., 1992).

As in the case of South Greenland (east of Qagssimiut area) it might be considered where local readvances locally already around c. 2.5 ka B.P. could have reached beyond present extension.

For the later phases of ice margin response Reeh (1983) by modelling calculated a minor readvance at A.D. 800-900 preceding the neoglacial maximum at 1600-1900.

- d) Storstrømmen area at 77°N at the northeastern slope of the ice sheet.

Quaternary studies made by Lister & Wyllie (1957) and Landvik (in press) reveals the early Holocene deglaciation of the area. ¹⁴C-determination of biogenic material collected by N. Reeh and H. Oerter (ages shown in fig. 1.) have dated the altithermal hiatus to 5-2 ka B.P. indicating that Germania Land in this period was an island, and that the front of Storstrømmen must have been in a position c. 70 km behind the frontal position of the 1980s.

Subsequent neoglacial readvances seem generally to have culminated as late as around A.D. 1900 but it is still unclear whether the ice margin deposits laid down during this event is the neoglacial maximum. This moraine is characteristically ice-cored but is surrounded by an older, but fresh, moraine without dead ice. It is presumed that a gradual transformation of the ice-cored moraines to older moraines occurred during the last century e.g. at Annekssø by comparison of photos and description of the 1908 situation (Koch & Wegener, 1912) to that of the present

situation. If true the neoglacial maximum then must be older but subsequent expansions with gradually minor extent has occurred.

Historically documented records on glacier fluctuations have been applied for the last c. 200 years on the west slope of the ice sheet and of the northeastern slope for the last c. 80 years. The purpose is to establish a more spatial picture of the details of the ice margin changes, describing the different modes of glacierization and attainment of submaxima for readvances.

So far the results imply geographical variations in advances where the neoglacial maximum seems to have occurred at a few places at around 1750, at others (most places) at around 1850-1890 and at some places (essentially highland areas) it is still not achieved. This picture could be given around 1950 but since then the situation has shifted since more and more segments of the ice sheet have initiated a readvance reaching close (or beyond) the extent of 1950. The shift (turn of the tide) seems to be explained by a model, presented by Huybrechts (1993). It concludes that the ice sheet as a whole is thickening at present and that this thickening especially is concentrated in the southwestern parts of the ice sheet. It is suggested that this represents a long-term trend caused by a purely dynamic reaction to the geometry which come out of the last glacial-interglacial transition but at the same time, that this is partly and in places matched by the instant effects of temperature variation on the ablation.

The glacio-isostatic effects of the changes of the ice cover is very obvious from the Quaternary investigations. During the period of ice marginal recession of the early Holocene the coast was subject to an emergence which presumably ended (West and South Greenland) around 3 ka ago where the relative sea level at places was 8-6 m below the present one. Subsequent submergence is apparent for the last millenium but the spatial and temporal variations of the individual regions are still unclear (Weidick 1993). The same trend of emergence followed by submergence can be stated for the areas north of Storstrømmen (Peary Land: Bennike, 1987), and to the south (Hochstetter Forland: Hjort 1981).

Acknowledgements

This research is supported by the European Community through contract number EV5V-CT91-0051.

References

- Bennike, O. 1987: Quaternary geology and biology of the Jørgen Brønlund area, North Greenland. *Meddr Grønland, Geosci.* **18**, 24 pp.
- Funder, S. 1971: C¹⁴-dates from the Scoresby Sund region 1971. *Rapp. Grønlands geol. Unders.*, **37**, 57-59.
- Huybrechts, P. 1993: Modelling the present evolution of the Greenland ice sheet. *In* Reeh & Oerter, H. (eds.): *Mass balance and related topics of the Greenland Ice Sheet.* Grønlands geol. Unders. Open File Series 93/5, 13-16.
- Hjort, Chr. 1981: Present and Middle Flandrian Coastal morphology in Northeast Greenland. *Norsk geogr. Tidsskrift* **35**, 197-207.
- Kelly, M. 1980: The Status of Neoglaciation in Western Greenland. *Rapp. Grønlands geol. Unders.* **96**, 24 pp.
- Koch, J. P. & Wegener, A. 1912: Die glaziologischen Beobachtungen der Danmark-Expedition. *Meddr Grønland*, **46**, 1, 77 pp.
- Landvik, J. (in press): The last glaciation of Germania Land and adjacent areas, Northeast Greenland.
- Lister, H. & Wyllie, P. J. 1957: The geomorphology of Dronning Louise Land. *Meddr Grønland* **158**, 1, 73 pp.
- Mörner, N.-A. and Funder, S. 1990: C¹⁴-dating of samples collected during the NORDQUA-86 expedition to Thule. *In* S. Funder (editor), *Late Quaternary Stratigraphy and Glaciology in the Thule Area, Northwest Greenland.* *Meddr Grønland, Geosci.*, **22**, 57-60
- Reeh, N. 1983: Ikke-stationær beregningsmodel for Indlandsisens randzone. *Grønlands geol. Unders. Gletscher-hydrol. Meddr* **83**, 7, 81 pp.
- Weidick, A. 1982: Klima- og gletscherændringer i det sydlige Vestgrønland de sidste 1000 år. *Grønland* **5-7**, 235-251.
- Weidick, A. 1993: Neoglaciation change of ice cover and the related response of the Earth's crust in West Greenland. *Rapp. Grønlands geol. Unders.* **159**, 121-126.
- Weidick, A., Oerter, H., Reeh, N., Thomsen, H. H. & Thorning, L. 1990: The recession of the Inland Ice margin during the Holocene climatic optimum in the Jakobshavn Isfjord area of West Greenland. *Palaeogeography, Palaeoclimatology, Palaeoecology (Global and Planetary Change Section)*, **82**, 389-399.

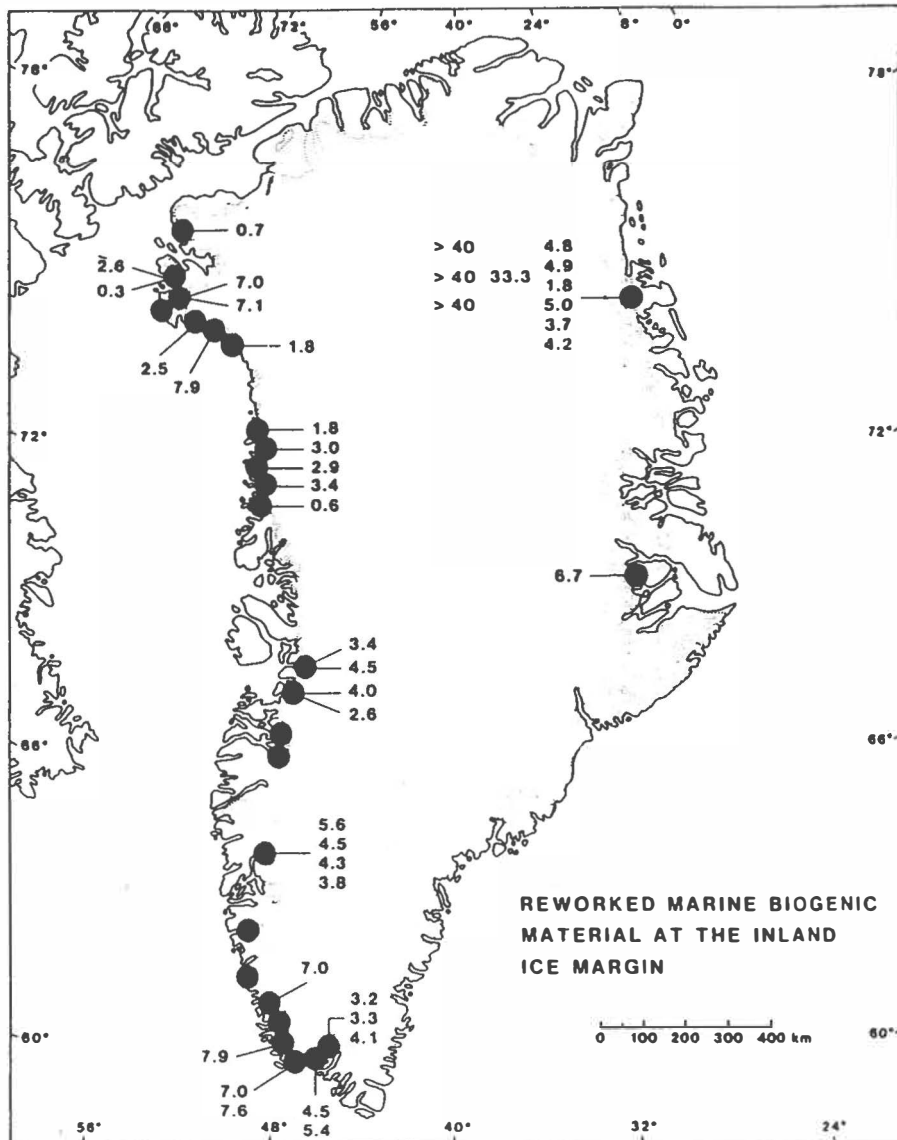


Fig. 1. Location of reworked biogenic material at the margin of the Inland Ice. All dates are given in ^{14}C kyr. Older sources of data from Funder 1971, Kelly 1980, Mörner & Funder 1990 and Weidick et al. 1990. The additional dates referred to here are clustered around 61°N (Qagssimiut), $64^\circ\text{-}65^\circ\text{N}$ (Kangersuneq) and 69°N Jakobshavn Isfjord) in West Greenland and at 77°N (Storstrømmen) in Northeast Greenland. Interstadial and/or interglacial ages will be noticed at some of the samples from Storstrømmen.

ALBEDO VARIATIONS IN THE MELTING ZONE OF THE GREENLAND ICE SHEET: OBSERVATIONS AND MODELLING

Zhizheng Zuo & Hans Oerlemans
Institute for Marine and Atmospheric Research Utrecht
Utrecht University, The Netherlands

Surface albedo varies strongly with the changing morphology of snow and ice cover, thus governing the surface energy balance and therefore the mass balance over glaciers and ice sheets. The crucial point is how we can construct a simple scheme capable of reproducing the main features of albedo patterns observed in the field.

Data on surface albedos collected during a meteorological experiment in the ablation zone of west Greenland in the summer of 1991, offer a good opportunity to design and test an albedo scheme for use in an energy/mass balance model. A striking finding in the field experiment was an unexpected decrease of the albedo (down to 0.27 in mid July) observed at the mid-elevation part (± 300 -1000 m) of the ice sheet. At the ice margin the albedo remains at rather constant values of 0.50-0.55. Comparison between the measurement of albedo and temperature indicates an inverse correlation between those two, that is, decreasing albedo coupled with increasing temperature. The reduction in the albedo seems to be related to the accumulation of melt water at the surface. Such an albedo pattern, opposite to what has been observed on mountain glaciers, has large implications for the energy budget and deserves careful study.

A surface energy balance model was developed to study the sensitivity of the Greenland ice sheet to changes of climate conditions. The model is a modified version of the one developed in Oerlemans (1991). One of the most important modifications in the model is the treatment of albedo. The albedo scheme is designed in such a way that it can simulate the following features observed in the field: 1) decay of snow albedo within a few days after a snowfall event; 2) decrease of albedo associated with accumulation of melt water. The runoff rate of melt water is

determined by surface slope and underlying snow depth. For the melt water budget, we use the formulation:

$$\frac{dW}{dt} = P_w - \frac{W}{t^*} \quad (1)$$

$$t^* = c_1 / (c_2 + S) + c_3 d \quad (2)$$

where W is the amount of melt water; P_w is the production of melt water, t^* is a time constant that depends on surface slope S and snow depth d , and c_1 , c_2 , c_3 are constants. The expression used for albedo that includes effect of melt water reads:

$$\alpha_e = \alpha_{\text{wat}} - (\alpha_{\text{wat}} - [\alpha_{\text{sn}} - (\alpha_{\text{sn}} - \alpha_{\text{ice}}) e^{-d/d^*}]) e^{-W/w^*} \quad (3)$$

with the following ageing effect of the snow:

$$\alpha_{\text{sn}} = \begin{cases} \alpha_0 & \text{if } T_a < 2^\circ\text{C} & \text{precipitation day} \\ \max\{\alpha_0 - 0.04 i; 0.65\} & \text{if } B > 0 & \text{other days} \\ \max\{\alpha_0 - 0.03 i; 0.70\} & \text{if } B \leq 0 & \text{other days} \end{cases} \quad (4)$$

$i = 1, \dots, 14.$

where α_{wat} is albedo of water, α_0 albedo of fresh snow, α_{ice} albedo of clean dry ice, α_{sn} albedo of old snow, d snow depth, d^* and w^* constants, i days after snowfall event, T_a air temperature and B energy budget.

Climatological data collected during the GIMEX expeditions in the summers of 1990 and 1991, as well as routine weather observations made by the Danish Meteorological Institute at the Søndre Strømfjord weather station, west Greenland, during 1990-1992, combined with the data reported in the existing literature were used as input to the model. The integration of the energy balance model was performed with a one-day time step. Calculations were done for a number of grid points up to 2300 m elevation. Five years of integration leads to a stationary balance profile with an equilibrium line altitude of 1375 m that is similar to the field data. The calculated mass balance profile is in good agreement with the observations. It appears that a better simulation of observed albedo can indeed be obtained if water at the surface is explicitly included in the model. When excluding the term of melt water in the model, the mass balance profile has a significant departure from the field data and the reduction of surface albedo, as observed in the field, disappears completely. The total ablation in this case would be reduced by 31%. This indicates that the presence of the surface melt water during the ablation season plays an important role in mass budget of the ice sheet in west Greenland. It is therefore

necessary to include this effect when constructing an energy balance model for the entire Greenland ice sheet.

Climate sensitivity has been studied with respect to mean air temperature, surface albedo and precipitation. Clearly in most cases the change in mass balance reaches its maximum close to the equilibrium line. Above the ela, the change in mass balance decreases with elevation, while at the lower part of the ice sheet the situation is vice versa. For typical climate conditions in west Greenland a 1K temperature change leads to a lifting in equilibrium line altitude of 142 m. This would increase the total ablation by about 32%. This large sensitivity is a consequence of a strong albedo feedback as well as a lengthening of the ablation season. For a uniform reduction of 0.05 in albedo, an effect of similar magnitude can be obtained, which shows the extreme importance of this quantity. This implies that the parameterization of surface albedo is the most critical point in the formulation of the energy/mass balance model.

To summarize, the energy balance model is capable of reproducing the observed albedo and mass balance features of the ice sheet in west Greenland. The effect of melt water at the surface during the ablation season is of great importance in studying physical processes of the Greenland ice sheet. A climate sensitivity test shows the clear response of a mass balance profile to climatic change. For a better understanding in the evolution of the Greenland ice sheet further time series observations as well as further development of the existing model are required.

References

- Oerlemans J. (1991). The mass balance of the Greenland ice sheet: sensitivity to climate change as revealed by energy-balance modelling. *The Holocene* **1** (1), 40-49.

